Western Graduate&PostdoctoralStudies

Western University
Scholarship@Western

Electronic Thesis and Dissertation Repository

8-24-2020 10:30 AM

A 3D Microvessel Model for the Study of Endothelial Cell Transluminal Pillar Formation

Emma Kate Prescott, *The University of Western Ontario*

Supervisor: Pickering, J. Geoffrey, *The University of Western Ontario*

A thesis submitted in partial fulfillment of the requirements for the Master of Science degree in Medical Biophysics

© Emma Kate Prescott 2020

Follow this and additional works at: https://ir.lib.uwo.ca/etd

Part of the Medical Biophysics Commons

Recommended Citation

Prescott, Emma Kate, "A 3D Microvessel Model for the Study of Endothelial Cell Transluminal Pillar Formation" (2020). *Electronic Thesis and Dissertation Repository*. 7240.
https://ir.lib.uwo.ca/etd/7240

This Dissertation/Thesis is brought to you for free and open access by Scholarship@Western. It has been accepted for inclusion in Electronic Thesis and Dissertation Repository by an authorized administrator of Scholarship@Western. For more information, please contact wlswadmin@uwo.ca.

ABSTRACT

BACKGROUND: Endothelial cells (ECs) line the blood vessel lumen and respond to fluid shear stress. ECs are also responsible for initiating the formation of new blood vessels. These new vessels can form either by sprouting angiogenesis or intussusceptive, or splitting, angiogenesis. The latter is poorly understood but recent evidence suggests that intussusception occurs in early vessels with ultra-low blood flow. However, the biomechanical and biochemical mechanisms of intussusceptive angiogenesis remain largely unknown and *in vitro* models do not exist.

The purpose of this thesis was to develop a three-dimensional EC culture model capable of forming transluminal pillars, a key step in angiogenesis, and to utilize this model to identify regulators of pillar formation.

METHODS: I developed a novel 3D microvessel model using microfluidic channels of dimensions 100 μm x 100 μm x 1 cm (h, w, l). The channels were circumferentially lined with a confluent monolayer of human umbilical vein endothelial cells (HUVECs). Programmable syringe pumps were used to expose cells to range of shear stresses from physiological (10 dyn/cm^2) to ultra-low (0.02 dyn/cm^2). Cells were immunostained for VE-Cadherin, ARL13b, and phosphorylated VEGFR2 (pVEGFR2). A similar microfluidic model in channels of dimensions 300 μm x 1000 μm x 1 cm (h, w, l) was used to co-culture RFP- and GFP-expressing HUVECs differentially treated with control or VEGFR2 siRNA and subjected to ultra-low shear stress to directly test the role of VEGFR2 in pillar formation.

RESULTS: Endothelial cells exposed to ultra-low shear stress showed marked changes in morphology compared to cells exposed to physiological shear stress, including a decrease in elongation, more random orientation, and a shift in F-

actin from stress fibres to cortical actin. Importantly, transluminal pillars were identified at the channel shoulders and pillar abundance was 8.8-fold higher under ultra-low shear stress. Furthermore, ARL13b expression was 1.9-fold higher in HUVECs exposed to ultra-low shear stress, suggesting an increase in primary cilia under ultra-low shear. Interestingly, ARL13b was also localized with transluminal pillars. Expression of pVEGFR2 decreased by 22% in cells subjected to ultra-low shear stress and was identified in the mid-region of pillars and lateralized to the upstream surface. A co-culture of RFP- and GFP-HUVECs differentially transfected with control siRNA or VEGFR2 siRNA demonstrated a 12.5-fold increase in pillar frequency in cells with reduced VEGFR2 content under ultra-low shear stress.

CONCLUSIONS: I established a 3D microfluidic culture model of endothelial cells that successfully yields transluminal endothelial pillars. Pillar formation was stimulated by ultra-low shear stress and further enhanced by VEGFR2 downregulation. Immunostaining for ARL13b and pVEGFR2 suggested shear-seeking behaviour may underlie pillar formation. This interplay between ultra-low flow and shear-seeking behaviour constitutes new insights into intussusceptive angiogenesis.

Keywords: endothelial cell, microfluidics, transluminal pillar, intussusceptive angiogenesis, primary cilia, VEGFR2, peripheral arterial disease, ischemic injury, shear stress

SUMMARY FOR LAY AUDIENCE

Peripheral arterial disease (PAD) is a disorder common among older individuals and diabetics wherein the arteries that supply blood to the muscles in the leg become blocked, starving the tissue of oxygen. New therapies for PAD include attempting to promote the growth of new blood vessels to return blood flow to these muscles. However, these therapies have seen little success in patients.

In this thesis, I developed a 3D model of a blood vessel using microfluidics to understand how new blood vessels form. I particularly investigated how a single vessel can split into two. I discovered that endothelial cells that line blood vessels can be made to take on a flow-seeking behaviour that motivates them to stretch across the blood vessel channel. This happens when the blood flow in the vessel is low. The study revealed the critical first steps in blood vessel duplication.

This knowledge could help in developing therapies that stimulate blood vessel development to restore blood flow to damaged leg muscles in patients with PAD.

CO-AUTHORSHIP STATEMENT

All chapters of this thesis were written by Emma Prescott and revised with recommendations from Dr. Hao Yin and Dr. Geoffrey Pickering. All schematics and artwork is original work created by Emma Prescott.

The data presented in Chapter 2 is in preparation for submission to a peer-reviewed journal. Emma Prescott was the primary contributor to all aspects of manuscript preparation including study design and experimentation, data acquisition and quantification, analysis, and writing. Contributions to the work in this chapter include Dr. John-Michael Arpino (execution of one microfluidic experiment and immunostaining in Figures 2.1, 2.4, and 2.5) and Sabrina Staples (cell culture for microfluidic experiments in Figures 2.2, 2.3, and 2.6). Collaborators included Dr. Daniel Lorusso, Dr. David Holdsworth, and Dr. Tamie Poepping who helped to design and fabricate the microfluidic device used in these experiments. Dr. J. Geoffrey Pickering conceived and coordinated the study.

Chapter 3 of this thesis represents original work by Emma Prescott included in a manuscript composed by Dr. John-Michael Arpino in preparation for submission to a peer-reviewed journal. Emma Prescott was responsible for study design and experimentation, data acquisition and quantification, analysis, and writing. Contributions to the work in this chapter includes Dr. Hao Yin who helped with generation of qPCR data for HUVECs transfected with control siRNA or VEGFR2 siRNA (Figure 3.3A). Collaborators included Dr. Daniel Lorusso, who helped with setup of the peristaltic pump and design and fabrication of the microfluidic device used in these experiments, along with Dr. David Holdsworth and Dr. Tamie Poepping. Dr. J. Geoffrey Pickering conceived and coordinated the study.

ACKNOWLEDGEMENTS

I would first like to thank my supervisor, Dr. Geoffrey Pickering, for his invaluable guidance and support over the past two years. I am thrilled to have been given the opportunity to work on such a unique and exciting project, and the advancements I made would not have been possible without his advice. I would also like to acknowledge my advisory committee members, Dr. Tamie Poepping and Dr. David Holdsworth, for their willingness to collaborate and constant enthusiasm for the project.

I would also like to thank my colleagues for their help and support. I would like to specifically thank Dr. Hao Yin for giving so much of his time and advice to helping me surpass countless hurdles as I completed this project. I would also like to thank Caroline O'Neil for making my time in the lab so enjoyable, alongside her constant technical support. I would like to thank Dr. Jason Lee, without whom I would never have been accepted to medical school, and Jacqueline Chevalier, who was a great friend during her time in the lab and after. Finally, I would to thank my mentors Dr. John-Michael Arpino, who taught me so much about high-quality research and was always willing to listen, and Dr. Daniel Lorusso, who was an invaluable resource on the field of microfluidics.

I would also like to thank my friends and family for their unwavering support and encouragement as I finished my degree and as I move on to a new chapter.

Table of Contents

ABSTRACT ..... **II**

SUMMARY FOR LAY AUDIENCE ..... **IV**

CO-AUTHORSHIP STATEMENT ..... **V**

ACKNOWLEDGEMENTS ..... **VI**

LIST OF FIGURES ..... **IX**

LIST OF TABLES ..... **XI**

LIST OF APPENDICES ..... **XII**

LIST OF ABBREVIATIONS ..... **XIII**

CHAPTER 1: GENERAL INTRODUCTION **1**

1.1 CARDIOVASCULAR DISEASE 3
1.1.1 Ischemic Cardiovascular Disease *3*
1.1.2 Peripheral Arterial Disease *3*
1.1.3 Therapeutics for Peripheral Arterial Disease Patients *4*
1.2 ANGIOGENESIS 5
1.2.1 Sprouting Angiogenesis *5*
1.2.2 Intussusceptive Angiogenesis *8*
1.2.3 Intussusceptive Angiogenesis in a Mouse Model of PAD *9*
1.3 ENDOTHELIAL CELL FLOW SENSING 11
1.3.1 Receptor Tyrosine Kinases *14*
1.3.2 Receptor Serine/Threonine Kinases *16*
1.3.3 G-Protein Coupled Receptors *17*
1.3.4 Notch1 ..... *18*
1.3.5 Ion Channels *18*
1.3.6 Endothelial Cell Adhesion Molecules *20*
1.3.7 Plasma Membrane Structures *21*
1.4 TOOLS FOR STUDYING ENDOTHELIAL CELL FLOW RESPONSE 22
1.4.1 Microfluidics *23*
1.5 AIMS OF THE THESIS 26
1.6 REFERENCES 26

CHAPTER 2: A NOVEL 3D MICROVESSEL MODEL FOR THE STUDY OF ENDOTHELIAL CELL TRANSLUMINAL PILLAR FORMATION **33**

2.1 INTRODUCTION 33
2.2 METHODS 35
2.2.1 Microfluidic Device Design and Fabrication *35*
2.2.2 Endothelialization of Microfluidic Channels *36*
2.2.3 Induction and Variation of Shear Stress within Microfluidic Channels *37*

2.2.4 Immunostaining of Endothelial Cells Lining Microfluidic Channels 37
2.2.5 Confocal Imaging and Analysis of Endothelial Cell Morphology and Pillar Formation 38
2.2.6 Statistical Analysis 40
2.3 Results 41
2.3.1 Engineering of a Novel 3D Microvessel Model 41
2.3.2 Ultra-Low Shear Stress Induces Endothelial Cell Rounding 41
2.3.3 Ultra-Low Shear Stress Causes Reorganization of the F-Actin Cytoskeleton 48
2.3.4 Endothelial Cells Exposed to Ultra-Low Shear Stress Become Randomly Oriented in the Direction of Flow 50
2.3.5 Ultra-Low Shear Stress is Conducive to Endothelial Cell Transluminal Pillar Formation 52
2.3.6 Ultra-Low Shear Stress Leads to an Increase in ARL13b Expression 52
2.3.7 Ultra-Low Shear Stress Results in a Decrease in Phosphorylated VEGFR2 55
2.4 Discussion 61
2.5 References 66

CHAPTER 3: THE ROLE OF VEGFR2 IN ENDOTHELIAL TRANSLUMINAL PILLAR FORMATION: A 3D MICROFLUIDIC STUDY 70

3.1 Introduction 70
3.2 Methods 72
3.2.1 Microfluidic Device Fabrication 72
3.2.2 VEGFR2 Knockdown and Co-Culture of Fluorescent HUVECs in the Microfluidic Channel 72
3.2.3 Introduction of VEGFR2 Knockdown Co-Culture to Ultra-Low Shear Stress 73
3.2.4 Confocal Microscopy and Analysis of Pillar Formation in HUVECs with and without Reduced VEGFR2 Expression 75
3.2.5 Statistics 75
3.3 Results 76
3.3.1 Endothelial Cells Lining a Rectangular Microfluidic Channel are Capable of Pillar Formation 76
3.3.2 Reduced VEGFR2 Expression Results in Less Elongated Endothelial Cells 82
3.3.3 Pillar Predisposition in Endothelial Cells with Reduced VEGFR2 Expression 82
3.4 Discussion 87
3.5 References 89

CHAPTER 4: GENERAL DISCUSSION AND CONCLUSIONS 92

4.1 Development of a Novel 3D Microvessel Model using Microfluidics 93
4.2 Ultra-Low Flow is Permissive to Transluminal Pillar Formation 94
4.3 Microfluidic Modeling of Pillar Morphogenesis 96
4.4 Mechanosensing Regulators of Pillar Formation 97
4.5 Future Directions 100
4.6 Conclusions 101
4.7 References 102

APPENDIX 106

LIST OF FIGURES

Figure 1.1 Sprouting Angiogenesis.....7

Figure 1.2 Intussusceptive Angiogenesis 9

Figure 1.3 Endothelial Cell Mechanosensing 13

Figure 2.1 3D microvessel modelling using a microfluidic device.....42

Figure 2.2 Generation of a healthy endothelial cell monolayer within a microfluidic channel. 44

Figure 2.3 Morphology and cytoskeletal reorganization in response to decrements of laminar shear stress.....46

Figure 2.4 Endothelial cell changes in morphology under various shear stress conditions.....49

Figure 2.5 Recreation of a transluminal pillar under ultra-low shear stress in a 3D *in vitro* microvessel model.....53

Figure 2.6 Increase in ARL13b expression in HUVECs exposed to ultra-low shear stress. 56

Figure 2.7 Ultra-low shear stress results in a decrease in pVEGFR2 expression in endothelial cells lining a 3D microfluidic channel. ...59

Figure 3.1 A 3D *in vitro* microvessel lined with a healthy endothelial cell monolayer. 77

Figure 3.2 Controlled endothelial cell transluminal pillar formation in a 3D microvessel model. 80

Figure 3.3 Endothelial cells with reduced VEGFR2 expression are less elongated in the direction of flow. 83

Figure 3.4 3D co-culture of endothelial cells transfected with control siRNA or VEGFR2 siRNA reveals an increase in pillar formation among cells with reduced VEGFR2 expression.....85

LIST OF TABLES

Table 1.1 Endothelial Cell Shear Stress Sensors 15

LIST OF APPENDICES

Appendix A: Legends for Supplemental Video Files.....106

LIST OF ABBREVIATIONS

αvβ3 Integrin	Alpha 5 Beta 3 Integrin
2D	2-dimensional
3D	3-dimensional
Akt	Protein Kinase B
Alk	Activin Receptor-like Kinase
ARL13b	Adenosine Diphosphate-Ribosylation Factor-like Protein 13B
ATP	Adenosine Triphosphate
β1 Integrin	Beta-1 Integrin
BMP9	Bone Morphogenetic Protein 9
Ca^{2+}	Calcium Ion
CAM	Chick Chorioallantoic Membrane
Cas9	CRISPR associated protein 9
CD44	Cluster of Differentiation 44
CFTR	Cystic Fibrosis Transmembrane Conductance Regulator
CLI	Critical Limb Ischemia
CO_2	Carbon Dioxide
CRISPR	Clustered Regularly Interspaced Short Palindromic Repeats
DAG	Diacylglycerol
DAPI	4',6-Diamidino-2-phenylindole
dyn/cm^2	dynes/cm^2
EC	Endothelial Cell
ECM	Extracellular Matrix
EGM-2	Endothelial Growth Medium-2

EGM-MV	Microvascular Endothelial Growth Medium
eNOS	Endothelial Nitric Oxide Synthase
ERK	Extracellular Signal-Regulated Kinase
F-actin	Filamentous Actin
FAK	Focal Adhesion Kinase
FGF	Fibroblast Growth Factor
FOV	Field of View
GDP	Guanosine Diphosphate
GFP	Green Fluorescent Protein
GPCR	G-Protein Coupled Receptor
GTP	Guanosine Triphosphate
HGF	Hepatocyte Growth Factor
HUVEC	Human Umbilical Vein Endothelial Cell
IA	Intussusceptive Angiogenesis
IP_3	Inositol Triphosphate
IQR	Interquartile Range
KDR	Kinase Insert Domain Receptor
KLF	Krüppel-Like Factor
NF-κB	Nuclear Factor-Kappa Beta
NO	Nitric Oxide
PAD	Peripheral arterial disease
PBS	Phosphate-Buffered Saline
PCR	Polymerase Chain Reaction
PDMS	Polydimethylsiloxane
PECAM-1	Platelet and Endothelial Cell Adhesion Molecule 1
PI(3)K	Phosphoinositide 3-Kinase

PIP_2	Phosphatidylinositol 4,5-bisphosphate
pVEGFR2	Phosphorylated-VEGFR2
RBC	Red Blood Cell
RFP	Red Fluorescent Protein
RhoA	Ras homolog family member A
RPM	Revolutions per minute
RSTK	Receptor Serine/Threonine Kinase
RTK	Receptor Tyrosine Kinase
Shh	Sonic hedgehog
siRNA	Small interfering RNA
SMAD	Mothers against decapentaplegic homolog
TGFβ	Transforming Growth Factor Beta
TRPV4	Transient Receptor Potential Cation Channel Subfamily V Member 4
VE-Cadherin	Vascular Endothelial Cadherin
VEGF	Vascular Endothelial Growth Factor
VEGFR2	Vascular Endothelial Growth Factor Receptor 2

CHAPTER 1:
GENERAL INTRODUCTION

Peripheral arterial disease (PAD) is a devastating type of ischemic disease that is caused by chronic arterial occlusion and leads to reduced oxygen and nutrient levels in downstream tissue. This leads to damage or death of the tissue and surrounding microvascular networks. Therapeutic strategies for PAD beyond surgery and catheter interventions are limited. Recently, considerable research has focused on therapeutic angiogenesis, i.e. stimulating new blood vessel growth to reperfuse the ischemic tissue. However, these methods of therapy have shown little clinical success, failing to produce long-term benefits for patients (Inampudi et al., 2018).

Currently, the most studied mode of blood vessel formation is sprouting angiogenesis. In this process, endothelial cells (ECs) lining the lumen of a vessel migrate into the surrounding tissue, lumenize, and anastomose to form new perfusable vessels from a pre-existing blood vessel (Carmeliet, 2000). Accumulating evidence reveals that the stimulatory and regulatory mechanisms of sprouting angiogenesis involve a wide variety of soluble biochemical factors, and extracellular matrix and biophysical cues, e.g. shear stress, that directly or indirectly impact EC biology. Nevertheless, angiogenesis can also occur via a less understood approach called intussusceptive, or splitting, angiogenesis (IA). During intussusceptive angiogenesis, ECs form a bridge called a transluminal pillar across a lumen with blood flow and extend this bridge along the length of the vessel (Djonov et al., 2000). This process effectively splits one large vessel into two smaller daughter vessels, constituting a quick and efficient way of vascular growth when compared to sprouting angiogenesis. However, little is known about the biochemical and biomechanical regulation of this angiogenic process.

Recently, our research group has undertaken a detailed investigation of angiogenesis in ischemic muscle of mice (Arpino et al., 2017a). In response to femoral artery excision and subsequent infarction of lower limb muscle, microvasculature in the skeletal muscle was obliterated and quickly regenerated in a coordinated manner with myofiber reconstitution. We also observed that intussusceptive angiogenesis was the predominant mode of angiogenesis for blood vessel regeneration, as opposed to sprouting angiogenesis which could only be identified occasionally (Arpino, 2017b). Notably, vessels undergoing intussusception demonstrated a markedly low blood flow, with <2% of normal shear compared to normal microvessels. Given the ability of ECs to sense and respond to blood flow, this unique ultra-low flow could be responsible for triggering intussusceptive angiogenesis. However, there is no *ex vivo* model to study intussusceptive behaviour of ECs. This greatly limits the research progress to understanding the biochemical and biophysical factors of intussusceptive angiogenesis.

The broad goal of my thesis was to develop an *in vitro* culture model of ECs that enables formation of an EC transluminal pillar, the early landmark of intussusceptive angiogenesis. Addressing this entailed generating a 3D micro-scale vessel-like structure and delivery of ultra-low flow. I subsequently utilized this model to study the role of endothelial mechanosensors and morphogenetic behaviours of ECs in the induction of intussusceptive angiogenesis.

My specific objectives were:

1) To develop an *in vitro* model of early forming, primordial blood vessels using 3D microfluidics and ultra-low flow.

2) To determine if transluminal endothelial pillars will form in the microfluidic model.

3) To determine the expression and localization of select shear stress sensors in endothelial cells subjected to ultra-low flow and pillar-forming conditions.

4) To determine the role of vascular endothelial growth factor receptor 2 (VEGFR2) in endothelial transluminal pillar formation, *in vitro*.

I hypothesize that endothelial cell transluminal pillar formation depends on altered shear stresses. I further hypothesize that pillar formation will entail changes in expression and/or activation of shear sensors, including VEGFR2.

1.1 Cardiovascular Disease

1.1.1 Ischemic Cardiovascular Disease

Cardiovascular disease is a debilitating class of disorders that dramatically reduces patient quality of life and can quickly lead to death without, and sometimes even despite, receiving the correct therapeutics. Within the large category of cardiovascular diseases, ischemic cardiovascular disease presents with one of the highest mortality rates. (Yusuf et al., 2001). This devastating disease is caused by the narrowing or occlusion of arterial vessels, reducing the flow of blood to downstream organs and tissues. Such ischemia and its outcomes can be seen among coronary artery disease and peripheral arterial disease.

1.1.2 Peripheral Arterial Disease

Peripheral arterial disease is a type of ischemic vascular disease affecting the extremities, most frequently the legs. PAD is a widespread health problem, with studies reporting 202 million people suffering from the disease globally, with greater than 8.5 million people above the age of 40 in North America alone (Benjamin et al., 2018). As the disease progresses, atherosclerotic lesions progress in the major arteries feeding these extremities, either partially blocking

or completely occluding the vessel (Annex, 2013). This arterial stenosis leads to a reduction in blood flow to downstream tissue, in turn reducing the amount of oxygen and nutrients delivered to the tissue. This can then result in ischemic injury and irrevocable tissue necrosis, if not addressed at an early stage. Common clinical symptoms of PAD include limb muscle fatigue, numbness, exercise-induced pain, and consequent reduction in limb function.

The most severe form of PAD manifests as critical limb ischemia (CLI), occurring in 1.3% of patients with PAD (Benjamin et al., 2018**)**. Patients with CLI suffer a worsening of PAD symptoms, including persistent rest pain, non-healing skin ulcers, gangrene, and even loss of toes or legs due to chronic, severe ischemia and/or infection.

1.1.3 Therapeutics for Peripheral Arterial Disease Patients

Despite the extremely poor outcomes of CLI, therapies that result in full recovery of the affected limb are limited. Currently, endovascular and open surgical revascularization procedures are the primary methods of CLI treatment (Kinlay, 2016). However, many CLI patients either undergo unsuccessful revascularization procedures or are not eligible for such procedures (Uccioli et al., 2018). In fact, a study performed by Chung et al. (2015) on a cohort of 8334 CLI patients found 46% of patients ultimately required major amputation. These types of major amputation, such as above-ankle amputation, are associated with greatly negative impacts on the quality of life of affected patients, as well as on costs of healthcare. Therefore, there is an urgent need to develop therapies for CLI that can effectively reduce the risk of amputation.

Therapeutic angiogenesis has recently been investigated as a means of treating various stages of PAD, including CLI. These therapies propose that the application of exogenous pro-angiogenic biochemical factors, such as vascular endothelial growth factor-A (VEGF-A), hepatocyte growth factor (HGF), and fibroblast growth factors (FGFs), can stimulate the growth of blood vessels in

ischemic tissue, thereby restoring blood flow and supporting the repair of chronically damaged skeletal muscle. However, despite promises derived from a variety of preclinical animal models, therapeutic angiogenesis has been met with limited success in clinical trials (Simons and Ware, 2003). Such clinical disappointment stresses on the requirement of a deeper understanding of the molecular and cellular mechanisms of blood vessel regeneration in ischemic tissue. In this regard, our group has demonstrated that, in a mouse model of CLI, ECs in ischemic skeletal muscle displayed a robust regenerative capacity to reconstitute a perfusable microvascular network in a tightly coordinated manner of skeletal muscle fiber reconstruction (Arpino et al., 2017a). Surprisingly, we observed intussusceptive angiogenesis as the major mode of blood vessel regrowth in ischemic muscle (Arpino, 2017b). The molecular cascades in ECs undergoing intussusception remain poorly characterized, largely attributed to lack of a proper *in vitro* cell model. In my thesis, I will present evidence for a first-in-kind EC culture model that recapitulates the early phase of intussusceptive angiogenesis.

1.2 Angiogenesis

1.2.1 Sprouting Angiogenesis

Sprouting angiogenesis is the most well-characterized form of new blood vessel growth in embryonic development, tumorigenesis, and regeneration of damaged adult tissue. This process is commonly triggered in tissue experiencing a certain level of hypoxia, or low oxygen content (Carmeliet, 2000). Parenchymal cells will begin to secrete a pro-angiogenic factor called vascular endothelial growth factor A (VEGF-A). VEGF-A binds to its cognate receptors on the surface of the EC membrane. The VEGF receptors are comprised of three family members: VEGFR1, 2 and 3, with VEGFR2 considered the major signal mediator to stimulate sprouting angiogenesis. VEGF-A-VEGFR2 binding causes the EC to secrete proteolytic enzymes to break down the extracellular matrix (ECM)

proteins and allow for this cell, now called the “tip cell”, to protrude into the surrounding tissue toward the source of VEGF-A, along an established VEGF-A gradient (Figure 1.1, Ribatti and Crivellato, 2012). Endothelial cells migrating into the surrounding tissue will then lumenize to create a blood vessel capable of receiving flow and successfully re-oxygenating the previously hypoxic tissue.

1.2.2 Intussusceptive Angiogenesis

Sprouting angiogenesis, while the most studied form of blood vessel growth, is not the only process of angiogenesis. Another, much less understood form of angiogenesis, is known as intussusceptive angiogenesis. During this process, pre-existing capillaries will enlarge and ECs primed to begin the process of angiogenesis will protrude into the lumen of the vessel rather than into the surrounding tissue (Djonov et al., 2000). This cell will reach for another EC on the opposite side of the vessel, fusing with this cell to form a bridge across a flowing vessel lumen termed an endothelial transluminal pillar (Figure 1.2). Multiple pillars then form down the length of this capillary, allowing fusion of neighbouring pillars to eventually create a wall that splits one large vessel into two smaller blood vessels.

The first studies to observe IA were in the developing rat lung microvasculature in 1986, followed by in the chick chorioallantoic membrane (CAM) in 1993. Caduff et al. (1986) identified small holes in the developing alveolar microvasculature by studying its casting using scanning electron microscopy, despite identifying no vessel sprouts to indicate sprouting angiogenesis. These “holes” were later proven to be pillars by Patan et al. (1993), who discovered the existence of transluminal EC bridges in a CAM model. To date, intussusceptive angiogenesis has been primarily identified during development of various tissues, including but not limited to the mammalian retina, ovary, kidney, as well as during tumour

Figure 1.1 Sprouting Angiogenesis

Sprouting angiogenesis is the best understood method of blood vessel growth. Central to this process is the secretion of VEGF-A by parenchymal cells that binds to and phosphorylates VEGFR2 on the surface of an endothelial cell lining a pre-existing vessel, now called a tip cell. This tip cell migrates into the surrounding tissue towards the hypoxic tissue, along a gradient of VEGF-A, and signals to its neighbouring stalk cells to proliferate and extend the length of the sprout.

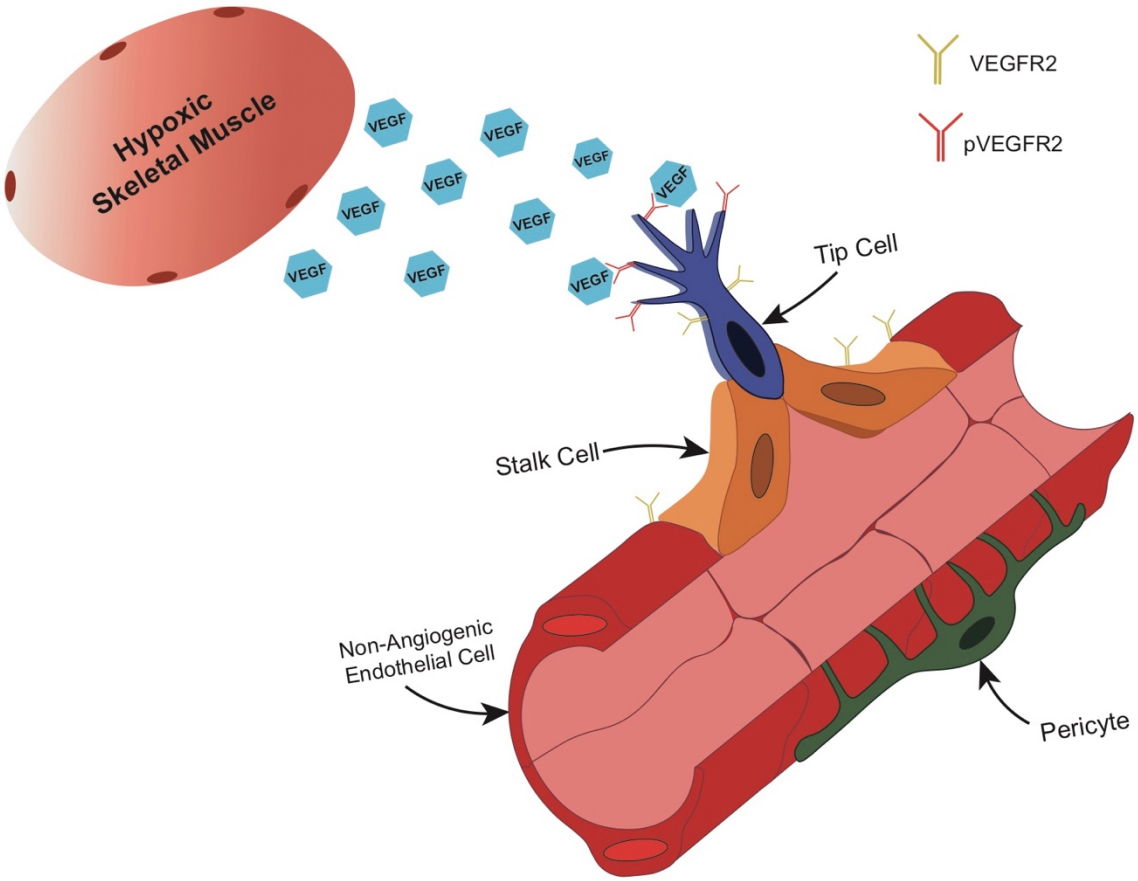
Hypoxic
Skeletal Muscle
VEGF
VEGFR2
pVEGFR2
Tip Cell
Stalk Cell
Non-Angiogenic
Endothelial Cell
Pericyte

Figure 1.2 Intussusceptive Angiogenesis

Intussusceptive angiogenesis is a poorly understood form of new blood vessel development from pre-existing blood vessels. In this method, an endothelial cell lining a pre-existing vessel will connect to ECs on the opposing side of the vessel lumen, forming an endothelial-based bridge known as an EC transluminal pillar. This pillar will extend down the long axis of the vessel, fusing with neighbouring pillars, to split one large blood vessel into two smaller daughter vessels.

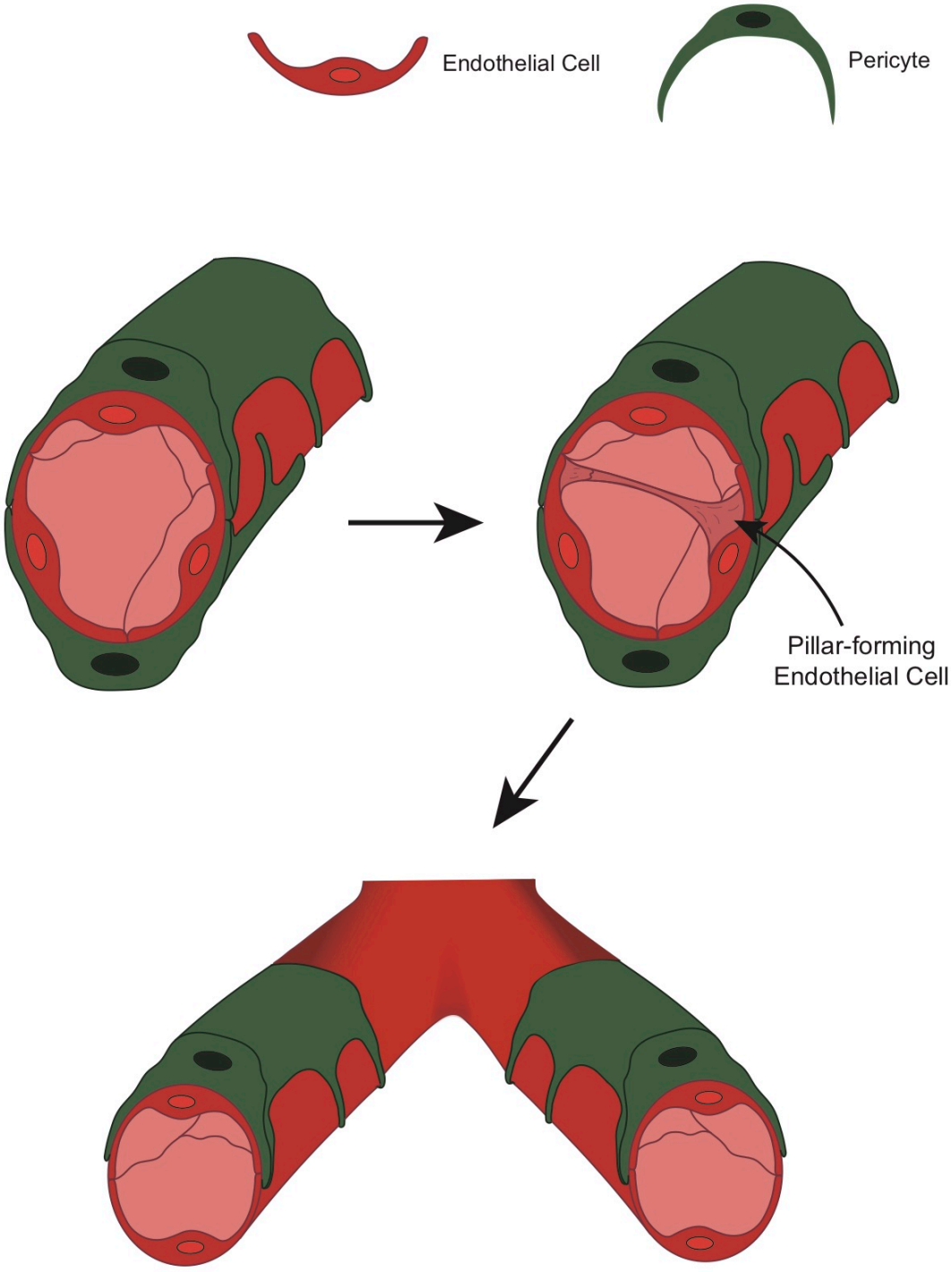
Endothelial Cell
Pericyte
Pillar-forming
Endothelial Cell

vascularization (Taylor et al., 2010; Macchiarelli et al., 2006; Makanya et al., 2005; Paku et al., 2011). Despite its identification in multiple human and animal tissues, the biochemical and molecular regulation of intussusceptive angiogenesis, specifically the formation of the transluminal pillar, remains under-studied and poorly understood.

1.2.3 Intussusceptive Angiogenesis in a Mouse Model of PAD

Recently, our research group has utilized a mouse model of PAD created by the excision of the hindlimb femoral artery to study regenerative angiogenesis in ischemic tissue, specifically skeletal muscle (Arpino et al., 2017a). Using this model, we have discovered a high incidence of enlarged capillaries which showed a high frequency of luminal EC protrusions akin to EC transluminal pillars (Arpino, 2017b). These results suggest regenerative angiogenesis in the ischemic hindlimb relies heavily on intussusceptive angiogenesis as opposed to sprouting angiogenesis. Moreover, the velocity of red blood cells (RBCs) in these primordial vessels was markedly slower than that seen in the microvascular network of healthy skeletal muscle. Whereas physiologic shear stress magnitudes range from 10 – 20 dynes/cm^2, in these vessels shear stress was an average of 0.08 dynes/cm^2. Characterization of VEGFR2 activation by immunostaining showed an overall decrease in phosphorylated VEGFR2 (pVEGFR2) within transluminal pillars. Moreover, the pVEGFR2 found within pillars was localized to the midsection. These findings suggest a potentially vital role for ultra-low flow as well as a reduction in VEGFR2 activity in the formation of transluminal pillars and subsequent progression of intussusceptive angiogenesis.

1.3 Endothelial Cell Flow Sensing

Healthy ECs are well-known for their ability to respond to changes in blood flow rate by sensing what is known as shear stress: the tangential force of the

blood flowing across the surface of the cell. Molecules and complexes activated both directly and indirectly by this force include, but are not limited to, receptor tyrosine kinases (RTKs), G-protein coupled receptors (GPCRs), ion channels, adhesion molecules, membrane microdomains, and transmembrane receptors (Figure 1.3; Ando and Yamamoto, 2013). Under normal physiologic flow, these molecules cause reorganization of the EC cytoskeleton, as well as cell-cell and cell-ECM interactions, to elongate cells in the direction of flow, redistribute focal adhesions via an increase in actin stress fibres, and suppress mitosis. Shear stress sensors, therefore, represent an important group of signalling molecules vital for vascular health and maintenance (Table 1.1).

1.3.1 Receptor Tyrosine Kinases

Receptor tyrosine kinases (RTKs) encompass a group of receptors located on the plasma membrane of various cell types. These receptors are activated by extracellular ligand-binding, which causes oligomerization of two or more receptors on the plasma membrane (Hubbard and Miller, 2007). This then leads to autophosphorylation of the tyrosine residues on the cytoplasmic domain. Sites of autophosphorylation can act as recruitment sites for signalling proteins that will activate a cascade of downstream signalling pathways. RTKs such as VEGFR2 and Tie-2 angiopoietin receptor are known to be important in shear stress sensing in vascular ECs.

VEGFR2, as previously noted, is a well-studied RTK whose ligand-dependent activation by VEGF is a key activator in the process of blood vessel growth known as sprouting angiogenesis. However, VEGFR2 can also be activated in a ligand-independent manner in response to shear stress. This RTK forms a mechanosensory complex with junctional proteins called platelet endothelial cell adhesion molecule-1 (PECAM-1 or CD31) and vascular endothelial cadherin (VE-Cadherin) located at the cell-cell junction (Baeyens et al., 2016). The activation and signal transduction pathway of this complex has

Figure 1.3 Endothelial Cell Mechanosensing

Endothelial cells are able to sense and respond to changes in blood flow via the tangential force created by the flowing blood across the surface of the cell, called shear stress. Molecules and complexes that are activated by shear stress, known as mechanosensors, include ion channels, GPCRs, RTKs, adhesion molecules, namely integrins, and membrane microdomains such as the glycocalyx and caveolae. An important shear stress sensor complex in endothelial cells consists of VEGFR2, PECAM-1, and VE-Cadherin, which is then linked to β-catenin.

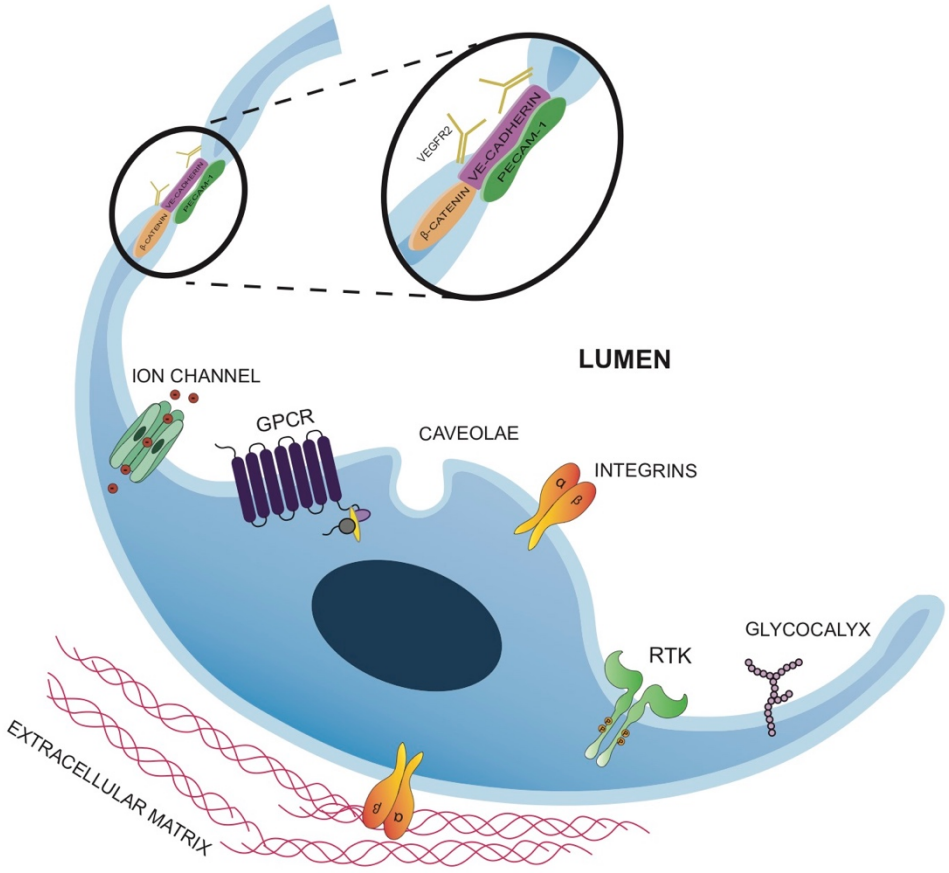
VEGFR2
VE-CADHERIN
PECAM-1
β-CATENIN
LUMEN
ION CHANNEL
GPCR
CAVEOLAE
INTEGRINS
RTK
GLYCOCALYX
EXTRACELLULAR MATRIX

Table 1.1 Endothelial Cell Shear Stress Sensors

Shear Stress Sensors		Function Under Shear Stress
Receptor Tyrosine Kinases (RTKs)	Vascular Endothelial Growth Factor Receptor 2 (VEGFR2)	Forms a complex with PECAM-1 and VE-Cadherin, and is phosphorylated independently of its ligand, activating PI(3)K.
	Tie2 Angipoietin Receptor	Phosphorylation is controlled by shear stress in a velocity-dependent manner, activating a PI(3)K/Akt signalling cascade.
G-protein Coupled Receptors (GPCRs)	G-protein Coupled Receptor 68 (GPR68)	Activation causes the release of calcium stores, opening Ca^{2+}- and K^{+}-gated channels and intiating NO synthesis.
Receptor Serine/Threonine Kinases (RSTKs)	Activin A Receptor-Like Kinase 1 (Alk1)	Forms a complex with endoglin, causing phosphorylation of SMAD proteins to regulate EC proliferation and migration.
Transmembrane Receptors	Notch1	Signals based on the magnitude of laminar shear stress to foster junctional integrity and elongation, and prevent mitosis.
Ion Channels	Piezo1	Opening of the channel due to shear stress causes an influx of Ca^{2+} into RBCs, causing ATP release and binding to ECs.
	P2X4	Activated via binding of ATP released by ECs in response to shear stress, allowing extracellular Ca^{2+} to enter the cell.
	Transient Receptor Potential Vanilloid 4 (TRPV4)	Shear stress causes an increase in surface expression of the Ca^{2+} channel, causing an increase in intracellular Ca^{2+}.
Adhesion Molecules	β1 Integrin	Senses unidirectional flow and transmits the tension to the cytoskeleton, causing increased Ca^{2+} via Piezo1 and TRPV4.
	αvβ3 Integrin	Increases affinity binding to the ECM due to shear stress, causing remodeling of focal adhesions via Rho activation.
	Platelet EC Adhesion Molecule-1 (PECAM-1)	Forms a complex with VEGFR2 and VE-Cadherin. Translates tension to cytoskeleton, triggering VEGFR2 phosphorylation.
	Vascular Endothelial Cadherin (VE-Cadherin)	Forms a complex with VEGFR2 and PECAM-1. Acts as an adaptor to form signaling complexes for PI(3)K activation.
Plasma Membrane Structures	Caveolae	Acts as a microdomain for various signaling molecules, rendering them inactive via binding in the absence of flow.
	Primary Cilia	Activated by bending of the cilium, activating KLF-2 either via cytoskeletal deformation or cation channel activation.
	Glycocalyx	Undergoes conformational changes that are transmitted to the cytoskeleton or transduced into biochemical signals.

*References can be found in Section 1.3 (pages 12-24).

been largely elucidated. Briefly, tension induced by shear stress causes the association of PECAM-1 with vimentin, an intermediate filament protein found in the cytoskeleton. This association then transfers the tension from the myosin within the cytoskeleton to PECAM-1, triggering activation of a Src-family kinase responsible for transphosphorylation of VEGFR2. VE-Cadherin plays the role of an adaptor within this mechanosensory complex along with its binding partner β-catenin, associating with VEGFR2 on the plasma membrane to facilitate its activation (Conway et al., 2013). Activated VEGFR2 will then bind phophoinositide 3-kinase (PI(3)K) and trigger a downstream signalling cascade involving protein kinase B (Akt) and endothelial nitric oxide synthase (eNOS; Jin et al., 2003). Ultimately, this signalling cascade leads to production of nitric oxide (NO), which modulates vascular tone, suppresses cell proliferation, and inhibits nuclear factor kappa B (NF-κB), thereby decreasing EC expression of adhesion molecules (Tousoulis et al., 2012).

Another RTK known to be responsible for shear stress sensing is the Tie-2 angiopoietin receptor. While less is known about the activation of the Tie2 receptor compared to VEGFR2, it is known that Tie-2 is autophosphorylated in a ligand-dependent manner via binding of angiopoietin 1 (Ang1). Its activation is more sustained than that of VEGFR2 and is also velocity-dependent, meaning activation increases as shear stress increases (Lee and Koh, 2003). Phosphorylation of Tie-2 activates a similar PI(3)K/Akt pathway to VEGFR2 phosphorylation and ultimately aids in EC survival and maintained cell integrity.

1.3.2 Receptor Serine/Threonine Kinases

Receptor serine/threonine kinases (RSTKs) are transmembrane receptors that function in a similar manner to RTKs. RSTKs can be classified as either type I receptors or type II receptors depending on their role in signal transduction (Piek et al., 1999). Briefly, following binding of a ligand to its corresponding RSTK, a heterodimer of type I and type II receptors will form on the plasma

membrane. The proximity of these receptors will allow the type II RSTK to phosphorylate specific serine and threonine residues located on the intracellular domain of the type I RSTK, thereby activating this receptor and allowing downstream signalling. A well-known pathway controlled by RSTK signalling is the transforming growth factor-β (TGF-β) pathway.

Recently, the role of one RSTK called activin A receptor-like kinase 1 (Alk1) in shear stress sensing has been uncovered. Baeyens et al. (2016) have hypothesized that shear stress causes endoglin, a membrane glycoprotein, to associate with Alk1 on the plasma membrane, resulting in an increase in the sensitivity of Alk1 to one of its ligands, bone morphogenic proteins 9 (BMP9). Ligand binding results in phosphorylation of SMAD1, SMAD5, and SMAD8, which will then translocate into the nucleus to act as a transcription factor (Franco and Gerhardt, 2016). The activation of this Alk1/endoglin pathway has proven to be important in regulating EC proliferation under flow. Importantly, Alk5 has been shown to be crucial for Alk1 activation by mediating its recruitment into a TGF-β receptor complex, allowing for this shear stress-induced signalling pathway to progress (Goumans et al., 2003).

1.3.3 G-Protein Coupled Receptors

G-protein coupled receptors (GPCRs) are seven-transmembrane domain receptors located on the plasma membrane responsible for transmitting extracellular signals into the cell using guanosine triphosphate (GTP), a common source of energy (Wettschureck and Offermanns, 2005). Extracellular ligand binding to a GPCR causes a conformational change in the protein that results in coupling of the receptor to a heterotrimeric G protein composed of α-, β-, and γ-subunits. This drives the exchange of guanosine diphosphate (GDP) to GTP on the α-subunit, which then dissociates from the plasma membrane G protein complex and goes on to modulate the activity of downstream signalling

molecules. While many GPCRs have been implicated in shear stress sensing, few have been proven to be essential for mechanosensing (Scholz et al., 2016).

GPR68 is a class A rhodopsin-like GPCR that has recently been shown to be activated in response to both laminar and disturbed flow (Xu et al., 2018). Unlike other GPCRs studied, this receptor has been proven to be expressed on the surface of ECs, and necessary for sensing flow. Due to its classification and its coupled G-protein complex, it is suspected that activation of GPR68 causes cleavage of phosphatidylinositol 4,5-bisphosphate (PIP_2) into inositol triphosphate (IP_3) and diacylglycerol (DAG), ultimately leading to the release of Ca^{2+} from intracellular stores. This likely leads to the synthesis of NO, among other effects, in order to regulate vascular tone.

1.3.4 Notch1

Notch1 is a single-pass transmembrane protein that has been suggested to act as a shear stress sensor. This receptor plays an important role in sprouting angiogenesis by regulating tip cell selection, among its other crucial roles (Ribatti and Crivellato, 2012). However, it has also been shown to be activated specifically by laminar shear stress in the adult vasculature (Mack et al., 2017). In this case, Notch1 is responsible for maintaining junctional integrity, encouraging EC elongation in the direction of flow, and suppressing cell proliferation, most likely by regulating intracellular Ca^{2+} concentrations.

1.3.5 Ion Channels

Ion channels are membrane proteins that form pores within the plasma membrane that allow the passage of specific charged ions through the membrane into and out of the cell. Many of these channels are gated, requiring a chemical signal or mechanical force to open and allow the passage of ions. Channels such as Piezo1, P2X4, and transient receptor potential vanilloid 4 (TRPV4) have been shown to activate in response to shear stress, changing mainly Ca^{2+} concentration within the cell.

Piezo1 is a mechanically activated cation channel expressed on the surface of ECs, as well as mature RBCs and neuronal stem cells. Recently, Piezo1 has been studied in-depth in RBCs and has been shown to be activated by shear stress (Cinar et al., 2015). This causes an influx of Ca^{2+} into the cells, thereby causing a release of adenosine triphosphate (ATP) from the RBCs. ATP can then bind to signalling molecules on the surface of vascular ECs, such as GPCRs, to induce synthesis and release of NO. The exact mechanism of ATP release from RBCs has not yet been elucidated. However, two pathways of activation have been suggested: 1) the influx of Ca^{2+} activates pannexin-1 channels, triggering ATP release from pools associated with the RBC membrane, or 2) this influx depolymerizes actin filaments, leading to activation of cystic fibrosis transmembrane conductance regulator (CFTR), a membrane chloride channel, and subsequent release of ATP (Cinar et al., 2015). The indirect effect of RBC-expressed Piezo1 on EC shear stress sensing could elucidate to a more direct role of EC shear stress sensing.

P2X4 is an ATP-gated ion channel highly expressed on the plasma membrane of vascular ECs. Laminar shear stress causes the release of ATP from ECs, which then binds to P2X4 to induce an influx of Ca^{2+} into the cell in a force-dependent manner (Ando and Yamamoto, 2013). Studies have suggested that this causes the ATP-induced expression of Krüppel-like factor 2 (KLF2), Krüppel-like factor 4 (KLF4), and eNOS (Sathanoori et al., 2015). KLF2 and KLF4 are well-understood to be upregulated in ECs due to laminar shear stress, imparting an atheroprotective phenotype and activating eNOS to control vascular tone. Therefore, the indirect activation of P2X4 due to shear stress is important for vascular health and EC survival under flow.

TRPV4 is another ion channel recently shown to be activated by shear stress. TRPV4 is a non-selective cation channel expressed in multiple different tissues, including the brain, cardiovascular system, liver, lung, and kidneys,

among others. In the vasculature, TRPV4 has been shown to regulate vascular tone (Ando and Yamamoto, 2013). This channel is activated by osmotic, chemical, and mechanical cues, notably shear stress. Shear stress causes an influx of Ca^{2+} through TRPV4 activation and, interestingly, recruitment of additional TRPV4 to the cell membrane, creating a potentiating response which enhances TRPV4 responsiveness to this mechanical force.

1.3.6 Endothelial Cell Adhesion Molecules

Adhesion molecules encompass a wide range of molecules, most of which are transmembrane proteins, that are responsible for facilitating interactions between cells, and between cells and the ECM. These molecules can be divided into five families: immunoglobulin-like adhesion molecules, integrins, cadherins, selectins, and the CD44 family (Murray et al., 1999). Adhesion molecules play an important role in translating the tension placed on the cell produced by shear stress into a biochemical response within the cell.

As previously mentioned, PECAM-1 and VE-Cadherin are parts of a well-studied, vital mechanosensory complex along with VEGFR2 found at the junctional border between cells. Integrins, however, also represent a category of adhesion molecules that have been widely implicated in the translation of shear stress tension to the cell. β1 integrin plays an adhesion role by anchoring the cell via actin filaments in the cytoplasm to the ECM on the basal surface. In this case, unidirectional and bidirectional flow cause both an increase and clustering of β1 integrin, allowing for the development of focal adhesions that develop within the cell as F-actin stress fibres (Ando and Yamamoto, 2013). This allows for alignment in the direction of flow.

Recently, β1 integrin has also been found on the apical surface of ECs and is hypothesized to act in a manner independent of β1 integrin located on the basal surface to respond to only unidirectional flow (Xanthis et al., 2019). Shear

stress tension placed on these apical pools of β1 integrin causes a change in its conformation in order to translate the force into downstream signalling, including the accumulation of Ca^{2+} via activation of Piezo1 and TRPV4. This, in turn, enhances EC alignment with the direction of unidirectional flow specifically.

Another integrin considered to act as an important shear stress sensor is αvβ3 integrin. Similar to β1 integrin, shear stress causes a conformational change in αvβ3 integrin that increases its binding affinity to its corresponding ECM component vitronectin (Shyy and Chien, 2002). This increased binding and subsequent aggregation of αvβ3 integrin proteins causes the adaptor molecules Shc and focal adhesion kinase (FAK) to associate with integrins on the membrane and become tyrosine phosphorylated. Shc association then activates the extracellular receptor kinase (ERK) pathway. Integrins including αvβ3 are also thought to regulate RhoA activation, leading to actin stress fibre formation under shear stress (Tzima et al., 2001).

1.3.7 Plasma Membrane Structures

The plasma membrane has many structures that are crucial to cell signalling, cell adhesion, and cell trafficking. These structures include glycocalyx, lipid rafts, caveolae, primary cilia, and others, alongside the previously discussed ion channels and signalling receptors. Caveolae, primary cilia, and glycocalyx specifically have been outlined in the literature as important for shear stress sensing and the subsequent translation of this force into biochemical signals.

Caveolae are plasma membrane invaginations similar to lipid rafts in that they are rich in cholesterol and sphingolipids compared to the rest of the plasma membrane (Shaul and Anderson, 1998). Unlike lipid rafts, these structures are also rich in a protein called calveolin-1. Their primary role in most cell types is the organization and accumulation of various signalling molecules including signalling receptors, ion channels, and intracellular membrane-associated

signalling molecules. In ECs, caveolae have been implicated in shear stress sensing by mediating the activation of the ERK pathway through the association of calveolin-1 with upstream signalling molecules located on the plasma membrane, such as integrins, G proteins, and GPCRs (Park et al., 2000).

Primary cilia are extracellular rod-like structures that protrude from the plasma membrane of cells. These structures are composed of doublets of microtubules connected to a microtubule organizing centre. Though the exact mechanism of shear stress sensing via primary cilia is unknown, two methods of mechanosensing have been hypothesized (Ando and Yamamoto, 2013). First, shear stress could cause bending of the cilia that translates to the cell via cytoskeletal deformation. Second, bending of the cilia due to shear stress causes the activation of ion channels that leads to an influx of Ca^{2+}–this results in NO production and a change in vascular tone. The presence of primary cilia regardless of activation method has been shown to cause an increase in KLF2 expression, a known marker of EC shear stress response.

The glycocalyx encompasses a carbohydrate-rich extracellular coating that lines the vascular endothelium on the luminal surface. The glycocalyx layer responds to shear stress in a similar fashion to integrins via conformational change that is translated into an intracellular signal through the cytoskeleton (Tarbell and Pahakis, 2006). This conformation change also translates into biochemical signals indirectly by changing various concentration gradients and a change in the regulation of ions, amino acids, and growth factors moving through the membrane. Both of these methods of signal transduction result in increased production of NO.

1.4 Tools for Studying Endothelial Cell Flow Response

Endothelial cells have a wide range of shear stress sensors that range from adhesion molecules to transmembrane receptors, each of which activates signalling pathways that lend information to the cell about the magnitude of the

force, the direction of the flow, and the type of flow, whether pulsatile or laminar. While the responses of ECs to physiologic flow rates have been studied extensively, responses to ultra-low shear stress levels, such as the 0.08 dynes/cm^2 shear stress magnitude characterized by our research group in our ischemic mouse model, remain unknown. Furthermore, examining the relationship between this ultra-low shear stress and the high incidence of transluminal pillar formation seen in this model could lead to a better understanding of the process of intussusceptive angiogenesis and its role in regenerating ischemic tissue.

The importance of EC mechanosensing in maintaining the health and integrity of tissues and their corresponding vasculature throughout the body cannot be underestimated. Therefore, the study of changes in EC behaviour under high flow and high shear stress has been a major focus in vascular biology using tools such as parallel plate flow systems and lab-on-a-chip devices (Coon et al., 2015; Shih et al., 2019). However, experiments studying both smaller order blood vessels and ultra-low flow rates are lacking. Moreover, the current strategies for addressing EC flow are largely 2D, not 3D. Therefore, the shape and configuration of these flow chambers do not closely mimic the physiology seen in the vasculature *in vivo*. Critical information concerning EC morphology, and 3D interactions and signalling remains elusive using current methods.

1.4.1 Microfluidics

Microfluidics is a recently emerging field that uses networks of channels within the micrometer range to manipulate and control fluid flow. These devices generally consist of an inlet leading into a single or branched channel, which then leads to an outlet. The inlet and outlet allow for the attachment of tubing that will directly connect a fluid source to the microfluidic channel. However, the design of the channel itself is readily customizable, allowing for varying channel heights, widths, and lengths that coordinate with specific study aims, as well as control of

flow rate. One important use of microfluidic devices seen in the literature is as cell culture systems, wherein the walls of these channels can be used as a surface on which to grow a wide range of cell types (Mannino et al., 2018; Osaki et al., 2018). Microfluidic systems could therefore allow for the development of a 3D cell culture system capable of mimicking the structure of the microvasculature more closely, along with the study of lower flow rates than have been previously tested. The overarching principle of my thesis is that microfluidic systems present a unique, novel opportunity to study and characterize EC morphologic and biochemical responses to ultra-low flow in 3D.

While the field of microfluidics and its subjects of study have diversified as the field has expanded, the materials used largely remain consistent. Microfluidics emerged and popularized in the 1970s with the use of silicon and glass, mainly for the sake of convenience. However, silicone is opaque and therefore not compatible with most microscopy techniques. Glass, while more commonly used, required expensive and sometimes complicated techniques to bond to silicone and create closed channels (Sackmann et al., 2014). These problems were solved in the 1980s with the introduction of polydimethylsiloxane (PDMS), a material used widely in current microfluidics research, and led to the development of soft lithography, a common microfluidic device fabrication technique. PDMS has many advantages, including: 1) its gas-permeability, 2) malleability, 3) it is inexpensive to use and easy to work with, 4) PDMS can easily bond with itself, as well as made to bond other materials such as glass using surface treatments, and 5) its hydrophobic surface can be tuned to be more hydrophilic to allow the attachment and growth of various cell types (Sackmann et al., 2014). The transition into using PDMS as the main structural component of microfluidic device fabrication has allowed the size, shape, arrangement, and use of microfluidics to broaden significantly.

As described above, the wide range of sizes, shapes, and arrangement of channels in microfluidics has broadened immensely and remains one of the main strengths of the field. Using PDMS and soft lithography in microfluidic fabrication allows channels to become highly customizable and tuned to the nature of the study. In EC studies specifically, many investigators focus on branched-channel designs that somewhat mimic the structure of the vasculature (Myers et al., 2012; Lee et al., 2018). However, as use of microfluidics has increased, more complicated channel designs have been introduced, including those connected to a reservoir or chamber, channels sprouting from the main channel, and more. Even when single straight channels are used, the size of the channels vary greatly from study to study. Many research groups focus mainly on the height of the device, which can range from 30 μm – 500 μm depending on the type of cell or vessel they intend to study (Esch et al., 2011; Bischel et al., 2013). However, when working with such small heights, the width of the channels tend to be relatively large, helping to offset any pressure that would be introduced by high flow rates in such a small channel. For example, Sakurai et al. (2018) used a microfluidic device 50 μm in height and 150 μm in width to create a vascularized bleeding model. Studies using channels with an equal height and width below 150 μm, while physiologically closer to what is seen *in vivo*, are rarely seen–even more so when using a single channel geometry.

Finally, microfluidics also allows fine-tuned control and variation of flow rate and shear stress, which can be modified to fit the cell or organ type being studied. Focusing on microfluidic studies concerning the vascular cell types, the majority of studies focus on high flow rates seen in healthy vessels. Microvascular studies mainly use shear stress levels around 10 dynes/cm^2, corresponding to the shear stress seen within capillaries (van der Meer et al., 2010; Regmi et al., 2017). Studies that do look at the effects of low shear stress do so in the context of atherosclerosis or wound healing. Moreover, many studies consider low shear stress to be on the order of 2–4 dynes/cm^2 (Khan and Sefton,

2011). Therefore, while a high shear stress environment has been consistently studied, the effects of low shear stress, and particularly ultra-low shear stress, remain largely untouched by research groups.

1.5 Aims of the Thesis

The rationale for my thesis is that there is a lack of knowledge concerning EC morphologic and biochemical responses to ultra-low flow rates, conditions that exist in disease and regeneration. In addition, there is no existing *in vitro* model for transluminal pillar formation, a phenomenon that can occur within ultra-low flow.

To address this, the overarching goals of my research were: 1) to develop an *in vitro* model of early forming, primordial blood vessels using 3D microfluidics and ultra-low flow (Chapter 2); 2) to determine if transluminal endothelial pillars will form in the microfluidic model (Chapter 2); 3) to determine the expression and localization of select shear stress sensors in endothelial cells subjected to ultra-low flow and pillar-forming conditions (Chapter 2); and 4) to determine the role of VEGFR2 in endothelial transluminal pillar formation, *in vitro* (Chapter 3).

1.6 References

Ando, J., and Yamamoto, K. 2013. Flow detection and calcium signalling in vascular endothelial cells. Cardiovasc Res *99*, 260-268.

Annex, B.H. (2013). Therapeutic angiogenesis for critical limb ischaemia. Nat Rev Cardiol *10*, 387-396.

Arpino, G.M. (2017b). Angiogenesis And Neo-Microcirculatory Function In Diseased Tissue Revealed By Intravital Microscopy. Electronic Thesis and Dissertation Repository, 4731.

Arpino, J.M., Nong, Z., Li, F., Yin, H., Ghonaim, N., Milkovich, S., Balint, B., O'Neil, C., Fraser, G.M., Goldman, D.*, et al.* (2017a). Four-Dimensional Microvascular Analysis Reveals That Regenerative Angiogenesis in

Ischemic Muscle Produces a Flawed Microcirculation. Circ Res *120*, 1453-1465.

Baeyens, N., Bandyopadhyay, C., Coon, B.G., Yun, S., and Schwartz, M.A. (2016a). Endothelial fluid shear stress sensing in vascular health and disease. J Clin Invest *126*, 821-828.

Baeyens, N., Larrivée, B., Ola, R., Hayward-Piatkowskyi, B., Dubrac, A., Huang, B., Ross, T.D., Coon, B.G., Min, E., Tsarfati, M.*, et al.* (2016b). Defective fluid shear stress mechanotransduction mediates hereditary hemorrhagic telangiectasia. J Cell Biol *214*, 807-816.

Benjamin, E.J., Virani, S.S., Callaway, C.W., Chamberlain, A.M., Chang, A.R., Cheng, S., Chiuve, S.E., Cushman, M., Delling, F.N., Deo, R.*, et al.* (2018). Heart Disease and Stroke Statistics-2018 Update: A Report From the American Heart Association. Circulation *137*, e67-e492.

Bischel, L.L., Young, E.W., Mader, B.R., and Beebe, D.J. (2013). Tubeless microfluidic angiogenesis assay with three-dimensional endothelial-lined microvessels. Biomaterials *34*, 1471-1477.

Caduff, J.H., Fischer, L.C., and Burri, P.H. (1986). Scanning electron microscope study of the developing microvasculature in the postnatal rat lung. Anat Rec *216*, 154-164.

Carmeliet, P. (2000). Mechanisms of angiogenesis and arteriogenesis. Nat Med *6*, 389-395.

Chung, J., Modrall, J.G., Ahn, C., Lavery, L.A., and Valentine, R.J. (2015). Multidisciplinary care improves amputation-free survival in patients with chronic critical limb ischemia. J Vasc Surg *61*, 162-169.

Cinar, E., Zhou, S., DeCourcey, J., Wang, Y., Waugh, R.E., and Wan, J. (2015). Piezo1 regulates mechanotransductive release of ATP from human RBCs. Proc Natl Acad Sci U S A *112*, 11783-11788.

Conway, D.E., Breckenridge, M.T., Hinde, E., Gratton, E., Chen, C.S., and Schwartz, M.A. (2013). Fluid shear stress on endothelial cells modulates

mechanical tension across VE-cadherin and PECAM-1. Curr Biol *23*, 1024-1030.

Coon, B.G., Baeyens, N., Han, J., Budatha, M., Ross, T.D., Fang, J.S., Yun, S., Thomas, J.L., and Schwartz, M.A. (2015). Intramembrane binding of VE-cadherin to VEGFR2 and VEGFR3 assembles the endothelial mechanosensory complex. J Cell Biol *208*, 975-986.

Djonov, V., Schmid, M., Tschanz, S.A., and Burri, P.H. (2000). Intussusceptive angiogenesis: its role in embryonic vascular network formation. Circ Res *86*, 286-292.

Esch, M.B., Post, D.J., Shuler, M.L., and Stokol, T. (2011). Characterization of in vitro endothelial linings grown within microfluidic channels. Tissue Eng Part A *17*, 2965-2971.

Franco, C.A., and Gerhardt, H. (2016). Blood flow boosts BMP signaling to keep vessels in shape. J Cell Biol *214*, 793-795.

Goumans, M.J., Valdimarsdottir, G., Itoh, S., Lebrin, F., Larsson, J., Mummery, C., Karlsson, S., and ten Dijke, P. (2003). Activin receptor-like kinase (ALK)1 is an antagonistic mediator of lateral TGFbeta/ALK5 signaling. Mol Cell *12*, 817-828.

Hubbard, S.R., and Miller, W.T. (2007). Receptor tyrosine kinases: mechanisms of activation and signaling. Curr Opin Cell Biol *19*, 117-123.

Inampudi, C., Akintoye, E., Ando, T., and Briasoulis, A. (2018). Angiogenesis in peripheral arterial disease. Curr Opin Pharmacol *39*, 60-67.

Jin, Z.G., Ueba, H., Tanimoto, T., Lungu, A.O., Frame, M.D., and Berk, B.C. (2003). Ligand-independent activation of vascular endothelial growth factor receptor 2 by fluid shear stress regulates activation of endothelial nitric oxide synthase. Circ Res *93*, 354-363.

Khan, O.F., and Sefton, M.V. (2011). Endothelial cell behaviour within a microfluidic mimic of the flow channels of a modular tissue engineered construct. Biomed Microdevices *13*, 69-87.

Kinlay, S. (2016). Management of Critical Limb Ischemia. Circ Cardiovasc Interv *9*, e001946.

Lee, H.J., and Koh, G.Y. (2003). Shear stress activates Tie2 receptor tyrosine kinase in human endothelial cells. Biochem Biophys Res Commun *304*, 399-404.

Lee, J., Estlack, Z., Somaweera, H., Wang, X., Lacerda, C.M.R., and Kim, J. (2018). A microfluidic cardiac flow profile generator for studying the effect of shear stress on valvular endothelial cells. Lab Chip *18*, 2946-2954.

Macchiarelli, G., Jiang, J.Y., Nottola, S.A., and Sato, E. (2006). Morphological patterns of angiogenesis in ovarian follicle capillary networks. A scanning electron microscopy study of corrosion cast. Microsc Res Tech *69*, 459-468.

Mack, J.J., Mosqueiro, T.S., Archer, B.J., Jones, W.M., Sunshine, H., Faas, G.C., Briot, A., Aragón, R.L., Su, T., Romay, M.C.*, et al.* (2017). NOTCH1 is a mechanosensor in adult arteries. Nat Commun *8*, 1620.

Makanya, A.N., Stauffer, D., Ribatti, D., Burri, P.H., and Djonov, V. (2005). Microvascular growth, development, and remodeling in the embryonic avian kidney: the interplay between sprouting and intussusceptive angiogenic mechanisms. Microsc Res Tech *66*, 275-288.

Mannino, R.G., Pandian, N.K., Jain, A., and Lam, W.A. (2018). Engineering "Endothelialized" Microfluidics for Investigating Vascular and Hematologic Processes Using Non-Traditional Fabrication Techniques. Curr Opin Biomed Eng *5*, 13-20.

Murray, P., Frampton, G., and Nelson, P.N. (1999). Cell adhesion molecules. Sticky moments in the clinic. BMJ *319*, 332-334.

Myers, D.R., Sakurai, Y., Tran, R., Ahn, B., Hardy, E.T., Mannino, R., Kita, A., Tsai, M., and Lam, W.A. (2012). Endothelialized microfluidics for studying microvascular interactions in hematologic diseases. J Vis Exp *64*, e3958.

Osaki, T., Sivathanu, V., and Kamm, R.D. (2018). Engineered 3D vascular and

neuronal networks in a microfluidic platform. Sci Rep *8*, 5168.

Paku, S., Dezso, K., Bugyik, E., Tóvári, J., Tímár, J., Nagy, P., Laszlo, V., Klepetko, W., and Döme, B. (2011). A new mechanism for pillar formation during tumor-induced intussusceptive angiogenesis: inverse sprouting. Am J Pathol *179*, 1573-1585.

Park, H., Go, Y.M., Darji, R., Choi, J.W., Lisanti, M.P., Maland, M.C., and Jo, H. (2000). Caveolin-1 regulates shear stress-dependent activation of extracellular signal-regulated kinase. Am J Physiol Heart Circ Physiol *278*, H1285-1293.

Patan, S., Haenni, B., and Burri, P.H. (1993). Evidence for intussusceptive capillary growth in the chicken chorio-allantoic membrane (CAM). Anat Embryol (Berl) *187*, 121-130.

Piek, E., Heldin, C.H., and Ten Dijke, P. (1999). Specificity, diversity, and regulation in TGF-beta superfamily signaling. FASEB J *13*, 2105-2124.

Regmi, S., Fu, A., and Luo, K.Q. (2017). High shear stresses under exercise condition destroy circulating tumor cells in a microfluidic system. Sci Rep *7*, 39975.

Ribatti, D., and Crivellato, E. (2012). "Sprouting angiogenesis", a reappraisal. Dev Biol *372*, 157-165.

role of microfluidics in biomedical research. Nature *507*, 181-189.

Sackmann, E.K., Fulton, A.L., and Beebe, D.J. (2014). The present and future

Sakurai, Y., Hardy, E.T., Ahn, B., Tran, R., Fay, M.E., Cicliano, J.C., Mannino, R.G., Myers, D.R., Qui, Y., Carden, M.A., *et al*. (2018). A microengineered vascularized bleeding model that integrates the principal components of hemostasis. Nat Commun *9*, 509.

Sathanoori, R., Rosi, F., Gu, B.J., Wiley, J.S., Müller, C.E., Olde, B., and Erlinge, D. (2015). Shear stress modulates endothelial KLF2 through activation of P2X4. Purinergic Signal *11*, 139-153.

Scholz, N., Monk, K.R., Kittel, R.J., and Langenhan, T. (2016). Adhesion GPCRs

as a Putative Class of Metabotropic Mechanosensors. Handb Exp Pharmacol *234*, 221-247.

Shaul, P.W., and Anderson, R.G. (1998). Role of plasmalemmal caveolae in signal transduction. Am J Physiol *275*, L843-851.

Shih, H.C., Lee, T.A., Wu, H.M., Ko, P.L., Liao, W.H., and Tung, Y.C. (2019). Microfluidic Collective Cell Migration Assay for Study of Endothelial Cell Proliferation and Migration under Combinations of Oxygen Gradients, Tensions, and Drug Treatments. Sci Rep *9*, 8234.

Shyy, J.Y., and Chien, S. (2002). Role of integrins in endothelial mechanosensing of shear stress. Circ Res *91*, 769-775.

Simons, M., and Ware, J.A. (2003). Therapeutic angiogenesis in cardiovascular disease. Nat Rev Drug Discov *2*, 863-871.

Tarbell, J.M., and Pahakis, M.Y. (2006). Mechanotransduction and the glycocalyx. J Intern Med *259*, 339-350.

Taylor, A.C., Seltz, L.M., Yates, P.A., and Peirce, S.M. (2010). Chronic whole-body hypoxia induces intussusceptive angiogenesis and microvascular remodeling in the mouse retina. Microvasc Res *79*, 93-101.

Tousoulis, D., Kampoli, A.M., Tentolouris, C., Papageorgiou, N., and Stefanadis, C. (2012). The role of nitric oxide on endothelial function. Curr Vasc Pharmacol *10*, 4-18.

Tzima, E., del Pozo, M.A., Shattil, S.J., Chien, S., and Schwartz, M.A. (2001). Activation of integrins in endothelial cells by fluid shear stress mediates Rho-dependent cytoskeletal alignment. EMBO J *20*, 4639-4647.

Uccioli, L., Meloni, M., Izzo, V., Giurato, L., Merolla, S., and Gandini, R. (2018). Critical limb ischemia: current challenges and future prospects. Vasc Health Risk Manag *14*, 63-74.

van der Meer, A.D., Poot, A.A., Feijen, J., and Vermes, I. (2010). Analyzing shear stress-induced alignment of actin filaments in endothelial cells with a microfluidic assay. Biomicrofluidics *4*, 11103.

Wettschureck, N., and Offermanns, S. (2005). Mammalian G proteins and their cell type specific functions. Physiol Rev *85*, 1159-1204.

Xanthis, I., Souilhol, C., Serbanovic-Canic, J., Roddie, H., Kalli, A.C., Fragiadaki, M., Wong, R., Shah, D.R., Askari, J.A., Canham, L.*, et al.* (2019). β1 integrin is a sensor of blood flow direction. J Cell Sci *132*.

Xu, J., Mathur, J., Vessières, E., Hammack, S., Nonomura, K., Favre, J., Grimaud, L., Petrus, M., Francisco, A., Li, J.*, et al.* (2018). GPR68 Senses Flow and Is Essential for Vascular Physiology. Cell *173*, 762-775.e716.

Yusuf, S., Reddy, S., Ounpuu, S., and Anand, S. (2001). Global burden of cardiovascular diseases: part I: general considerations, the epidemiologic transition, risk factors, and impact of urbanization. Circulation *104*, 2746-2753.

CHAPTER 2:
A NOVEL 3D MICROVESSEL MODEL FOR THE STUDY OF ENDOTHELIAL CELL TRANSLUMINAL PILLAR FORMATION

2.1 Introduction

Critical limb ischemia (CLI) is the most severe form of peripheral arterial disease (PAD) characterized by a marked and irreversible reduction in blood supply to the affected lower limb. This reduction in blood supply leads to a decrease in oxygen diffusion to the skeletal muscle within the leg causing pain in the leg at rest and non-healing ulcers, and resulting in ischemic injury (Varu, 2010). There has been considerable interest in therapies for CLI that centre around strategies to encourage new blood vessel formation in a process called therapeutic angiogenesis in order to reperfuse the damaged skeletal muscle. However, these methods have shown little clinical success in translating into long term benefits for the patient (Inampudi et al., 2018). Therefore, there may be a critical lack of knowledge surrounding blood vessel growth in an ischemic setting.

The growth of new blood vessels in an existing microvascular network is best understood to occur via sprouting angiogenesis. In this process, endothelial cells (ECs) lining the lumen of an existing blood vessel will be stimulated by nearby low-oxygen conditions to migrate into the surrounding tissue. From there, these cells will lumenize to allow blood flow within this new vessel, which will then help with reperfusion of the previously hypoxic tissue (Carmeliet, 2000). However, there is another form of blood vessel growth that is understudied called intussusceptive angiogenesis. In this case, ECs lining the vessel will protrude into the blood-perfused lumen to create a structure known as a transluminal pillar (Djonov et al., 2000). Multiple EC pillars will then form along the length of the

vessel and fuse with neighbouring pillars to create a wall down the length of the vessel, splitting one large capillary into two smaller daughter capillaries (Mentzer and Konerding, 2014). While this phenomenon has been previously reported in a number of different tissues, including the mammalian retina, kidney, lung and tumour (Taylor et al., 2010; Hlushchuk et al., 2017; Hlushchuk, et al., 2008), little is known about the biochemical and mechanical regulation of intussusceptive angiogenesis.

Our research group has recently uncovered novel information on intussusceptive angiogenesis in ischemic skeletal muscle (Arpino, 2017b). We utilized a mouse model of PAD with the excision of the hindlimb femoral artery to characterize regenerative angiogenesis in ischemic skeletal muscle and discovered a high incidence of transluminal EC pillars within the early stages of microvascular regeneration. This finding suggests that regeneration of the microvasculature within the ischemic hindlimb skeletal muscle may be largely dependent on intussusceptive angiogenesis. Furthermore, we observed that pillar-bearing vessels exhibited a drastic decrease in blood flow and shear stress compared with normal capillaries. Endothelial cells possess the unique ability to sense and respond to changes in the mechanical force caused by flowing blood, known as shear stress, using a variety of shear stress sensors (Ando and Yamamoto, 2013). Our findings could therefore suggest that a decrease in shear stress within a given vessel could be necessary for blood vessel growth via the process of intussusceptive angiogenesis.

However, *ex vivo* models for studying EC transluminal pillar formation and its relationship to shear stress are not available. There are several *ex vivo* models to study fluid shear stress, most commonly parallel plate flow systems, and lab-on-a-chip devices, wherein cells are grown on the surface of a microchannel physiologically similar in size to microvessels, but studied largely using only the bottom surface of the channel (Wong et al., 2017; Varma and

Voldman, 2015). These designs are therefore 2D and consequently lack the 3D geometry needed for pillar formation. Therefore, development of a novel 3D system to study endothelial responses to shear stress is required to directly study this EC phenomenon.

Herein, we report the development of a novel 3D *in vitro* microvessel model using microfluidics capable of creating EC transluminal pillars and enabling the study of mechanisms of pillar formation. We report an increase in pillar formation under ultra-low shear stress conditions that mimic the flow in early-stage regenerative microvessels in ischemic muscle. We further characterize the expression and localization of select shear stress sensors such as primary cilia, and the activation of vascular endothelial growth factor receptor 2 (VEGFR2) under ultra-low shear stress conditions. The findings uncover novel information on the regulation of EC transluminal pillar formation that could have implications for microvascular network growth and repair in injured tissues.

2.2 Methods

2.2.1 Microfluidic Device Design and Fabrication

The microfluidic device used in these experiments was designed in collaboration with the Poepping and Holdsworth Labs at the University of Western Ontario. The master mold of the device was made of acrylic and generated by the Machine Shop at the University of Western Ontario via micro-milling. The device was designed to contain three parallel channels 100 μm in width, 100 μm in height, and 1 cm in length, although only two channels were used in any given experiment. Each channel also contained a circular inlet and outlet. Microfluidic devices were generated using a silicone-based organic polymer called polydimethylsiloxane (PDMS). A negative of the master mold was generated using a 10:1 mixture of PDMS elastomer base (10 g, Sylgard184, Sigma) and silicone curing agent (1 g, Sylgard184, Sigma) and fashioned to a 35 mm glass-bottom dish (MatTek) coated in a thin layer of PDMS semi-cured using

a hot plate set to 60º. Polyethylene tubing (Intramedic™, 0.5 mm, BD Biosciences) cut at 45º was then inserted into the inlet and outlet of the microchannels.

Before cell culture, microchannels were washed with PBS to remove any debris and/or air within the channel. The two channels were then coated with 250 µg/mL bovine plasma fibronectin (Sigma, F1141) in an incubator at 37ºC and 5% CO_2 via programmable syringe pumps (NE-300, New Era Pump Systems, Inc.). The microchannels were then washed with Endothelial Growth Media-2 (EGM-2) supplemented with EGM-2 Bullet kit (CC-3156, Lonza) containing 0.1 µg/mL L-ascorbic acid (A4034, Sigma) via syringe pump set 1 µL/min to create an environment conducive to cell attachment and growth. The device remained in an incubator at 37ºC and 5% CO_2 until perfusion of the cell suspension.

2.2.2 Endothelialization of Microfluidic Channels

Human umbilical vein endothelial cells (HUVECs; Lonza) were grown in EGM-2 containing Gibco™ Amphotericin B (1:500, ThermoFisher Scientific) on 10 mm culture dishes (Corning) in an incubator at 37ºC and 5% CO_2. HUVECs were used to develop the microfluidic model because they were relatively easy to grow within the channels where volume to surface area ratio is low. Between 3-6 passages, HUVECs were trypsinized and resuspended in a mixture of 8% Dextran in EGM-2 supplemented with L-ascorbic acid to create a cell suspension at a concentration of $1x10^7$ cells/mL used for seeding one microfluidic channel. Cells were then infused into the channel by hand, guided by Hoffman modulation phase contrast microscopy (Axiovert S100 with Hoffman Modulation Contrast, Zeiss), allowing for visualization and control of the flow of cells within the channel in order to increase cell adherence. The microfluidic device was left stationary at 37ºC and 5% CO_2 for one hour, after which channels were washed by hand with fresh EGM-2 supplemented with L-ascorbic acid before being left stationary at 37ºC and 5% CO_2 for 24 h.

2.2.3 Induction and Variation of Shear Stress within Microfluidic Channels

Once both microfluidic channels reached 100% confluency, the channels were connected to programmable syringe pumps and pre-conditioned with EGM-2 degassed in a vacuum dessicator (Bel-Art^{TM}) and delivered at a flow rate of 1 µL/min, corresponding to a shear stress of 1 dyn/cm^2, for 1-4 days to allow cells to become accustomed to moderate flow. The flow rate was then adjusted to 10 µL/min, 0.2 µL/min, or 1 µL/hr, corresponding to shear stresses of 10 dyn/cm^2, 0.2 dyn/cm^2, and 0.02 dyn/cm^2, respectively, or left at 1 dyn/cm^2. Shear stress was calculated using an equation for parallel-plate flow chambers derived from the Navier-Stokes and continuity equations (Ahsan and Nerem, 2010). The viscosity of culture medium used was 0.0078 cPoise (dela Paz et al., 2012). Importantly, the device remained inside the incubator during the entire procedure to prevent temperature fluctuation-induced air bubbles that could result in cell death. Cells were subjected to experimental shear stress for 24-48 hours, followed by immunostaining.

2.2.4 Immunostaining of Endothelial Cells Lining Microfluidic Channels

Cells lining all four walls of each channel were fixed by delivery of 4% paraformaldehyde (Alfa Aesar, A11313) using programmable syringe pumps at 1 µL/min at room temperature for 25 min. The cells were then permeabilized by delivering 0.1% or 0.5% Triton-X 100 (Sigma, T8787) in PBS at 1 µL/min for 15 min, after which the solution was left static inside the channels for an additional 15 min. Blocking was performed by delivery of 5% donkey serum at 1 µL/min for 15 min before the blocking solution was left stationary in the device for 1.5-2 hr. Endothelial cell-cell junctions were immunostained by delivery of rabbit monoclonal anti-human VE-Cadherin primary antibody (1:200, Cell Signaling Technologies, D87F2) at 1 µL/min for 15 min. The device was placed on a flat surface and empty 1 mL syringes were attached to the inlet and outlet tubing of both channels. The syringes were taped in place to ensure equal tubing height to reduce residual flow within the channel. The device was stored in static

conditions overnight at 4ºC. After 24 hr, HUVECs were washed by infusion of PBS at 1 µL/min for 30 min. The VE-Cadherin cell-cell junctions were visualized using Alexa Fluor-546 (1:400, Life Technologies, A10040) or DyLight-550 (1:400, Abcam, ab96920) conjugated donkey anti-rabbit IgG perfused at 1 µL/min for 15 min. The secondary antibody was left static at room temperature for 2 hr and then washed by delivery of PBS at 1 µL/min for 30 min. Next, the F-actin cytoskeleton was visualized by perfusion of Alexa Fluor-488 conjugated phalloidin (1:30 or 1:40, Invitrogen, A12379) at 1 µL/min for 15 min, followed by a washing step via infusion of PBS for 30 min. Finally, the nuclei were visualized using either DAPI (1000 nM, Sigma, D9542) or DRAQ5^{TM} (1:200 or 1:500, ThermoFisher Scientific, 62254) and Fluoromount-G (SouthernBiotech, 0100-01) was perfused through the channel for 25 min.

The immunostaining methods listed above were also used to visualize primary cilia, and phosphorylated VEGFR2 (pVEGFR2). To locate primary cilia, a protein localized to the axoneme of cilia called ADP-ribosylation factor-like protein 13b (ARL13b) was immunostained by delivery of rabbit polyclonal anti-human ARL13b primary antibody (1:400, Proteintech, 17711-1-AP) and visualized using DyLight-550 conjugated donkey anti-rabbit IgG (1:200). Phosphorylated VEGFR2 was immunostained by delivery of rabbit polyclonal anti-human VEGFR2 (phospho Y1054 + Y1059) primary antibody (1:100, Abcam, ab5473). The receptor was visualized using DyLight-550 conjugated donkey anti-rabbit IgG (1:100).

2.2.5 Confocal Imaging and Analysis of Endothelial Cell Morphology and Pillar Formation

Endothelial cells lining all four walls of the microfluidic channels were imaged using a Leica TCS SP8 Confocal Microscope using a 40x oil-immersion objective and Diode 405, OPSL 488, and OPSL 552 lasers or a Nikon A1R Confocal Laser Scanning System using a 40x oil-immersion objective and

405nm, 488nm, 561nm, and 647nm lasers. Seven fields of view (FOV) were taken down the length of each channel, beginning 1 mm from the channel inlet and moving toward the channel outlet. Regions of interest imaged using the Galvano or Resonance scanner from the Nikon microscope were generated using up to 120, 0.3 μm-thick z-slices at a pixel resolution of 300 nm. Z-slices were reconstructed using Image Viewer (Leica) or NIS Elements Software (Nikon) into 3D volume images, as well as maximum intensity planar projections showing only the bottom surface of the channel, and orthogonal projections.

Endothelial cell elongation in the direction of flow was evaluated quantitatively under each shear stress condition, whether 10 dyn/cm^2, 1 dyn/cm^2, 0.2 dyn/cm^2, or 0.02 dyn/cm^2, by measuring both the length of each cell in the direction of flow and the aspect ratio of each cell. The maximum intensity planar projection of 7 FOVs was used to outline each individual cell and, using the "Centroid" and "Fit ellipse" tools in ImageJ (NIH), the major axis and minor axis through the centroid of the cell area were measured and divided to generate the aspect ratio. The length of each cell was quantified by measuring the length of each cell along the flow axis.

Alignment of ECs in the direction of flow was evaluated quantitatively by measuring the angular deviation of both the cell axis and the nuclear axis from the axis of flow. To measure angular deviation of the cell axis from the axis of flow, the intracellular area of each cell was again outlined in ImageJ (NIH) and, using the "Centroid" and "Fit ellipse" tools, the major axis was calculated and the angle between the major axis and the x-axis of the image, in this case set to be the axis of flow. Angular deviation of the nuclear axis from the axis of flow was measured by hand using the "Angle" tool in ImageJ, quantifying the angle between the long axis of each cell nucleus and the axis of flow.

Endothelial cell F-actin, ARL13b, and pVEGFR2 content was quantified using background-corrected integrated density measurements. When measuring

F-actin and ARL13b content, the intracellular area of each cell in the maximum intensity projection was outlined following the internal border of each cell in ImageJ to ensure no cortical F-actin was measured. When measuring F-actin content, 5-7 FOVs were used and, when measuring ARL13b and pVEGFR2 were being measured, 7 FOVs were used. Then, the channels were split, and the areas outlined were imported onto the green channel image when measuring F-actin and red channel image when measuring ARL13b. When measuring pVEGFR2 content, the border of each cell was outlined to measure the content of the cellular junctions. The area and integrated density of each outlined cell were generated using the "Integrated Density" and "Area" tools. Then, a random area outside of the channel walls was measured for background using the "Mean Grey Value" tool. Finally, the corrected integrated density was generated using the following equation: Integrated Density – (Mean Grey Value*Area).

Pillar frequency within the channels was quantified using the seven equidistant regions of interest down the length of each channel exposed to both 1 dyn/cm^2 and 0.02 dyn/cm^2. The 3D volume reconstructions of each FOV of dimensions 206.21 μm x 318.01 μm x 45.00 μm (XYZ) were used to determine the number of cells forming a pillar and the number of cells not participating in a pillar. The number of cells participating in a pillar was then divided by the total number of cells on the bottom surface of the channel to generate the pillar frequency.

2.2.6 Statistical Analysis

All data sets were tested for normality using a D'Agostino and Pearson omnibus normality test and none were shown to be normally distributed. Comparisons were made among all four shear stress conditions using a Kruskal-Wallis test with Dunn's *post hoc* test using Graphpad Prism. Comparisons among pillar frequency and the integrated densities of ARL13b and pVEGFR2 were made using a Mann-Whitney test. Statistical significance was set at $p<0.05$.

2.3 Results

2.3.1 Engineering of a Novel 3D Microvessel Model

In order to study the effects of shear stress on EC transluminal pillar formation, we developed a 3D *in vitro* model of a microvessel using a microfluidic device containing two channels 100 μm in height, 100 μm in width, and 1 cm in length (Figure 2.1 A-B). A square channel geometry was developed to allow close proximity of the channel walls, creating an environment where pillar formation could occur. Each channel was circumferentially lined with a monolayer of endothelial cells and fluorescently stained to visualize the F-actin cytoskeleton, VE-cadherin intercellular junctions, and nuclei using laser-scanning confocal microscopy (Figure 2.1 C).

Healthy ECs are known to respond to high shear stress by elongating and aligning in the direction of flow *in vivo* (Tzima et al., 2005). We found that HUVECs lining the microfluidic channels subjected to a high shear stress of 10 dyn/cm^2, a shear stress seen in capillaries *in vivo*, underwent such an alignment. That is, cells appeared elongated in shape and aligned in the direction of flow. This was associated with cells having an abundance of F-actin stress fibres, which were similarly aligned in the direction of flow (Figure 2.2). These findings indicated healthy EC monolayers lining the microfluidic device capable of responding to physiologic shear stress.

2.3.2 Ultra-Low Shear Stress Induces Endothelial Cell Rounding

Following the construction and optimization of our 3D microvessel model, we looked to examine the morphological responses of ECs under a range of shear stress conditions. To accomplish this, we subjected ECs to four shear stress conditions, including ultra-low shear: 10 dyn/cm^2, 1 dyn/cm^2, 0.2 dyn/cm^2, and 0.02 dyn/cm^2 (Figure 2.3). EC morphology and elongation in the direction of

Figure 2.1 3D microvessel modelling using a microfluidic device.

A-B. Generation of a microfluidic device entails design and fabrication of a microfluidic master mold containing three channels 100 μm in height, 100 μm in width, and 1 cm in length, each beginning with an inlet and ending with an outlet. A negative mold of these channels is then developed using cured PDMS, which is attached to a glass-bottom dish spin-coated with a thin layer of PDMS. Tubing is inserted to the inlet and outlet of two channels to allow perfusion of fluids through the microfluidic channels. **C.** A 3D volume image (XYZ) reconstructed from 365 confocal z-slices showing HUVECs immunostained for VE-Cadherin and stained for F-actin lining all four walls of the microfluidic channel.

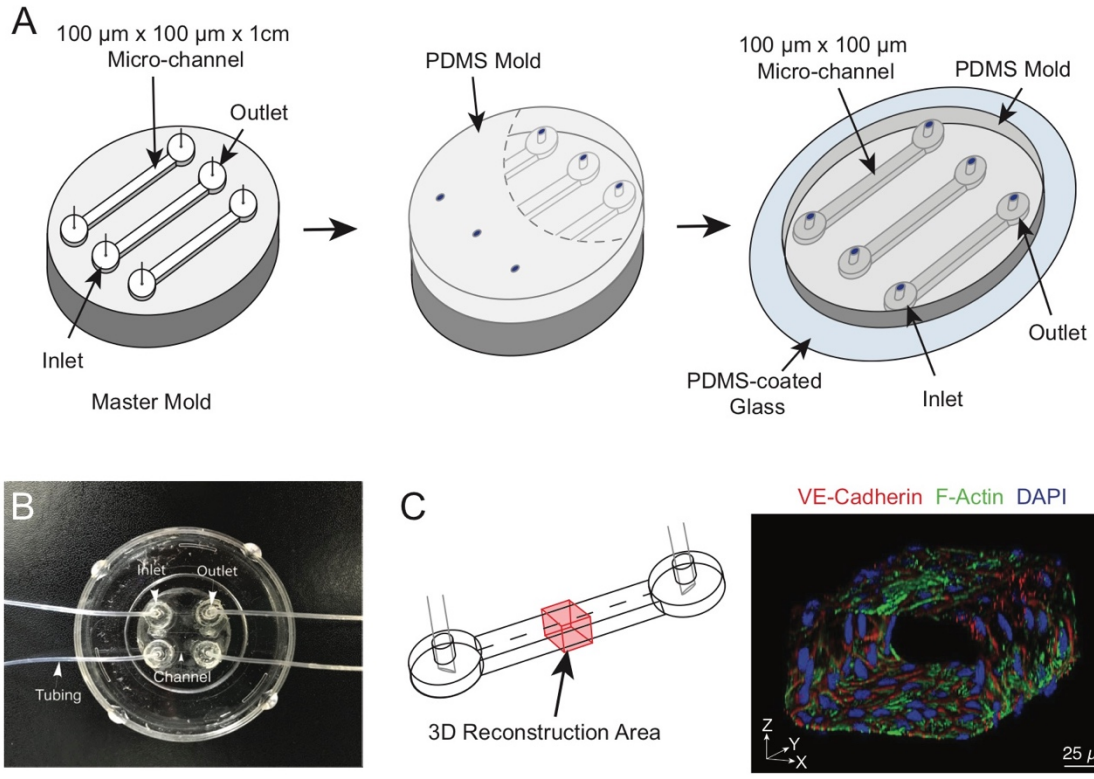
A
100 µm x 100 µm x 1cm
Micro-channel
Outlet
Inlet
Master Mold
PDMS Mold
100 µm x 100 µm
Micro-channel
PDMS Mold
Outlet
PDMS-coated
Glass
Inlet
B
Inlet
Outlet
Channel
Tubing
C
3D Reconstruction Area
VE-Cadherin F-Actin DAPI
Z
Y
X
25 µm

Figure 2.2 Generation of a healthy endothelial cell monolayer within a microfluidic channel.

Confocal planar projection images (XY) of HUVECs lining the bottom surface of a microfluidic channel immunostained for VE-Cadherin and stained to visualize F-actin and nuclei (120 z-slices, 0.25 μm step-size) showing healthy ECs capable of responding to high shear stress of 10 dyn/cm^2 by elongating and aligning in the direction of flow, with a high number of F-actin stress fibres.

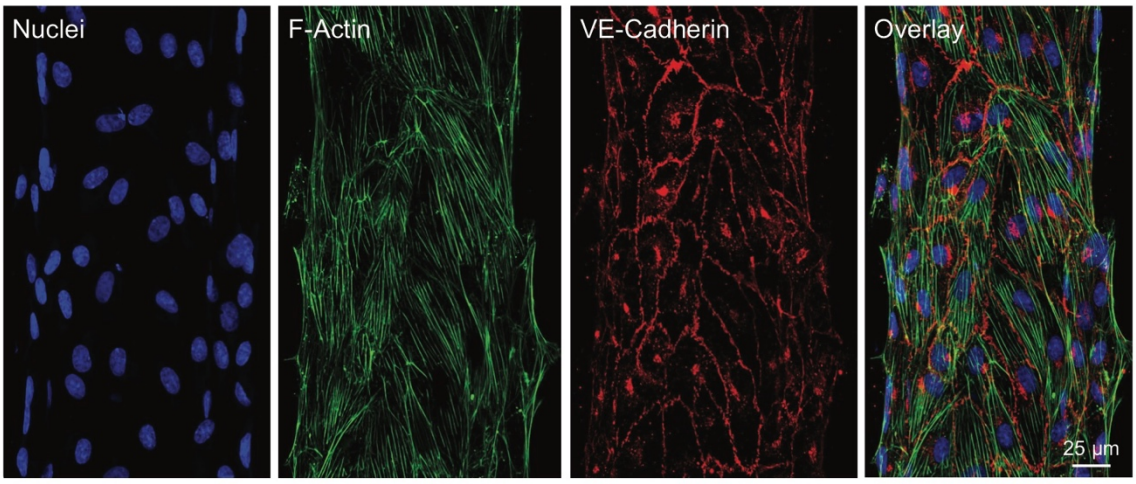
Nuclei
F-Actin
VE-Cadherin
Overlay
25 µm

Figure 2.3 Morphology and cytoskeletal reorganization in response to decrements of laminar shear stress.

HUVECs lining the bottom surface of a microfluidic device revealed using confocal planar projection images (XY) stained to visualize F-actin cytoskeleton (upper row) and immunostained for VE-Cadherin (middle row) (120 z-slices, 0.25 μm step-size). Cells exposed to physiologically relevant shear stress conditions of 10 dyn/cm^2 and 1 dyn/cm^2 (first and second columns, respectively) showed typical EC morphology under high shear stress, appearing elongated in shape and aligned in the direction of flow with high number of F-actin stress fibres. Cells exposed to ultra-low shear stress conditions of 0.2 dyn/cm^2 and 0.02 dyn/cm^2 (third and fourth columns, respectively) showed a decrease in elongation and alignment with the direction of flow, instead appearing rounded in shape and more randomly oriented. Under these conditions, the F-actin cytoskeleton was reorganized from F-actin stress fibres to cortical actin bordering the cell-cell junctions.

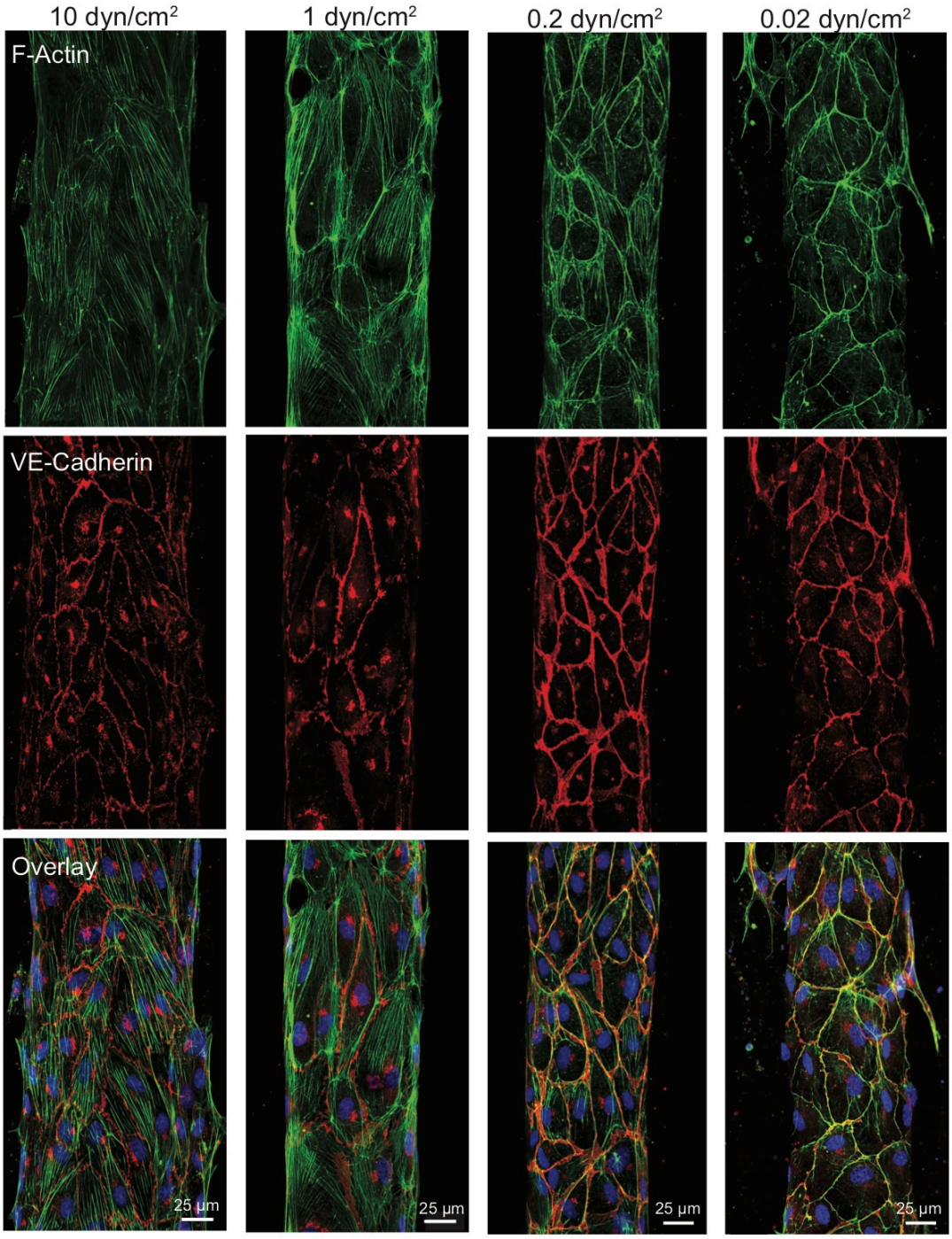
10 dyn/cm²
1 dyn/cm²
0.2 dyn/cm²
0.02 dyn/cm²
F-Actin
VE-Cadherin
Overlay
25 µm
25 µm
25 µm
25 µm

flow were quantified by measuring the length of each cell in the direction of flow and the cellular aspect ratio. Cells exposed to physiologic shear stress of 10 dyn/cm^2 displayed a median cell length of 78.7 μm (IQR = 63.7 μm to 100.8 μm). Under 1 dyn/cm^2 the median cell length was also 69.04 μm (IQR = 55.5 μm to 85.1 μm, Figure 2.4 A). Cells exposed to 0.2 dyn/cm^2 (56.2 μm, IQR = 47.2 μm to 72.1 μm) and 0.02 dyn/cm^2 (56.9 μm, IQR = 46.5 μm to 70.0 μm) showed a 28% and 19% decrease in median cell length when compared to 10 dyn/cm^2 and 1 dyn/cm^2, respectively ($p<0.0001$).Quantitative analysis of cellular aspect ratio revealed a similar trend. Cells exposed to physiologic shear stress of 10 dyn/cm^2 and 1 dyn/cm^2 had a median aspect ratio of 4.2 (IQR = 2.9 to 6.0) and 3.3 (IQR = 2.3 to 4.6), respectively (Figure 2.4 B). Cells exposed to 0.2 dyn/cm^2 experienced a 25% and 18% decrease in aspect ratio compared to 10 dyn/cm^2 and 1 dyn/cm^2 (IQR = 2.1 to 3.9, $p<0.0001$), respectively. A similar reduction was seen in cells exposed to 0.02 dyn/cm^2 (IQR = 1.8 to 3.3, $p<0.0001$). These results reveal that cells become rounder and less elongated as shear stress decreases. Nevertheless, they remained viable and adherent to the channels walls.

2.3.3 Ultra-Low Shear Stress Causes Reorganization of the F-Actin Cytoskeleton

In response to decreased shear stress, we observed a shift in the F-actin cytoskeleton organization of HUVECs in micro-channels. Specifically, cells exposed to higher shear showed a high number of thick F-actin stress fibres. However, as shear decreased, the number of F-actin stress fibres progressively decreased. Instead, cortical actin lining the border of each cell became prominent (Figure 2.3). Quantitative analysis of intracellular F-actin showed that exposure to a shear of 0.2 dyn/cm^2 results in a 37% and 36% decrease compared to 10 and 1 dyn/cm^2, respectively ($p=0.0001$, $p<0.0001$) (Figure 2.4 C). A 21% and 19% reduction in F-actin content was seen when cells were exposed to shear stress of 0.02 dyn/cm^2 ($p<0.0001$, $p=0.0177$). A shear of 0.02 dyn/cm^2 led to a slight peculiar increase of F-actin content as compared with 0.2 dyn/cm^2 ($p<0.0001$).

Figure 2.4 Endothelial cell changes in morphology under various shear stress conditions.

A. Graph depicting changes in length of the cell in the direction of flow at 10 dyn/cm^2 (n=348 ECs), 1 dyn/cm^2 (n=345 ECs), 0.2 dyn/cm^2 (n=372 ECs), and 0.02 dyn/cm^2 (n=345 ECs). **B.** Scatter plot showing cell aspect ratio determined by the length of the major axis of the cell divided by the minor axis at 10 dyn/cm^2 (n=348 ECs), 1 dyn/cm^2 (n=322 ECs), 0.2 dyn/cm^2 (n=373 ECs), and 0.02 dyn/cm^2 (n=345 ECs). **C.** Plot depicting the presence of F-actin stress fibres quantified using intracellular F-actin content at 10 dyn/cm^2 (n=284 ECs), 1 dyn/cm^2 (n=283 ECs), 0.2 dyn/cm^2 (n=307 ECs), and 0.02 dyn/cm^2 (n=283 ECs). **D-E.** Graphs showing angular deviation of the nucleus of cells from the direction of flow at 10 dyn/cm^2 (n=396 ECs), 1 dyn/cm^2 (n=377 ECs), 0.2 dyn/cm^2 (n=382 ECs), and 0.02 dyn/cm^2 (n=376 ECs), as well as angular deviation of the major axis of the cell from the direction of flow at 10 dyn/cm^2 (n=347 ECs), 1 dyn/cm^2 (n=345 ECs), 0.2 dyn/cm^2 (n=373 ECs), and 0.02 dyn/cm^2 (n=345 ECs). All graphs were generated using data from 3 microfluidic channels per shear stress condition.

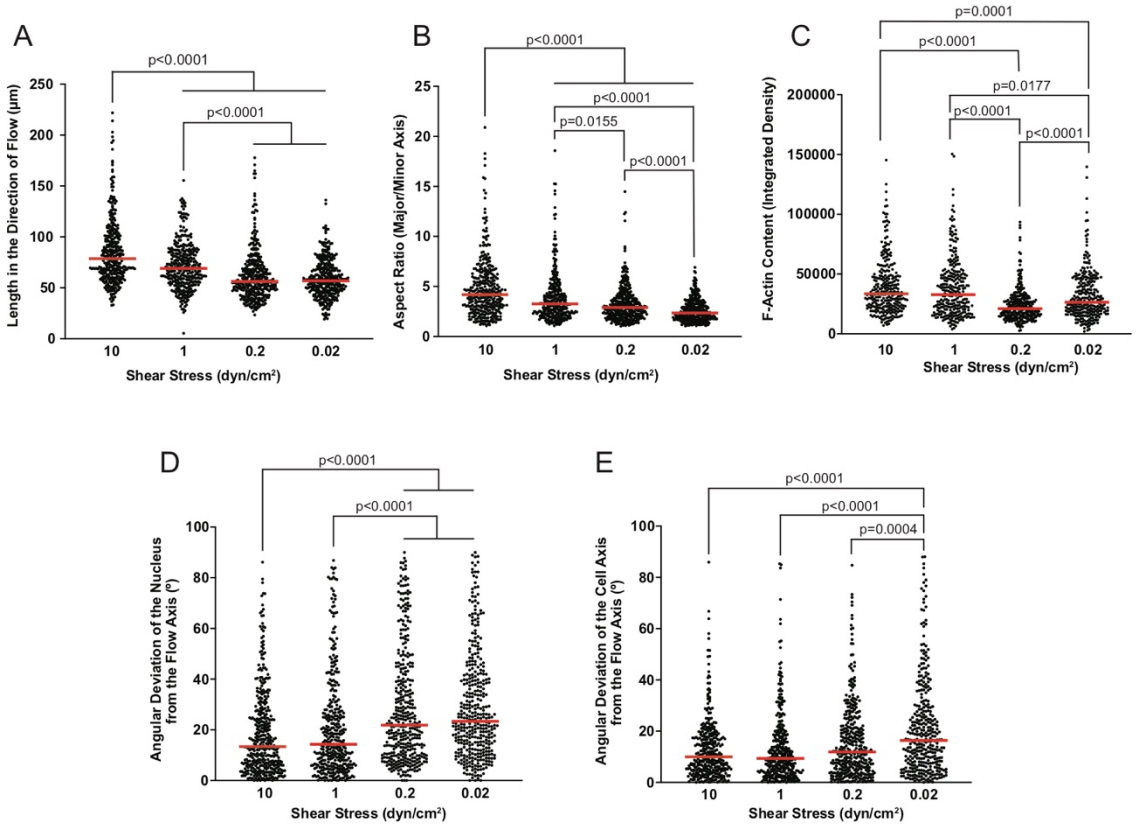
A
p<0.0001
p<0.0001
Length in the Direction of Flow (µm)
250
200
150
100
50
0
10
1
0.2
0.02
Shear Stress (dyn/cm²)
B
p<0.0001
p<0.0001
p=0.0155
p<0.0001
Aspect Ratio (Major/Minor Axis)
25
20
15
10
5
0
10
1
0.2
0.02
Shear Stress (dyn/cm²)
C
p=0.0001
p<0.0001
p=0.0177
p<0.0001
p<0.0001
F-Actin Content (Integrated Density)
200000
150000
100000
50000
0
10
1
0.2
0.02
Shear Stress (dyn/cm²)
D
p<0.0001
p<0.0001
Angular Deviation of the Nucleus from the Flow Axis (°)
100
80
60
40
20
0
10
1
0.2
0.02
Shear Stress (dyn/cm²)
E
p<0.0001
p<0.0001
p=0.0004
Angular Deviation of the Cell Axis from the Flow Axis (°)
100
80
60
40
20
0
10
1
0.2
0.02
Shear Stress (dyn/cm²)

These results reflect the decrease in F-actin stress fibres seen in cells exposed to ultra-low shear stress.

2.3.4 Endothelial Cells Exposed to Ultra-Low Shear Stress Become Randomly Oriented in the Direction of Flow

We next evaluated EC alignment in the direction of flow among the various shear stress conditions. To do so, I measured the angular deviation of the long axis of the cell nucleus from the axis of flow, as well as the angular deviation of the major axis of the cell body from the axis of flow. Cells exposed to physiologic shear stress conditions of 10 dyn/cm^2 and 1 dyn/cm^2 showed a median nuclear angular deviation of 13.4º (IQR = 6.0º to 26.6º) and 14.3º (IQR = 6.3º to 27.9º), respectively (Figure 2.4 D). The angle of the nuclear axis of cells exposed to 0.2 dyn/cm^2 showed respective 63% and 53% increases when compared to cells subjected to 10 dyn/cm^2 and 1 dyn/cm^2. (IQR = 10.6º to 41.1º, $p<0.0001$). Cells exposed to 0.02 dyn/cm^2 experienced a 75% and 64% increase in nuclear angular deviation when compared to the higher shear stress conditions (IQR = 12.9º to 40.2º, $p<0.0001$).

Quantitative analysis of the angular deviation of the major axis of the cell body from the direction of flow also revealed more randomly oriented ECs as shear stress decreased. When exposed to 10 dyn/cm^2 and 1 dyn/cm^2, cells showed a median angular deviation of 10.0º (IQR = 4.8º to 17.8º) and 9.34º (IQR = 4.3º to 17.9º), respectively (Figure 2.4 E). When exposed to 0.2 dyn/cm^2, cells showed a median angular deviation of 11.8º (IQR = 5.2º to 21.6º). Cells exposed to 0.02 dyn/cm^2 showed a 64% and 75% increase in angular deviation of the cell axis when compared to 10 dyn/cm^2 and 1 dyn/cm^2, respectively (IQR = 7.4º to 28.6º, $p<0.0001$). Interestingly, cells subjected to 0.02 dyn/cm^2 also had a 38% increase in angular deviation compared to cells exposed to 0.2 dyn/cm^2 ($p=0.0004$). Taken together, these results show an overall increase in angular

deviation from the direction of flow and generally more random orientation in cells exposed to ultra-low shear stress.

2.3.5 Ultra-Low Shear Stress is Conducive to Endothelial Cell Transluminal Pillar Formation

Next, we sought to determine if the microfluidic model was capable of recreating an EC transluminal pillar. To accomplish this, HUVECs exposed to 1 dyn/cm^2 and 0.02 dyn/cm^2 were visualized using both orthogonal and 3D volume reconstructions of confocal z-slices. Remarkably, these orthogonal and volume images revealed a number of transluminal pillars. These appeared as endothelial-based projection that crossed from one side of the lumen to the other, connecting cells on the bottom surface to cells lining the wall of the microfluidic channel (Figure 2.5 A-B). Remarkably, we also observed multiple pillars formed within the same region of interest within the microfluidic channel (Figure 2.5 B, see Online Video 4.1in Appendix A). Interestingly, filopodial projections varied in morphology–81% of pillars appeared as thin F-actin protrusions crossing the lumen, while the other 19% appeared wider, having extended down the long axis of the channel, often with a nucleus participating within the filopodial structure (Figure 2.5 B). Wider pillars also experienced some overlap, suggesting fusing of neighbouring pillars.

We next sought to compare the prevalence of pillar formation under each of the shear stress conditions. ECs subjected to physiologic flow showed a mean pillar prevalence of 0.6% (Figure 2.5 C). Interestingly, quantitative analysis of EC pillar prevalence showed an 8.8-fold increase in pillar formation under ultra-low shear stress conditions ($p<0.0001$). This finding reveals that ultra-low shear stress facilitates EC transluminal pillar formation.

2.3.6 Ultra-Low Shear Stress Leads to an Increase in ARL13b Expression

Primary cilia are extracellular structures found on the surface of cells composed of microtubules that are widely thought to act as shear stress sensors.

Figure 2.5 Recreation of a transluminal pillar under ultra-low shear stress in a 3D *in vitro* microvessel model.

A. Confocal orthogonal projections (XZ) depicting HUVECs exposed to 0.02 dyn/cm^2 lining the bottom and side walls of a microfluidic channel immunostained for VE-Cadherin (red) and stained to visualize F-actin (green). Endothelial cell transluminal pillars formed across the channel lumen stretching from the bottom surface to the side wall (arrows), with and without the presence of a nucleus within the pillar (top and middle rows versus bottom row, respectively). **B-C.** 3D volume images (XYZ) reconstructed from confocal z-slices (120 z-slices, 0.25 μm step-size) showing multiple transluminal pillars formed within one region of interest (arrows) (**B**, see Online video 4.1 in Appendix A), as well as pillars widened down the long axis of the channel and beginning to overlap at the base of the pillars (arrow) (**C**). **D.** Bar graph depicting transluminal pillar frequency, calculated as the number of cells participating in a pillar divided by the total number of cells within a microfluidic channel across 7 FOVs, showing an increase in EC pillar formation under ultra-low flow ($p<0.0001$, $n=4$ microfluidic channels per shear stress condition).

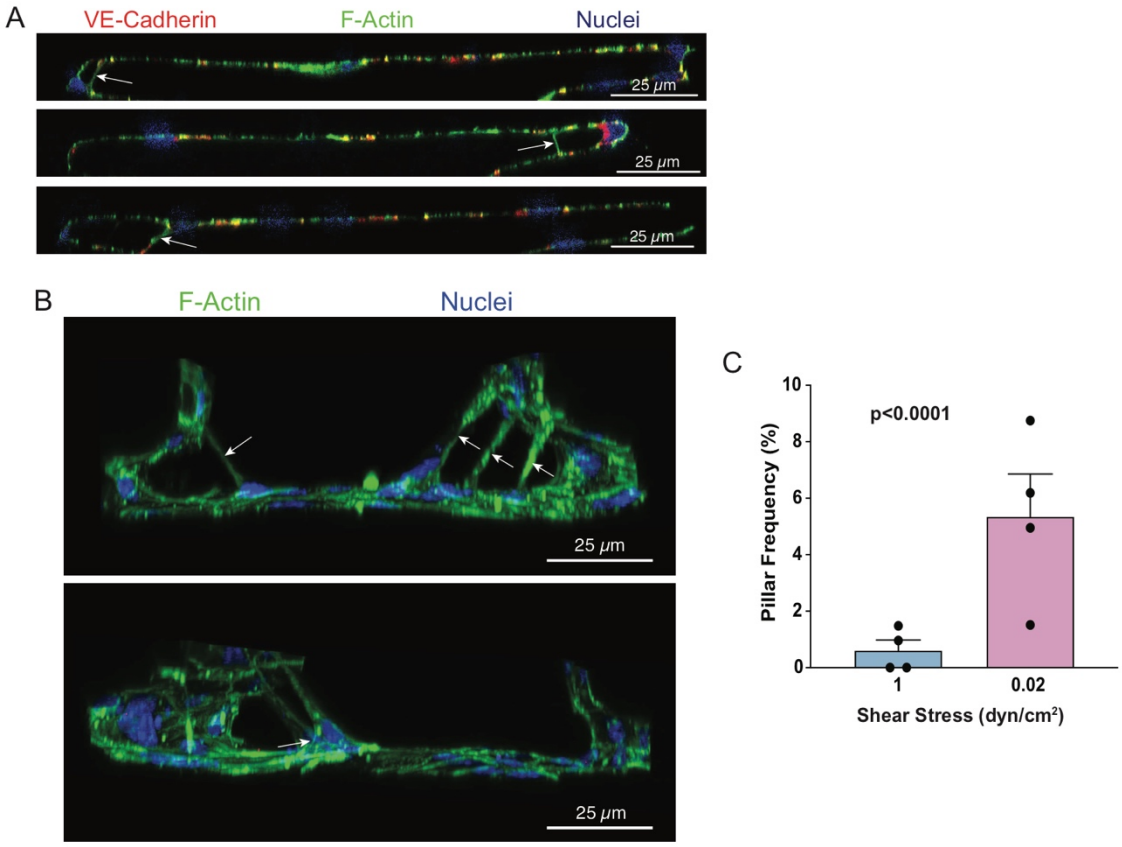
A
VE-Cadherin
F-Actin
Nuclei
25 μm
25 μm
25 μm
B
F-Actin
Nuclei
25 μm
25 μm
C
p<0.0001
Pillar Frequency (%)
10
8
6
4
2
0
1
0.02
Shear Stress (dyn/cm²)

ADP-ribosylation factor-like protein 13b (ARL13b) is a GTPase localized along the axoneme of these cilia and is responsible for F-actin cytoskeleton reorganization via the Sonic hedgehog (Shh) pathway (Caspary et al., 2007; Renault et al., 2010). Given that the role of primary cilia as a shear stress sensor has been studied mainly under high shear stress conditions (Ando and Yamamoto, 2013), we asked whether these could sense ultra-low shear stress. By immunostaining for ARL13b, we identified primary cilia under a shear stress of 1 dyn/cm^2 and an ultra-low shear stress of 0.02 dyn/cm^2. Notably, we observed a 1.9-fold increase in ARL13b content under the ultra-low shear condition (Figure 2.6 A-B). This finding indicates that endothelial primary ciliogenesis is stimulated by ultra-low shear, potentially increasing the cell's sensitivity to this force.

Most intriguing was the identification and localization of ARL13b within the EC transluminal pillar structure. When scrutinizing a 3D volume image, we observed ARL13b localized to a primary cilium above the nucleus within a pillar bridging across the microfluidic channel lumen (Figure 2.6 C), suggesting the presence of a primary cilium protruding out of the pillar. However, ARL13b was only associated with pillars larger in width as opposed to thinner strands of pillars. This novel information concerning primary cilium localization within a transluminal pillar could uncover a potential active, spatially-specific role for these cilia in pillar formation.

2.3.7 Ultra-Low Shear Stress Results in a Decrease in Phosphorylated VEGFR2

We next sought to determine the change in activation of VEGFR2 by phosphorylation. To do so, we subjected ECs lining the microfluidic device to shear stress conditions of 1 dyn/cm^2 and an ultra-low shear stress of 0.02 dyn/cm^2. Immunostaining of phosphorylated VEGFR2 (pVEGFR2) revealed signal along the borders of ECs at cell-cell junctions. Notably, we observed a

Figure 2.6 Increase in ARL13b expression in HUVECs exposed to ultra-low shear stress.

A. Confocal planar projection images (XY) of HUVECs lining the bottom surface of microfluidic channels immunostained for ARL13b (red) and stained to visualize the F-actin cytoskeleton (green) showing an increase in ARL13b expression under ultra-low shear stress of 0.02 dyn/cm^2 (120 z-slices, 0.25 μm step size). **B.** Graph depicting ARL13b content in cells exposed to 1 dyn/cm^2 (n=408 ECs) and 0.02 dyn/cm^2 (n=360 ECs) ($p<0.0001$, n=3 microfluidic channels per shear stress condition). **C.** A 3D volume image (XYZ) reconstructed from confocal z-slices depicting a transluminal pillar with localized ARL13b (arrow) extending from the bottom surface to the side wall of an EC-lined microfluidic channel.

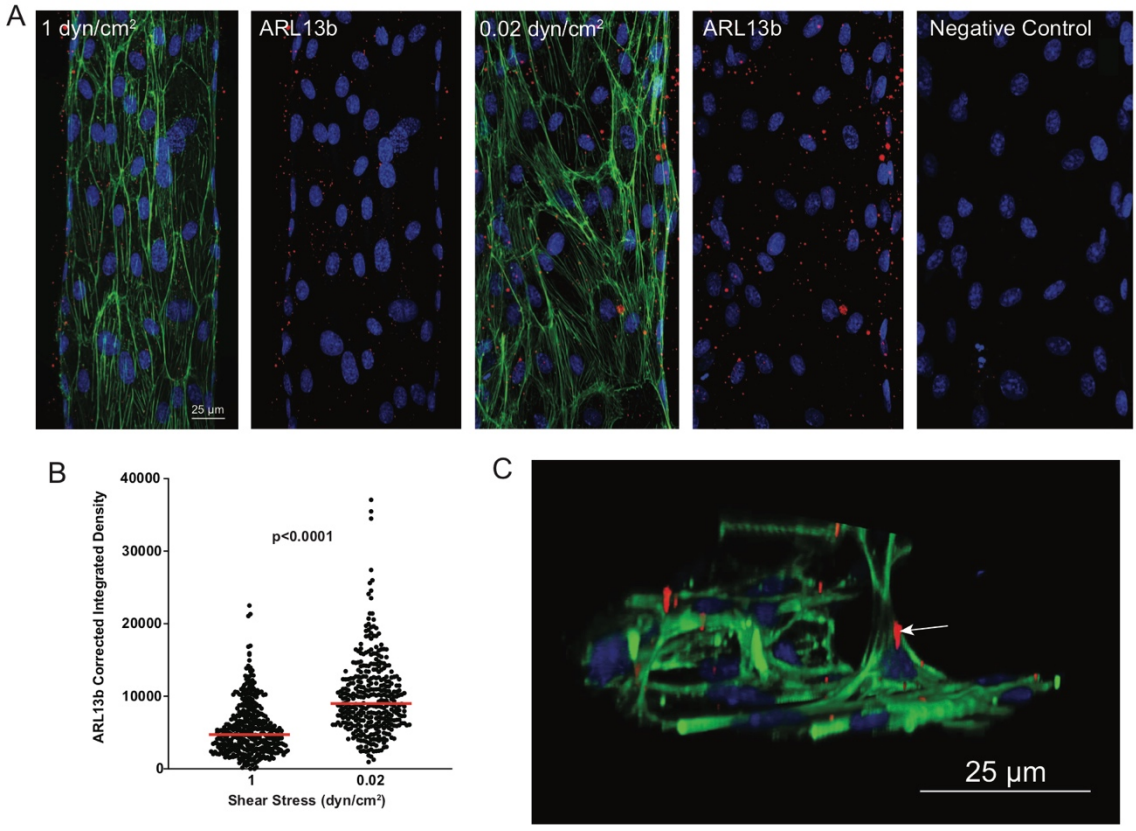
A
1 dyn/cm²
ARL13b
0.02 dyn/cm²
ARL13b
Negative Control
25 µm
B
ARL13b Corrected Integrated Density
40000
30000
20000
10000
0
p<0.0001
1
0.02
Shear Stress (dyn/cm²)
C
25 µm

statistically discernible 22% decrease in pVEGFR2 abundance in cells exposed to ultra-low shear stress conditions compared to cells exposed to 1 dyn/cm^2 ($p<0.0001$, Figure 2.7 A-B). Of note, this decrease in pVEGFR2 suggests activation of VEGFR2 is positively correlated with shear stress magnitude in my microfluidic design. This adds to and is consistent with the previous report that increased laminar shear activates VEGFR2 (Tzima et al., 2005).

Interestingly, pVEGFR2 immunoreactivity was also observed at EC transluminal pillars. To accurately study pVEGFR2 localization within transluminal pillars, 3D volume images of regions of interest were reconstructed using *z*-slices taken using confocal laser scanning. These images revealed pVEGFR2 staining localized to the middle region of the pillar away from either end of the pillar-wall interface (Figure 2.7 C). Moreover, this signal appeared to be lateralized to the upstream side the pillar bridging the channel lumen (Figure 2.7 D). This finding of localized and lateralized pVEGFR2 expression within transluminal pillars outlines a potential role for VEGFR2 in pillar morphogenesis, especially after initial stage of pillar formation.

Figure 2.7 Ultra-low shear stress results in a decrease in pVEGFR2 expression in endothelial cells lining a 3D microfluidic channel.

A. Confocal planar projection images (XY) of ECs lining the bottom surface of microfluidic channels immunostained for pVEGFR2 (red) and stained to visualize the F-actin cytoskeleton (green). pVEGFR2 appears along the border of cells, overlapping cell-cell junctions (120 z-slices, 0.25 μm step size). **B.** Graph depicting pVEGFR2 content quantified within endothelial cell-cell junctions showing a decrease in pVEGFR2 expression in cells under ultra-low shear stress of 0.02 dyn/cm^2 (n=211 ECs) compared to 1 dyn/cm^2 (n=214 ECs) ($p<0.0001$, n=2 microfluidic channels per shear stress condition). **C-D.** 3D volume images (XYZ) reconstructed from 120 confocal z-slices (0.25 μm step-size) showing the presence of pVEGFR2 in the mid-region of a transluminal pillar (arrow) (C) lateralized to the upstream side of the pillar (D) extending from the bottom surface to the side wall of a microfluidic channel circumferentially lined with ECs.

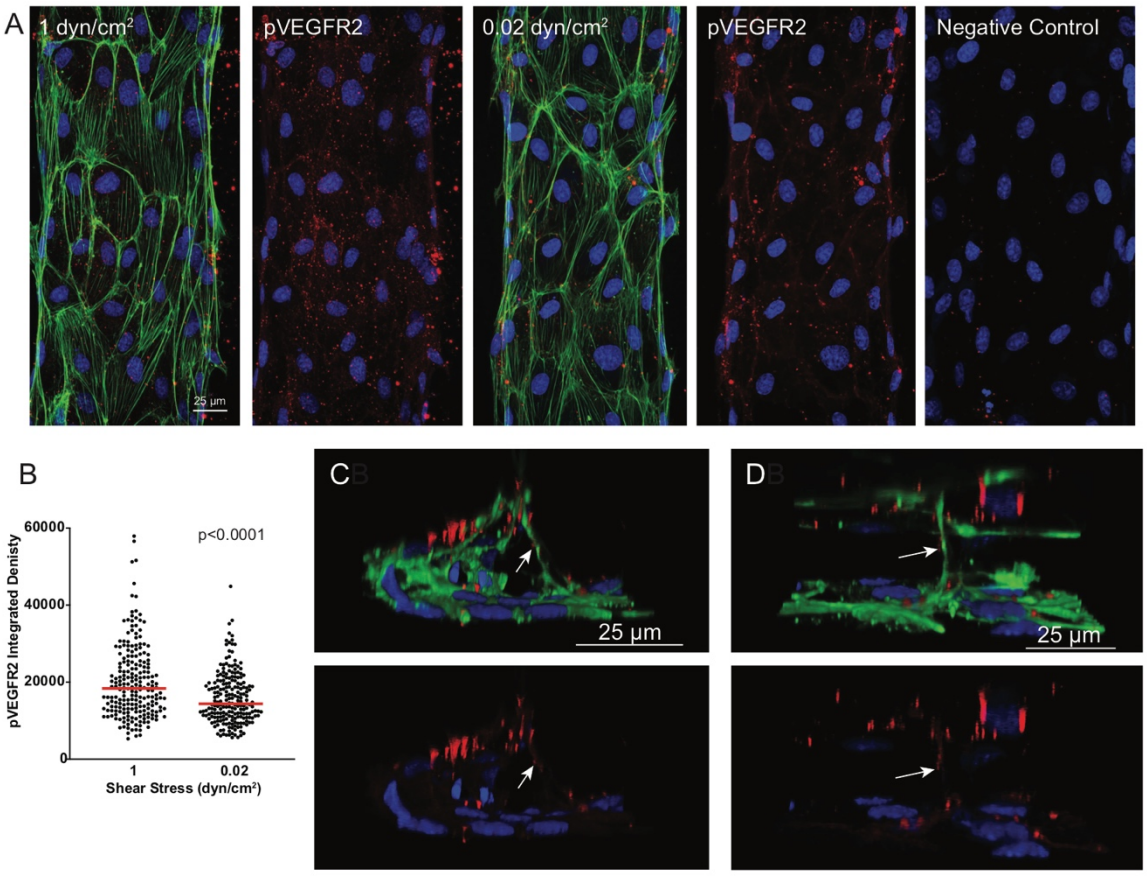
A
1 dyn/cm²
pVEGFR2
0.02 dyn/cm²
pVEGFR2
Negative Control
25 µm
B
p<0.0001
pVEGFR2 Integrated Denisty
60000
40000
20000
0
1
0.02
Shear Stress (dyn/cm²)
C
25 µm
D
25 µm

2.4 Discussion

Regenerative angiogenesis in the context of ischemic injury has recently been determined by our research group to rely on intussusceptive angiogenesis, discernible by the formation of endothelial transluminal pillars (Arpino, 2017b). Moreover, vessels undergoing intussusception also experienced a pronounced decrease in blood flow and, consequently, shear stress. However, the biochemical and biomechanical regulation of this growth process remains poorly understood. In this study, we developed a novel 3D microvessel model capable of forming pillars and elucidating the regulation of EC transluminal pillar formation. Notably, we report an 8.8-fold increase in transluminal pillar formation under ultra-low shear stress conditions. This suggests ultra-low shear stress is permissive to the progression of intussusception angiogenesis via pillar formation.

The model developed in this study uses a square channel design that approximates microvessel physiology in terms of size. Our model is also unique in that cells line all four surfaces of the channel to create a contiguous 3D structure wherein the opposing cells monolayers are close enough in proximity to resemble a microvessel. Despite the expansion of the field of microfluidics, there remains a large variation in both the size and geometry of microchannels used to study EC flow response. Many research groups make use of rectangular channels, using the channel height to reflect microvessel physiology and increasing the width of the channel to offset pressure introduced by high flow rates (Park et al., 2019; Reinitz et al., 2015; Sakurai et al., 2018). Moreover, the majority of microfluidics studies concentrate on cells lining the bottom surface of the channel, generating 2D models indicative of changes in the EC monolayer, but not in the channel as a whole (Shih et al., 2019; Maoz, et al., 2018). The system developed herein not only allows for the controlled study of EC response

to shear stress, but also accounts for the communication between cells not only adjacent but physically opposing each other as would be the case *in vivo*.

Among 3D microfluidic microvessel models, most commonly studied is endothelial response to high shear stress conditions seen within healthy microvascular networks. Under these conditions, ECs have been shown to elongate and align in the direction of flow (Tzima et al., 2005). Our findings of EC morphology changes under low shear are consistent with prior data. A vascular cast study by Langille and Adamson (1981) of rabbit and mouse arterial branch sites showed ECs lacked orientation and appeared rounded in shape in areas of low shear stress. Moreover, our finding of cytoskeletal reorganization from F-actin stress fibres to cortical actin under low shear stress conditions echoes a recent study of ECs within a microfluidic channel (Inglebert et al., 2020). However, these studies, both *in vivo* and *ex vivo*, concentrate on low shear stress either in areas of turbulent flow or in conditions of laminar flow of 2-4 dyn/cm^2. Therefore, while similar findings were seen within the low shear stress conditions of our *ex vivo* microvessel model, the study of EC response to shear stress below 1 dyn/cm^2 is lacking, with only one study by Park et al. (2011), interestingly using microfluidics, interrogating shear stress at this magnitude.

The 3D microvessel model developed in this study represents the first *ex vivo* model to achieve suitable conditions for controlled endothelial transluminal pillar formation. While the existence of transluminal pillars as a marker of intussusception has been known for many years, the role of shear stress in the formation of these pillars has only recently become a focus. Some studies have suggested that acute increases in shear stress rapidly lead to transluminal pillar formation and subsequent vessel splitting in mouse skeletal muscle (Gianna-Barrera et al., 2013). Computational studies in chick chorioallantoic membrane (CAM) models of adaptive angiogenesis have suggested that pillars form in zones where shear stress is <1 dyn/cm^2, constrained by regions of high shear

stress (Lee et al., 2011). However, *in vitro* models capable of recreating a 3D transluminal pillar have not yet been established. Therefore, the finding of increased pillar frequency under an ultra-low shear stress of 0.02 dyn/cm^2 is the first to definitively and directly confirm the role of low shear stress in pillar formation.

The progression of intussusceptive angiogenesis is widely understood to involve the formation of multiple pillars down the length of a single vessel. These pillars will then enlarge to extend down the length of the vessel, fusing with adjacent pillars to fully split the vessel into two daughter vessels (Gianna-Barrera et al., 2013). Interestingly, the transluminal pillars seen in our 3D microvessel model showed a variation in size and thickness that could be representative of the enlargement of pillars as seen *in vivo*. In this case, thin filopodial projections would represent the beginning stages of intussusception wherein the pillar had first formed. Moreover, endothelial projections or bridges that had widened along the long axis of the microfluidic channel and contained a nucleus may represent pillars that had begun to enlarge. We also observed overlapping of these widened pillars that could reflect the fusing of neighbouring pillars. Furthermore, we observed multiple pillars of varying thickness within the same region of interest, reflective of the process that occurs in vivo. The observations in our microvessel model closely mimic what has been reported *in vivo*, which presents the first physiologically relevant, controlled method of studying not only a single transluminal pillar, but potentially the progression of intussusceptive angiogenesis via pillar formation and fusion.

Following interrogation of the biomechanical regulation of EC transluminal pillar formation by shear stress, I discovered novel information concerning the biochemical regulation of pillar formation. Specifically, I observed an increase in the abundance of primary cilia marker ARL13b in ECs subjected to ultra-low shear stress. Primary cilia are extracellular rod-like structures on the plasma

membrane of cells, composed of microtubule doublets, forming what is called an axoneme, connected to a microtubule organizing centre. ARL13b, the protein used to visualize the localization of these cilia, is a GTPase located along the axoneme and is responsible for regulating Shh signalling (Caspary et al., 2007). Non-canonical Shh signalling leads to reorganization of the actin cytoskeleton (Renault et al., 2010). These structures have been suggested to act as shear stress sensors on ECs, helping to trigger signalling cascades relaying changes in shear stress magnitude and direction to the cell via bending of the cilia (Ando and Yamamoto, 2013). The increase in ARL13b observed here suggests an increase in either the number of ARL13b GTPases lining a single primary cilium or an increase in the number of primary cilia themselves. Interestingly, studies within the chicken embryonic endocardium as well as the vasculature of the mouse retina reported a similar increase in number as well as length of primary cilia under low shear stress (Van der Heiden et al. 2005; Vion et al. 2018). It is tempting to consider the possibility of a role for primary cilia in the establishment of flow-seeking behaviour in ECs exposed to ultra-low shear stress. A decrease in shear stress corresponding to an increase in primary cilia suggests a mechanism by which the cell increases its capacity to sense shear stress under ultra-low conditions by increasing the number of flow-sensing structures on its plasma membrane.

I also discovered accumulation of ARL13b within the structure of the pillar itself. This novel finding further implicates a role for primary cilia in the formation or maintenance of EC transluminal pillars. In fact, this finding could support the establishment of flow-seeking behaviour in intussusceptive ECs even further. It could be suggested that under ultra-low shear stress conditions primary cilia increase in number, creating a flow-seeking behaviour that then guides the formation of a transluminal pillar. Assuming pillar formation is a protrusive event, primary cilia could exist to guide the cell body towards the centre of the lumen where shear stress would be more concentrated. This is further supported by the

increase in ARL13b observed, as an increase in this protein could magnify shear stress signalling via primary cilia and lead to the specific reorganization of the F-actin cytoskeleton that results in extension of the EC cell body to form a pillar.

It is worth noting, however, that in this study I visualized primary cilia by means of an antibody against ARL13b, a GTPase localized specifically to along the axoneme of the primary cilia (Caspary et al., 2007). While this method has been used in previous studies to identify primary cilia in EC culture (Vion et al., 2018; Eisa-Beygi et al., 2018), it is important to note that this protein may not reveal the entire structure of the primary cilia in a 3D capacity. Therefore, while I can derive the localization of primary cilia within the ECs in this study, I cannot infer structural information regarding the length or direction of the primary cilia identified.

Interestingly, in addition to observing a decrease in the activation of VEGFR2 within HUVECs lining the walls of the channel, localized pVEGFR2 was discovered within the endothelial-based protrusion of the transluminal pillar. Specifically, puncta/foci of pVEGFR2 was found within the mid-section of the pillar, away from either base where the pillar connected to a cell within the monolayer. Moreover, this pVEGFR2 was lateralized to the side of the pillar directly facing oncoming flow. This finding suggests a high magnitude of shear stress along the mid-section of the transluminal pillar due to localized hemodynamic forces. Computational models of pillars within a flowing vessel support these findings, demonstrating high shear stress within the mid-section of the pillar on the upstream side compared to “dead zones” on the downstream surface and at the pillar-wall interface (Filipovic et al., 2009). Therefore, migration from the wall, where shear stress is low, to the lumen could further imply a flow-seeking behaviour that motivates ECs to undergo intussusceptive angiogenesis, thereby forming a transluminal pillar.

In conclusion, we have developed the first *in vitro* model capable of EC transluminal pillar formation and the progression of intussusceptive angiogenesis. We further utilized this model to demonstrate that ultra-low shear stress is permissive to pillar formation and uncovered important relationships with primary cilia and VEGFR2. The findings described help to further elucidate the regulation of intussusceptive angiogenesis, which is an important but enigmatic angiogenic process.

2.5 References

Ahsan, T., and Nerem, R.M. (2010). Fluid shear stress promotes an endothelial-like phenotype during the early differentiation of embryonic stem cells. Tissue Eng Part A *16*, 3547-3553.

Ando, J., and Yamamoto, K. (2013). Flow detection and calcium signaling in vascular endothelial cells. Cardiovasc Res *99*, 260-268.

Arpino, G.M. (2017b). Angiogenesis And Neo-Microcirculatory Function In Diseased Tissue Revealed By Intravital Microscopy. Electronic Thesis and Dissertation Repository, 4731.

Carmeliet, P. (2000). Mechanisms of angiogenesis and arteriogenesis. Nat Med *6*, 389-395.

Caspary, T., Larkins, C.E., and Anderson, K.V. (2007). The graded response to Sonic Hedgehog depends on cilia architecture. Dev Cell *12*, 767-778.

dela Paz, N.G., Walshe, T.E., Leach, L.L., Saint-Geniez, M., and D'Amore, P.A. (2012). Role of shear-stress-induced VEGF expression in endothelial cell survival. J Cell Sci *125*, 831-843.

Djonov, V., Schmid, M., Tschanz, S.A., and Burri, P.H. (2000). Intussusceptive angiogenesis: its role in embryonic vascular network formation. Circ Res *86*, 286-292.

Eisa-Beygi, S., Benslimane, F.M., El-Rass, S., Prabhudesai, S., Khatib Ali Abdelrasoul, M., Simpson P.M., Yalcin, H.C, Burrows, P.E., and Ramchandran, R. (2018). Characterization of Endothelial Cilia Distribution

During Cerebral-Vascular Development in Zebrafish (*Danio rerio*). Arterioscler Thromb Vasc Biol *38*, 2806-2818.

Filipovic, N., Tsuda, A., Lee, G.S., Miele, L.F., Lin, M., Konerding, M.A., and Mentzer, S.J. (2009). Computational flow dynamics in a geometric model of intussusceptive angiogenesis. Microvasc Res *78*, 286-293.

Gianna-Barrera, R., Trani, M., Fontanellaz, C., Heberer, M., Djonov, V., Hlushchuk, R., and Banfi, A. (2013). VEGF over-expression in skeletal muscle induces angiogenesis by intussusception rather than sprouting. Angiogenesis *16*, 123-136.

Hlushchuk, R., Riesterer, O., Baum, O., Wood, J., Gruber, G., Pruschy, M., and Djonov, V. (2008). Tumor recovery by angiogenic switch from sprouting to intussusceptive angiogenesis after treatment with PTK787/ZK222584 or ionizing radiation. Am J Pathol *173,* 1173-1185.

Hlushchuk, R., Styp-Rekowska, B., Dzambazi, J., Wnuk, M., Huynh-Do, U., Makanya, A., and Djonov, V. (2017). PLoS One *12,* e0182813.

Inampudi, C., Akintoye, E., Ando, T., and Briasoulis, A. (2018). Angiogenesis in peripheral arterial disease. Curr Opin Pharmacol *39*, 60-67.

Inglebert, M., Locatelli, L., Tsvirkun, D., Sinha, P., Maier, J.A., Misbah, C., and Bureau, L. (2020). The effect of shear stress reduction on endothelial cells: A microfluidic study of the actin cytoskeleton. Biomicrofluidics *14*, 024115.

Langille, B.L., and Adamson, S.L. (1981). Relationship between blood flow direction and endothelial cell orientation at arterial branch sites in rabbits and mice. Circ Res *48*, 481-488.

Lee, G.S., Filipovic N., Lin, M., Gibney, B.C., Simpson, D.C., Konerding, M.A., Tsuda, A., and Mentzer, S. (2011). Intravascular pillars and pruning in the extraembryonic vessels of chick embryos. Dev Dyn *240*, 1335-1343.

Maoz, B.M., Herland, A., FitzGerald, E.A., Grevesse, T., Vidoudez, C., Pacheco, A.R., Sheehy, S.P., Park, T.E., Dauth, S., Mannix, R., et al. (2018). A

linked organ-on-a-chip model of the human neurovascular unit reveals the metabolic coupling of endothelial and neuronal cells. Nat Biotechnol *36*, 865-874.

Mentzer, S.J., and Konerding, M.A. (2014). Intussusceptive angiogenesis: expansion and remodeling of microvascular networks. Angiogenesis *17*, 499-509.

Park, J.Y., White, J.B., Walker, N., Kuo, C.H., Cha, W., Meyerhoff, M.E., and Takayama, S. (2011). Responses of endothelial cells to extremely slow flows. Biomicrofluidics 5, 22211.

Park, T.E., Mustafaoglu, N., Herland, A., Hasselkus, R., Mannix, R., FitzGerald, E.A., Prantil-Baun, R., Watters, A., Henry, O., Benz, M., et al. (2019). Hypoxia-enhanced Blood-Brain Barrier Chip recapitulates human barrier function and shuttling of drugs and antibodies. Nat Commun *10*, 2621.

Reinitz, A., DeStefano, J., Ye, M., Wong, A.D., and Searson, P.C. (2015). Human brain microvascular endothelial cells resist elongation due to shear stress. Microvasc Res *99*, 8-18.

Renault, M.A., Roncalli, J., Tongers, J., Thorne, T., Klyachko, E., Misener, S., Volpert, O.V., Mehta, S., Burg, A., Luedemann, C., et al. (2010). Sonic hedgehog induces angiogenesis via Rho kinase-dependent signaling in endothelial cells. J Mol Cell Cardiol *49*, 490-498.

Sakurai, Y., Hardy, E.T., Ahn, B., Tran, R., Fay, M.E., Cicliano, J.C., Mannino, R.G., Myers, D.R., Qui, Y., Carden, M.A., *et al*. (2018). A microengineered vascularized bleeding model that integrates the principal components of hemostasis. Nat Commun *9*, 509.

Shih, H.C., Lee. T.A., Wu, H.M., Ko, P.L., Liao, W.H., and Tung, Y.C. (2019). Mircofluidic Collective Cell Migration Assay for Study of Endothelial Cell Proliferation and Migration under Combinations of Oxygen Gradients, Tensions, and Drug Treatments. Sci Rep *9*, 8234.

Taylor, A.C., Seltz, L.M., Yates, P.A., and Peirce, S.M. (2010). Chronic whole-body hypoxia induces intussusceptive angiogenesis and microvascular remodeling in the mouse retina. Microvasc Res *79*, 93-101.

Tzima, E., Irani-Tehrani, M., Kiosses, W.B., Dejana, E., Schultz, D.A., Engelhardt, B., Cao, G., Delisser, H., and Schwartz, M. A. (2005). A mechanosensory complex that mediates the endothelial cell response to fluid shear stress. Nature *437*, 426-31.

Van der Heiden, K., Groenendijk, B.C.W., Hierck, B.P., Hogers, B., Koerten, H.K., Mommaas, M., Gittenberger-de Groot, A.C, and Poelmann, R.E. (2005). Monocilia on chicken embryonic endocardium in low shear stress areas. Dev Dyn *235*, 19-28.

Varma, S., and Voldman, J. (2015). A cell-based sensor of fluid shear stress for microfluidics. Lab Chip *15*, 1563-1573.

Varu, V.N., Hogg, M.E., Kibbe, M.R. (2010). Critical limb ischemia. J Vasc Surg *51*, 230-241.

Vion, A.C., Alt, S., Klaus-Bergmann, A., Szymborska, A., Zheng, T., Perovic, T., Hammoutene, A., Oliveira, M.B., Bartels-Klein, E., Hollfinger, I., et al. (2018). Primary cilia sensitize endothelial cells to BMP and prevent excessive vascular regression. J Cell Biol *217*, 1651-1665.

Wong, A.K., LLanos, P., Boroda, N., Rosenberg, S.R., and Rabbany, S.Y. (2017). A parallel-plate flow chamber for mechanical characterization of endothelial cells exposed to laminar shear stress. Cell Mol Bioeng *9*, 127-138.

CHAPTER 3:
THE ROLE OF VEGFR2 IN ENDOTHELIAL TRANSLUMINAL PILLAR FORMATION: A 3D MICROFLUIDIC STUDY

3.1 Introduction

Ischemic injury is a severe consequence of peripheral arterial disease (PAD), wherein atherosclerotic plaques within the femoral artery of the leg hinder oxygen delivery to the downstream skeletal muscle (Annex, 2013). This reduction in oxygen content also results in damage to the microvasculature responsible for feeding the tissue. Recently developed strategies used to reperfuse the deoxygenated skeletal muscle and restore muscle function include therapeutic angiogenesis, involving induction of angiogenesis in the affected leg and informed by current knowledge of sprouting angiogenesis (Cooke and Losordo, 2015). However, translation of these therapies from preclinical animal models to clinical trials has been met with limited success (Iyer and Annex, 2017).

Sprouting angiogenesis is the most well-understood form of angiogenesis and has been extensively studied to elucidate the biochemical regulation of the process. Central to the progression of blood vessel growth via this mechanism is vascular endothelial growth factor receptor 2 (VEGFR2) and its corresponding ligand vascular endothelial growth factor A (VEGF-A) (Carmeliet, 2000). VEGF-A-VEGFR2 binding on the surface of an endothelial cell (EC) lining a pre-existing blood vessel causes this cell to migrate into the surrounding tissue and lumenize (Ribatti and Crivellato, 2012).

However, another form of angiogenesis also exists called intussusceptive angiogenesis (IA), wherein ECs lining opposing sides of a pre-existing vessel

protrude into the flowing lumen and fuse to create a bridge termed an EC transluminal pillar. However, the exact biochemical and biomechanical regulation of this process remains elusive. Interestingly, recent research from our group has uncovered the importance of this mode of angiogenesis in repairing microvasculature damaged by ischemic injury in a mouse model of PAD (Arpino, 2017b).

VEGFR2 is known not only for its important role in sprouting angiogenesis, but also for its importance in shear stress sensing. ECs possess the unique ability to sense and respond to changes in the force created by the flowing blood, known as shear stress. These changes result in signalling cascades that ultimately modulate vascular tone, control cell proliferation, dictate the organization of the actin cytoskeleton, and more (Ando and Yamamoto, 2013). VEGFR2 itself forms a critical shear stress sensing complex at the junction of ECs, along with VE-Cadherin and PECAM-1, which upon stimulation by flow activates the Src-family kinases to phosphorylate VEGFR2 in a ligand-independent manner and trigger downstream activation of protein kinase B (Akt) and endothelial nitric oxide synthase (eNOS; Jin et al., 2003). Considered alongside its essential role in sprouting angiogenesis, the importance of VEGFR2 as a shear stress sensor could point to a potential role for VEGFR2 in intussusceptive angiogenesis.

Herein, we utilized the 3D microvessel model optimized in Chapter 2 to generate a co-culture of fluorescently labelled ECs transfected with siRNA designed to knockdown VEGFR2 or control siRNA. Notably, we report an increase in transluminal pillar formation in cells with reduced expression of VEGFR2. This finding uncovers novel information concerning the role of this essential endothelial cell-specific receptor in intussusceptive angiogenesis.

3.2 Methods

3.2.1 Microfluidic Device Fabrication

The microfluidic device used herein was designed in collaboration with the Poepping and Holdsworth Labs at the University of Western Ontario to generate one microchannel of dimensions 300 μm x 1000 μm x 1 cm (h, w, l). Microfluidic devices were constructed via soft lithography using a 10:1 mixture of polydimethylsiloxane (PDMS) elastomer base (10 g, Sylgard184, Sigma) and silicone curing agent (1 g, Sylgard184, Sigma). The negative mold containing the patterned PDMS was attached to a 35 mm glass-bottom dish (MatTek) spin-coated with a thin layer of PDMS using heat, after which tubing was inserted into the inlet and outlet of the channel to facilitate perfusion through the channel. Prior to cell culture, the channel was infused with 250 μg/mL of fibronectin (Sigma) at 37ºC and 5% CO_2 using a programmable syringe pump (NE-300, New Era Pump Systems, Inc.). Fibronectin was then washed from the channels via perfusion of Microvascular Endothelial Growth Media (EGM-MV) supplemented with EGM-MV Bulletkit (CC-3125, Lonza) containing 0.1 μg/mL L-ascorbic acid (Sigma) to prepare for cell seeding.

3.2.2 VEGFR2 Knockdown and Co-Culture of Fluorescent HUVECs in the Microfluidic Channel

Human umbilical vein endothelial cells (HUVECs) stably expressing either RFP or GFP (cAP-0001RFP, cAP-0001GFP, Angio-Proteomie) were cultured in EGM-MV. Upon reaching 60% confluency, passage 4-8 fluorescent HUVECs were transfected with 42 nM of either KDR/VEGFR2 siRNA or universal scrambled negative control siRNA (SR302557, SR3004, Origene) using Lipofectamine RNAiMAX (13778075, ThermoFisher Scientific). The transfection solution was applied for 6 h before fresh media was delivered and cells were left to recover at 37ºC and 5% CO_2 overnight. Before use in any experiments, the efficiency of the KDR/VEGFR2 siRNA knockdown was confirmed via reverse

transcription-quantitative PCR using SYBR Green chemistry and a ViiA 7 Real Time PCR System (ThermoFisher Scientific). Primers (Origene) for the human KDR gene were 5'-GGAACCTCACTATCCGCAGAGT-3' and 3'-CCAAGTTCGTCTTTTCCTGGGC-5'.

Following recovery from transfection, GFP-HUVECs and RFP-HUVECs were trypsinized and combined in equal amounts and resuspended in a mixture of EGM-MV and 8% Dextran (Sigma) in EGM-MV supplemented with L-ascorbic acid to encourage cell adherence to the channel surface. The cell suspension was generated at a bulk cell concentration of $3x10^6$ cells/mL and injected into the channel by hand guided by Hoffman modulation phase contrast microscopy (Axiovert S100 with Hoffman Modulation Contrast, Zeiss) to allow for visualization and control of the velocity of cells flowing through the channel. After 1 h, fresh media was perfused through the channel by hand and the channel was then left stationary at 37ºC and 5% CO_2 for 24 h to allow for cell growth into a complete EC monolayer. Similar methods were used for culture of non-fluorescent HUVECs within the microfluidic channel to assess the health of ECs and the cell monolayer within the channel.

3.2.3 Introduction of VEGFR2 Knockdown Co-Culture to Ultra-Low Shear Stress

The co-culture of fluorescently labelled VEGFR2 knockdown HUVECs and siRNA control HUVECs was introduced to flow via perfusion of fresh EGM-MV using a peristaltic pump (MiniPuls3, Gilson) at 14 RPM corresponding to 116 µL/min. The shear stress within the channel was calculated to be 1 dynes/cm^2 using an equation for parallel-plate flow chambers derived from the Navier-Stokes and continuity equations and used frequently in microfluidic studies (Ahsan and Nerem, 2010). Cells were subjected to a shear stress of 1 dynes/cm^2 for 4 h, a shear stress shown to produce adequate alignment and elongation in ECs lining the microfluidic channel. Flow of the medium was then reduced to 4

RPM on the peristaltic pump for 6 h, corresponding to a flow rate of 33 μL/min and resulting in shear stress of 0.29 dynes/cm^2.

Following induction of ultra-low shear stress, ECs were fixed via perfusion of 4% paraformaldehyde (Alfa Aesar, A11313) using programmable syringe pumps at 3 μL/min at room temperature for 25 min. Cells were then permeabilized using 0.1% Triton-X 100 (Sigma, T8787) in PBS delivered at 3 μL/min for 15 min, after which the solution was left stationary for 15 min and washed with PBS at 3 μL/min for 15 min. Blocking was performed by delivery of 5% donkey serum at 3 μL/min for 15 min before blocking solution was left stationary for 1.5-2 hr. Non-fluorescent HUVECs cultured within the microfluidic channel were then immunostained for endothelial cell-cell junctions by delivery of rabbit monoclonal anti-human VE-Cadherin primary antibody (1:200, D87F2, Cell Signalling Technologies) at 3 μL/min for 15 min. The device was then laid flat and empty 1 mL syringes were attached to the inlet and outlet tubing of both channels, ensuring tubing was at equal heights, to reduce residual flow within the channel. The device was stored in static conditions overnight at 4ºC. The next day, HUVECs were washed by infusion of PBS at 3 μL/min for 30 min. VE-Cadherin cell-cell junctions visualized using Alexa Fluor-546 conjugated donkey anti-rabbit IgG (1:400, A10040, Life Technologies) delivered at 3 μL/min for 15 min. The secondary antibody was left static at room temperature for 2 hr, and was then washed by delivery of PBS at 3 μL/min for 30 min. The F-actin cytoskeleton was visualized using Alexa Fluor-488 conjugated phalloidin (1:40, A12379, Invitrogen) delivered at 3 μL/min for 15 min, followed by a static phase for 30 min and a washing step with PBS delivered at 3 μL/min for 30 min. The nuclei of both non-fluorescent and fluorescently labelled HUVECs were visualized using DAPI (1000 nM, D9542, Sigma).

3.2.4 Confocal Microscopy and Analysis of Pillar Formation in HUVECs with and without Reduced VEGFR2 Expression

Endothelial cells lining the microfluidic channels were imaged using a Nikon A1R Confocal Laser Scanning System with a 40x oil-immersion objective and 405 nm, 488 nm, and 561 nm lasers. Regions of interest imaged using the Resonance scanning system were taken using up to 250, 0.25 μm-thick z-slices at a pixel resolution of 300 nm, while those imaged using the Galvano scanning system were taken using up to 150, 0.25 μm-thick z-slices with a pixel resolution of 300 nm. Z-slices were then reconstructed into 3D volume images, as well as maximum intensity planar projections and orthogonal projections using NIS Elements Software (Nikon).

Aspect ratio among RFP- and GFP-HUVECs was quantified using maximum planar projections of 14-20 regions of interest generated from z-slices of the same regions. Individual cells were outlined in ImageJ (NIH) and, using the "Centroid" and "Fit ellipse" tools, the major axis and minor axis through the centroid of the cell area were measured and divided to generate the aspect ratio. Pillar frequency among RFP- and GFP-expressing ECs was quantified using 3D volume images of dimensions 320 μm x 320 μm x 60 μm (XYZ) from 14-20 regions of interest reconstructed using z-slices of those same regions. The frequency of pillars among VEGFR2 knockdown and control cells was determined first by outlining a pillar-competent zone, defined as a 40 μm x 40 μm (XZ) zone along the bottom surface and side wall of the channel. Second, the number of cells participating in a pillar was expressed relative to the total cell number within that zone.

3.2.5 Statistics

Statistical analysis of pillar frequency was performed using Prism 8 (Graphpad Software). The data set was tested for normality using D'Agostino and Pearson omnibus normality test. Normally distributed data is presented as

mean ± SEM, and non-normally distributed data is presented as median and IQR. Comparisons among VEGFR2 knockdown and control cells were made using a t-test. Statistical significance was set at $p<0.05$.

3.3 Results

3.3.1 Endothelial Cells Lining a Rectangular Microfluidic Channel are Capable of Pillar Formation

Current research surrounding the biochemical and biomechanical regulation of intussusceptive angiogenesis remains elusive. However, some have suggested a role for VEGFR2 signalling due to its vital function in both sprouting angiogenesis and shear stress sensing (Gianni-Barrera et al., 2013; Gianni-Barrera et al., 2018). To explore the relationship between VEGFR2 and EC transluminal pillar formation, we utilized the protocol developed in Chapter 2 for the creation of a 3D in vitro microvessel model. To successfully generate a 3D microfluidic channel lined with a co-culture of RFP- and GFP-HUVECs transfected with siRNA designed to knockdown VEGFR2 or control siRNA, we designed and fabricated microchannels 300 μm in height, 1000 μm in width, and 1 cm in length. Notably, these channels had a larger volume to surface area ratio to increase the viability of transfected HUVECs (Sfriso et al., 2018). We lined the channel with non-transfected ECs to ensure this new channel design was capable of culturing a healthy EC monolayer, utilizing immunostaining techniques to visualize the F-actin cytoskeleton, VE-Cadherin intercellular junctions, and nuclei via confocal microscopy. Importantly, maximum intensity and orthogonal projections of ECs lining the channel generated a complete, continuous monolayer along the surfaces of the channel, as indicated by endothelial cell-cell junctions outlined by VE-Cadherin staining (Figure 3.1 A-B).

Interestingly, despite the 300 μm height of the microchannel used in this study, we observed EC transluminal pillar formation throughout the channel. Microfluidic devices used in this study were constructed in such a way as to

Figure 3.1 A 3D *in vitro* microvessel lined with a healthy endothelial cell monolayer.

A. Confocal planar projection of HUVECs lining the bottom surface of the microfluidic channel immunostained for VE-Cadherin (red) and stained for F-actin (green) (150 z-slices, 0.25 μm step-size) showing a healthy EC monolayer. **B-C.** Orthogonal projections of HUVECs lining the bottom surface and side wall of the microfluidic channel immunostained for VE-Cadherin (red) and stained for F-actin (green) showing a healthy EC monolayer (**B**) and the formation of endothelial cell pillars (arrows) within the microfluidic channel (**C**).

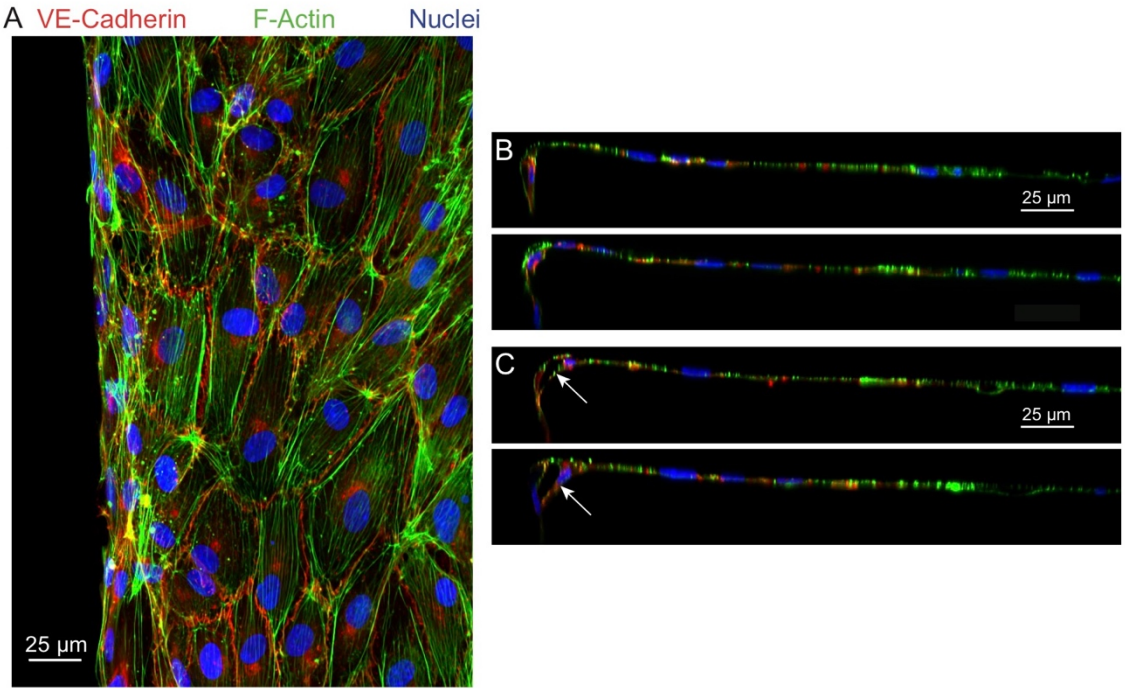
A VE-Cadherin
F-Actin
Nuclei
25 µm
B
25 µm
C
25 µm

generate “shoulders”. These “shoulders” were intentionally created by subtle over-curing of the PDMS-coated glass-bottom dish. This caused a shift in the PDMS side wall at the site of adhesion to the glass-bottom dish, generating a geometry wherein pillar formation was possible due to the existence of a shoulder with a height of 30-40 μm. Under ultra-low shear stress conditions alone, a proportion of ECs situated close to the side wall of the channel revealed a projection spanning across the channel lumen identified as a pillar (Figure 3.1 C). Moreover, these pillars also varied in appearance, with some existing as thin filopodial projections crossing the lumen, while other appeared to include nuclei within the structure of the pillar itself.

Reconstruction of the 3D volume image occurred by merging 150 z-slices (0.25 μm step-size), overlapping each image in the X, Y, and Z planes to create an image that could be reoriented to view the microfluidic channel at any angle. This 3D image showed a confluent EC monolayer along both the bottom surface and sidewall of the microfluidic channel as evidenced by nuclei and VE-Cadherin junctions. Close examination of the 3D volume image of an endothelial-based protrusion across the channel lumen provided evidence for the existence of an EC transluminal pillar within this microfluidic model (Figure 3.2). Notably, the EC monolayer was continuous on the channel wall behind the pillar and on the bottom surface surrounding the pillar when looking at the volume image from various angles. The pillar itself also remained consistent when viewed from various angles (see Online video 4.2 in Appendix A). It is also important to observe the definitive presence of multiple cellular organelles within 3D-reconstructed pillars, including VE-Cadherin-positive vesicles/junctions and nuclei. Taken together, the high-resolution imaging technique demonstrated that this pillar is not simply a visual overlay artifact, but a natural extension of the endothelial cell body bridging the adjacent walls of microchannel.

Figure 3.2 Controlled endothelial cell transluminal pillar formation in a 3D microvessel model.

A 3D volume image reconstructed from 150 confocal z-slices (0.25 μm) of HUVECs lining the bottom surface and side wall of a microfluidic channel immunostained for VE-Cadherin (red) and stained for F-actin showing an EC transluminal pillar (arrow) extending from the bottom surface and connected to an EC on the side wall of the channel (see Online Video 4.2 in Appendix A).

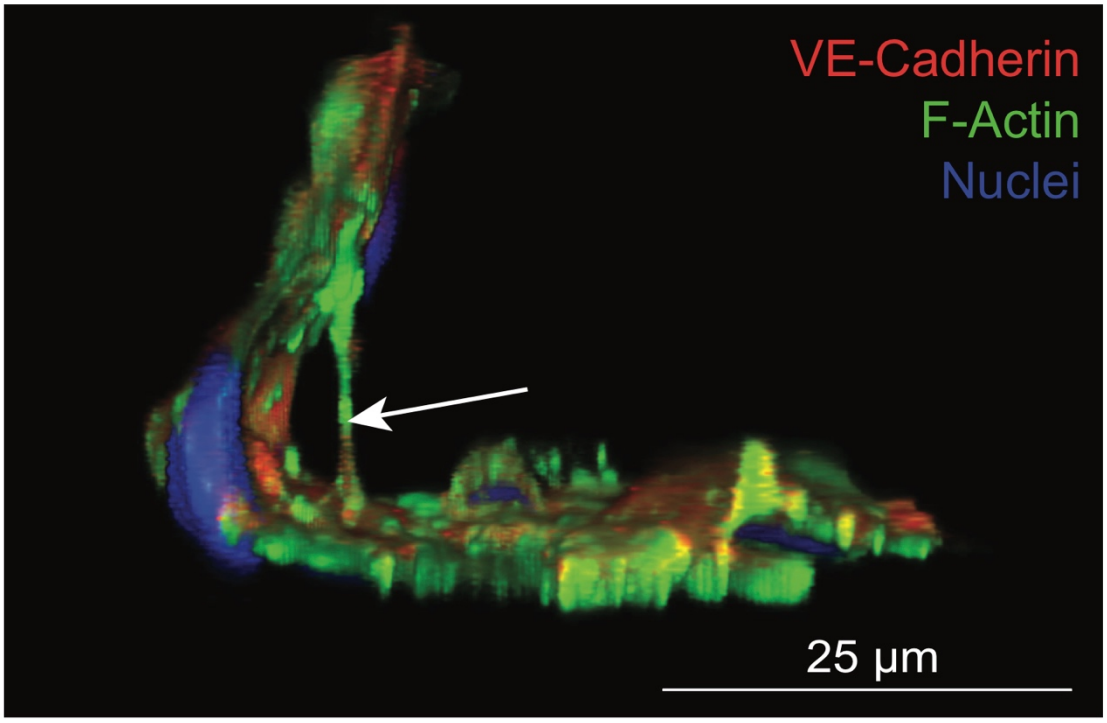
VE-Cadherin
F-Actin
Nuclei
25 µm

3.3.2 Reduced VEGFR2 Expression Results in Less Elongated Endothelial Cells

Following the generation of our 3D model capable of controlled EC pillar formation, we sought to directly examine the role of VEGFR2 expression, and consequently activity, in pillar formation. To do this, we created a co-culture of RFP- and GFP-expressing HUVECs differentially transfected with either VEGFR2 siRNA or control siRNA within the microchannel. Cells were seeded at a 2:3 knockdown to control cell ratio. Furthermore, cells transfected with VEGFR2 siRNA displayed a 88±5% knockdown efficiency (Figure 3.3 A). Under ultra-low shear stress conditions, cells transfected with control siRNA showed an aspect ratio of 2.7. However, transfection with VEGFR2 siRNA resulted in a 21% decrease in aspect ratio, suggesting reduction of VEGFR2 activity alone lead to cytoskeletal reorganization and rounding of ECs ($p<0.0001$, Figure 3.3 B).

3.3.3 Pillar Predisposition in Endothelial Cells with Reduced VEGFR2 Expression

As was the case with non-transfected ECs, pillars were identified as endothelial-based projections crossing the lumen of the channel, connecting with a cell on the adjacent wall (Figure 3.4 A-C). Under ultra-low flow, HUVECs transfected with control siRNA acted as pillar-forming cells, forming the endothelial-based protrusion, only 0.4% of the time. Remarkably, cells with reduced VEGFR2 expression showed a 12.5-fold increase in pillar formation under identical ultra-low shear stress conditions ($p=0.0008$, Figure 3.4 D). However, while the majority of pillar-forming cells were cells with reduced VEGFR2 expression, the pillar formed connected to a cell on the side wall of the channel that had high VEGFR2 expression.

The finding of increased pillar formation in cells with reduced VEGFR2 expression suggests the downregulation of VEGFR2 signalling could be essential

Figure 3.3 Endothelial cells with reduced VEGFR2 expression are less elongated in the direction of flow.

A. Graph showing VEGFR2 abundance measured by qPCR in HUVECs transfected with control siRNA and HUVECs transfected with siRNA designed to knockdown VEGFR2 (n=4 samples, p=0.0016). **B.** Plot from individual cell quantification showing a decrease in aspect ratio of HUVECs transfected with VEGFR siRNA (n=4 microfluidic devices, n=395 siCNTRL endothelial cells, n=379 siVEGFR2 endothelial cells, $p<0.0001$).

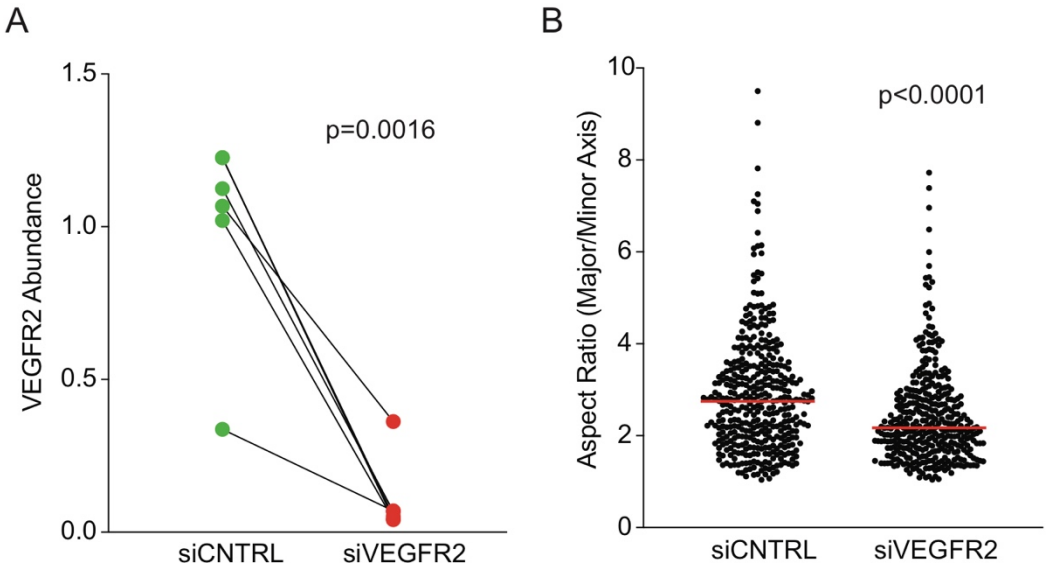
A
1.5
1.0
0.5
0.0
VEGFR2 Abundance
p=0.0016
siCNTRL
siVEGFR2
B
10
8
6
4
2
0
Aspect Ratio (Major/Minor Axis)
p<0.0001
siCNTRL
siVEGFR2

Figure 3.4 3D co-culture of endothelial cells transfected with control siRNA or VEGFR2 siRNA reveals an increase in pillar formation among cells with reduced VEGFR2 expression.

A-C. Confocal 3D volume images reconstructed using 150 z-slices (0.25 μm step-size) of the corner of a microfluidic channel lined with a co-culture of RFP- and GFP-HUVECs transfected with control siRNA or siRNA designed to knockdown VEGFR2 showing transluminal pillars (arrows) formed by HUVECs with reduced VEGFR2 expression (**A-B**, red, and **C**, green). **D.** Quantitative data of EC transluminal pillar frequency, determined by the number of control or VEGFR2 cells contributing to a pillar divided by the total number of cells within a pillar-competent zone, showing an increase in pillar formation in cells with reduced VEGFR2 expression (40 μm x 40 μm, XZ) (n=4 microfluidic devices, p=0.0008).

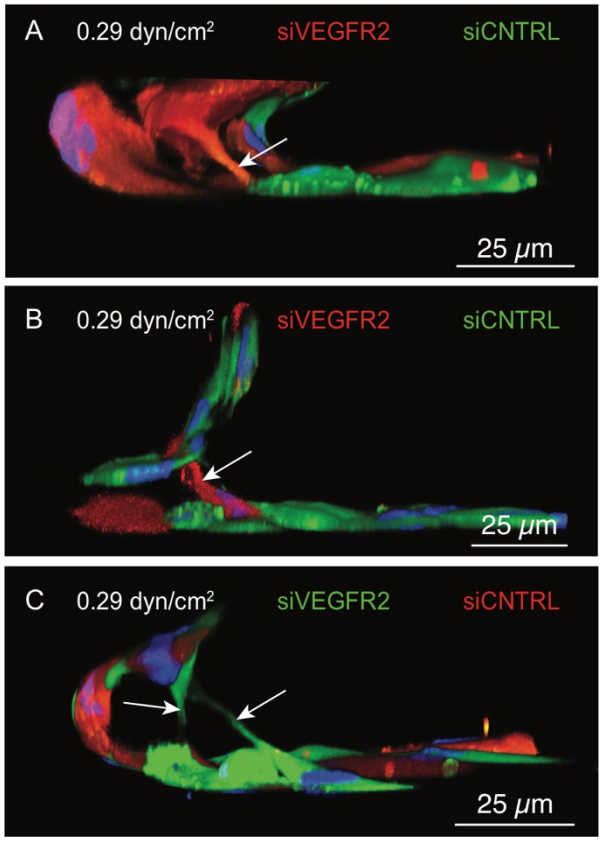
A
0.29 dyn/cm²
siVEGFR2
siCNTRL
25 μm
B
0.29 dyn/cm²
siVEGFR2
siCNTRL
25 μm
C
0.29 dyn/cm²
siVEGFR2
siCNTRL
25 μm

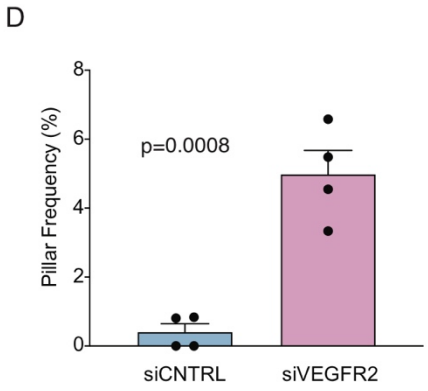
D
Pillar Frequency (%)
8
6
4
2
0
p=0.0008
siCNTRL
siVEGFR2

in the progression of intussusceptive angiogenesis via EC transluminal pillar formation.

3.4 Discussion

Recent research from our lab has shown that regeneration of damaged microvasculature following ischemic injury in the skeletal muscle relies heavily on intussusceptive angiogenesis. The biochemical and biomechanical regulation of intussusceptive angiogenesis is poorly understood. I have shown, using a novel model of pillar formation that, in contrast to sprouting angiogenesis, pillar formation is driven by ECs with low VEGFR2.

Studies performed in mouse skeletal muscles have shown an increase in pillar formation upon delivery of exogenous VEGF, suggesting a potential role for VEGFR2 signalling within this process of blood vessel growth (Gianni-Barrera et al., 2018). However, no direct evidence has been reported for the causal relationship between VEGFR2 and intussusceptive angiogenesis. In this study, we utilized a novel 3D microvessel model to induce controlled endothelial pillar formation, a critical step of intussusception. Co-culture of GFP- and RFP-HUVECs differentially transfected with VEGFR2 or control siRNA within the microfluidic channel revealed a 12.5-fold increase in pillar formation in cells with reduced VEGFR2 expression. This suggests the absence of VEGFR2 signalling is permissive to EC transluminal pillar formation in intussusceptive angiogenesis. This would appear to be in contrast with the aforementioned study showing an increase in intussusceptive angiogenesis in response to VEGF. However, there may be differences between newly formed blood vessels, as in the current study, and pre-existing blood vessels.

The microfluidic channel model used in this study was designed to be rectangular in geometry with the dimensions 300 μm x 1000 μm x 1 cm (h, w, l). Compared to our microfluidic channel designed to be square in nature discussed

in Chapter 2, this channel shows less of a resemblance to the normal physiology of the microvasculature being modelled. Despite this, the microfluidic model maintains its 3D design, which is essential to creating an *in vitro* microvessel model capable of controlled pillar formation. The design of the microfluidic channel, while seemingly less reflective of blood vessel geometry, was generated in a way that made co-culture of ECs differentially labelled with either VEGFR2 or control siRNA possible. The width to height ratio allowed for the optimization of the viability of cells within the channel, which were less resilient considering the numerous interventions (Sfriso et al., 2018). The rectangular shape therefore allowed for an increase in the volume to surface area ratio within the channel, favouring nutrient delivery to individual cells within the monolayer. Our microfluidic model featuring a co-culture of RFP- and GFP-HUVECs differentially labelled with either VEGFR2 siRNA or control siRNA presents the first 3D *ex vivo* assessment of VEGFR2 signalling in pillar formation. This unique approach allowed for direct control of VEGFR2 expression in a subset of ECs within a given population, with the ability to track the specific cell type in pillar formation and without confounding factors presented *in vivo*.

The finding of increased pillar formation in cells with reduced VEGFR2 expression reveals important information on the involvement of VEGFR2 in pillar formation. This receptor plays a major role in the more well-studied type of angiogenesis, sprouting angiogenesis–induction of the signalling cascade that ultimately triggers ECs lining a blood vessel lumen to migrate into the surrounding tissue and lumenize is dependent on activation of VEGFR2 by its ligand VEGF-A (Ribatti and Crivellato, 2012). Moreover, this receptor also participates in a complex with VE-Cadherin and PECAM-1 that is essential for endothelial cells' ability to sense and respond to changes in flow (Baeyens et al., 2016a). Given the importance of shear stress in pillar formation previously discussed and what is currently known about sprouting angiogenesis in the microvasculature, it is tempting to look to VEGFR2 as a regulator of

intussusceptive angiogenesis as well. To that end, studies using the mouse vasculature have suggested that increased doses of VEGF, and subsequently increased VEGFR2 activation, leads to pillar formation (Gianna-Barrera et al., 2013; Groppa et al., 2018). However, it is important to note that these studies observed dilation of the vessels as a direct result of VEGF delivery, while no measure of VEGFR2 activation was assessed on an individual cell basis. Moreover, recent research in our lab using a mouse model of ischemic injury within the skeletal muscle found instead that inhibition of VEGFR2 resulted in accentuated EC pillar formation within the early regenerating microvasculature (Arpino, 2017b). The finding of increased pillar formation among cells with reduced VEGFR2 activity therefore directly supports a role for VEGFR2 in inhibiting pillar formation. Taken together with the impact of shear stress elaborated in Chapter 2, we stipulate that cells with a reduced VEGFR2 signalling capacity are predisposed to form transluminal pillars, a process which is then encouraged by introduction of ultra-low shear stress.

In summary, the microfluidic model developed herein enables direct study of the role of VEGFR2 in endothelial pillar formation. From this, we discovered that ECs with a lower capacity for activating VEGFR2 were primed to participate in pillar formation under ultra-low flow conditions. These findings further characterize the biomechanical and biochemical cascades of intussusceptive angiogenesis, suggesting reconsideration of current therapeutic angiogenesis techniques used to treat patients with peripheral vascular disease.

3.5 References

Ahsan, T., and Nerem, R.M. (2010). Fluid shear stress promotes an endothelial-like phenotype during the early differentiation of embryonic stem cells. Tissue Eng Part A *16*, 3547-3553.

Ando, J., and Yamamoto, K. 2013. Flow detection and calcium signalling in vascular endothelial cells. Cardiovasc Res *99*, 260-268.

Annex, B.H. (2013). Therapeutic angiogenesis for critical limb ischaemia. Nat Rev Cardiol *10*, 387-396.

Arpino, G.M. (2017b). Angiogenesis And Neo-Microcirculatory Function In Diseased Tissue Revealed By Intravital Microscopy. Electronic Thesis and Dissertation Repository, 4731.

Baeyens, N., Bandyopadhyay, C., Coon, B.G., Yun, S., and Schwartz, M.A. (2016a). Endothelial fluid shear stress sensing in vascular health and disease. J Clin Invest *126*, 821-828.

Carmeliet, P. (2000). Mechanisms of angiogenesis and arteriogenesis. Nat Med *6*, 389-395.

Cooke, J.P, and Losordo, D.W. (2015). Modulating the vascular response to limb ischmia: angiogenic and cell therapies. Circ Res *9*, 1561-1578.

Gianna-Barrera, R., Butschkau, A., Uccelli A., Certelli, A., Valente, P., Bartolomeo, M., Groppa, E., Burger, M.G., Hlushchuk, R., Heberer, M. et al. (2018). PDGF-BB regulates splitting angiogenesis in skeletal muscle by limiting VEGF-induced endothelial proliferation. Angiogenesis *21*, 883-900.

Gianna-Barrera, R., Trani, M., Fontanellaz, C., Heberer, M., Djonov, V., Hlushchuk, R., and Banfi, A. (2013). VEGF over-expression in skeletal muscle induces angiogenesis by intussusception rather than sprouting. Angiogenesis *16*, 123-136.

Groppa, E., Brkic, S., Uccelli, A., Wirth, G., Korpisalo-Pirinen, P., Filippova, M., Dasen, B., Sacchi, V., Muraro, M.G., Trani, M. et al. (2018). EphrinB2/EphB4 signaling regulates non-sprouting angiogenesis by VEGF. EMBO Rep *19*, e45054.

Iyer, S.R., and Annex, B.H. (2017). Therapeutic Angiogenesis for Peripheral Artery Disease: Lessons Learned in Translation Science. JACC Basic Transl Sci *2*, 503-512.

Ribatti, D., and Crivellato, E. (2012). "Sprouting angiogenesis", a reappraisal.

Dev Biol *372*, 157-165.

Sfriso, R., Zhang, S., Bichsel, C.A., Steck, O., Despont, A., Guenat, O.T., and Rieben, R. (2018). 3D artificial round section micro-vessels to investigate endothelial cells under physiological flow conditions. Sci Rep *8*, 5898.

CHAPTER 4:
GENERAL DISCUSSION AND CONCLUSIONS

The findings presented in this thesis uncover new insights into the biochemical and biomechanical regulation of intussusceptive angiogenesis via endothelial cell (EC) pillar formation. In this study, I present the first *in vitro* method for the study of transluminal pillar formation. I developed the first 3D *ex vivo* microvessel model created using polydimethylsiloxane (PDMS) microfluidics capable of controlled recreation of an EC transluminal pillar. Using this model, I established several new insights into pillar formation. First, I discovered a permissive role for ultra-low shear stress in pillar formation, reporting an 8.8-fold increase in pillar formation under ultra-low shear stress compared to physiologic shear stress conditions. Second, I discovered the potential participation of primary cilia in the mechanical regulation of transluminal pillar formation, reporting an increase in ADP-ribosylation factor-like protein 13b (ARL13b) density under ultra-low shear stress. Remarkably, primary cilia were also observed within the pillar structure. Third, I utilized the 3D microvessel model developed herein to directly investigate the role of vascular endothelial growth factor receptor 2 (VEGFR2) activation in pillar formation. Under ultra-low shear stress, I reported a 22% decrease in phosphorylated VEGFR2 (pVEGFR2) abundance, indicating a decrease in VEGFR2 activation. Notably, I also observed a 12.5-fold increase in pillar formation among cells with decreased VEGFR2 expression. Based on the findings herein, I propose a permissive role for ultra-low shear stress as a biomechanical regulator of pillar formation. Biochemical regulation of pillar formation is then potentially regulated by primary cilia and, in parallel, occurs in cells with a lower capacity for VEGFR2 activation.

4.1 Development of a Novel 3D Microvessel Model using Microfluidics

The methodological approach developed in this study to characterize the biomechanical and biochemical regulation of EC pillar formation was accomplished using microfluidics. I was able to create the first *ex vivo* 3D microvessel model enabling controlled pillar formation, utilizing the ability to manipulate flow that is inherent to microfluidics. Microfluidics is a recent development within the field of bioengineering that focuses on the use of channels microns in size to study fluid flow. This method of study has many advantages compared to systems such as parallel flow plates, including a customizable channel design in terms of both the network of microchannels and channel geometry, and the ability to control and manipulate the velocity of fluid flow within the channel. Therefore, in the context of cellular models, this approach provides a unique opportunity to study vascular biology, specifically EC response to shear stress.

Endothelial cell microfluidic models have been used extensively to study: 1) EC permeability (Akbari et al., 2018), 2) EC migration (Shih et al., 2019), 3) the function of the blood-brain barrier (Ahn et al., 2020; Park et al., 2019), 4) tumor angiogenesis (Amann et al., 2017), and 5) wound healing and hematologic diseases (Lin et al., 2019; Tsai et al., 2012), among others. The large variability in the application contexts of microfluidic devices, consequently, leads to a wide variety of microfluidic channel designs. However, most microfluidic studies utilize a rectangularly shaped channel or a channel with multiple branching points, choosing to render the height of the channel similar to blood vessel geometry, but not the width (Kong et al., 2016; Myers et al., 2012). These design features help to compensate for the pressure created within the channel by high flow rates. The model developed in Chapter 2 of this study is therefore unique in that the height and width are equal, each being 100 μm in size, and create a microvessel model more reflective of *in vivo* blood vessel physiology. The microfluidic channel design in Chapter 3 was similar to others in the literature,

with a height of 300 μm and a width of 1000 μm. In this case, the microfluidic design was used to increase the viability of cells already less resilient to cell culture due to multiple interventions, including ultra-low flow, siRNA challenge and, particularly VEGFR2 knockdown (Sfriso et al., 2018).

Moreover, the 3D nature of the microfluidic channel was strategically used to recreate an environment conducive for pillar formation, wherein cells were lining all four walls and were therefore capable of bridging between two adjacent channel walls. Interestingly, within a literature search of endothelialized microfluidic models, few intentionally aim to develop a similar 3D microvascular model, while most focus on cells lining the bottom surface of the channel (Maoz, et al., 2018). The microfluidic microvessel model developed in this study therefore advances the field by rationally utilizing the 3D nature of microchannels to create an environment conducive to pillar formation for the first time *ex vivo*.

4.2 Ultra-Low Flow is Permissive to Transluminal Pillar Formation

Utilizing the full circumferential lining of a microfluidic channel with ECs, I characterized both EC morphology and pillar formation under ultra-low shear stress. First, I discovered changes in the shape, alignment, and actin cytoskeletal organization of cells under ultra-low shear stress. Capillaries experience a shear stress magnitude of 10-20 dyn/cm^2 in vivo (Aird, 2005). Endothelial cells under these conditions have been well-studied and shown to increase their alignment in the direction of flow, becoming elongated in shape (Tzima et al., 2005). Moreover, the actin cytoskeleton under high shear stress is organized into a high abundance of F-actin stress fibres, contractile bundles of actin filaments that use focal adhesions to anchor the cytoskeleton to the extracellular matrix (Tojkander et al., 2012). Under ultra-low shear stress, I identified an overall decrease in cellular alignment, showing cells more randomly oriented to the direction of flow, and a decrease in cellular elongation, associated with a more rounded cell shape. I also observed a decrease in the density of stress fibres, while actin was

reorganized into cortical bundles along the cell border. Interestingly, EC responses to low shear stress have largely been studied in the context of disturbed or turbulent flow, wherein flow patterns are irregular and unpredictable (Tovar-Lopez et al., 2019). A study by Park et al. (2011) was the only study found in a literature search to interrogate laminar flow under shear stress conditions <1 dyn/cm^2, demonstrating the degree to which ultra-low shear stress is understudied. This study found that, under ultra-low flow, ECs are randomly oriented, showing little alignment with the direction of flow with a high incidence of cortical actin. This directly supports the findings reported herein.

The finding of increased pillar formation under ultra-low shear stress conditions presents novel information on the biomechanical regulation of intussusceptive angiogenesis. Specifically, this is the first study to: a) generate an *ex vivo* microvessel model capable of reconstitution of EC transluminal pillars and b) provide direct evidence of the permissive role of ultra-low shear stress in pillar formation.

Interestingly, research into the role of shear stress in the progression of intussusceptive angiogenesis via pillar formation leads to divided understandings. For many years, researchers had proposed that high shear stress was critical for the induction of EC transluminal pillar formation (Egginton et al., 2001; Zhou et al., 1998). A study performed by Ogawa dating back to 1977 gave one of the first descriptions of intussusceptive angiogenesis using electron microscopy, wherein he postulated that increased blood flow to the rat skeletal muscle due to exercise lead to an increase in vascularity by intussusception. However, recent research using computational modeling of angiogenesis in the chick chorioallantoic membrane (CAM) microvasculature has shown different findings. It suggested that pillar formation occurs in “dead zones” where the shear stress levels are below 1 dyn/cm^2, and that pillars are constrained by

surrounding areas of high shear stress (Lee et al., 2011). These computational models directly support the findings reported herein.

Moreover, the findings within the microfluidic model I developed are in keeping with findings previously reported by our research group using a mouse model of peripheral arterial disease (PAD), wherein a high incidence of transluminal pillars was observed in early regenerating microvessels alongside a ultra-low shear stress condition (Arpino, 2017b). My discovery of increased pillar formation under conditions of ultra-low shear stress therefore presents the first concrete *in vitro* evidence of the permissive role of low shear stress in pillar formation. Given this information, my findings raise the prospect to reevaluate current methods of therapeutic angiogenesis in patients with severe PAD, which rely heavily on pathways promoting sprouting angiogenesis as opposed to intussusception (Said et al., 2013).

4.3 Microfluidic Modeling of Pillar Morphogenesis

Intussusceptive angiogenesis is the process of angiogenesis whereby ECs lining a preexisting blood vessel will protrude into the flowing lumen and connect to cells on the opposing wall of the vessel, forming an endothelial-based projection known as a transluminal pillar (Djonov et al., 2000). Multiple pillars will form down the length of the vessel, which will then expand along the long axis of the vessel and fuse with neighbouring pillars to split one large vessel into two smaller vessels (Gianna-Barrera et al., 2013; Mentzer and Konderding, 2014). Interestingly, in the 3D microvessel model developed in this study, I observed a spectrum of pillar structures, as well as multiple pillars within the same region of interest, that parallel the *in vivo* morphogenesis of pillars described. Frequently, I identified transluminal pillars with an appearance of slender endothelial-based projections immuno-positive of F-actin. However, I also observed transluminal pillars that were wider in nature, appearing to have expanded down the long axis within the channel. Many of these pillars contained a nucleus within the widened

base of the pillar structure, but clearly above the plane of the monolayer. Furthermore, there was one instance of pillar overlap–in this case, two neighboring pillars had appeared to widen down the axis of the channel and fuse, overlapping at their bases just above the cell monolayer along the bottom surface of the channel.

While the exact mechanism of pillar extension is unknown, the variation in pillar structure reported herein could be considered as an *in vitro* model for pillar morphogenesis of different phases/stages. The first phase of initial pillar formation would occur via endothelial-based projections across the channel/lumen that appear slender. The second phase would then involve the extension of pillar along the long axis of the channel, correlated with the migration of the nucleus into the pillar. This would then be followed by a theoretical final phase, wherein neighbouring pillars fuse to create a secondary lumen. This latter phase might be observed with future developments of microfluidic designs and culture conditions (such as circulating growth factors/cytokines, basement membrane-like ECM, mural cell or leukocyte co-culture). Taken together, the model developed in this study demonstrates a novel in vitro methodology to interrogate the occurrence and progression of intussusceptive angiogenesis, providing new insights into pillar morphogenesis without potential confounding factors seen in studies performed in vivo.

4.4 Mechanosensing Regulators of Pillar Formation

Transluminal pillar formation, as discussed above, was shown to correlate directly with changes in the magnitude of shear stress sensed by ECs, suggesting mechanosensing is crucial for EC pillar morphogenesis. To further characterize EC transluminal pillar formation, I studied several candidate shear stress sensors previously reported in the literature to have a specific relevance to EC functionality (Ando and Yamamoto, 2013). My thesis work described herein focuses explicitly on the expression and subcellular localization of shear sensors

including primary cilia and activation of VEGFR2 in ECs circumferentially lining a microfluidic channel. I further characterize the responses of these sensors to a pillar-permissive ultra-low shear stress. Under these shear stress conditions, I observed: 1) an increase in primary cilia via ARL13b, 2) a decrease in pVEGFR2 expression, and 3) an increase in pillar formation in ECs with reduced VEGFR2 expression. Furthermore, both primary cilia and activation of VEGFR2 were discovered within the pillar structure protruding into the lumen of the channel. Notably, pVEGFR2 was localized within the middle of the pillar and lateralized to the upstream side of the pillar, signifying elevated levels of shear stress in this region. While the increase in primary cilia within ECs under ultra-low flow alludes to an active role for primary cilia in pillar formation, the decrease in pVEGFR2 and increase in pillar formation in cells with reduced VEGFR2 suggests that the downregulation of VEGFR2 signalling promotes pillar formation. Taken together, these findings suggest that particular shear stress sensors have differing roles in the formation and progression of pillar morphogenesis and outline the potential for specific signalling pathways important for regulating this process.

Furthermore, the findings outlined above support the notion that transluminal pillar formation in intussusceptive angiogenesis is encouraged when ECs adopt a flow-seeking behaviour. Under conditions of ultra-low shear stress, ECs lining a microvessel may struggle to sense shear stress caused by the flowing blood. The increase in primary cilia demonstrated in this study would therefore act as a direct response to the cell's difficulty to sense flow: by increasing primary cilia, cells within the monolayer increase the presence of shear stress sensors on their plasma membranes and magnify the signal transmitted by these sensors to the cell. In a similar manner, pillar formation could therefore be considered as a migratory act of flow-seeking. Endothelial cells lining the vessel wall with a diminished capacity to activate VEGFR2 then form a bridge across the flowing lumen, migrating towards the centre of the vessel lumen where shear stress would be higher and allowing the cell to sense

the magnitude of shear stress more easily. This model of pillar formation is supported by the discovery of pVEGFR2 localized and lateralized to the middle, upstream side of EC transluminal pillars in this study, suggesting elevated shear stress within the lumen of the channel. Interestingly, a computational CAM model of EC transluminal pillars by Filipovic et al. (2009) have demonstrated elevated shear stress in the mid-section and on the upstream side of EC pillars, further supporting this flow-seeking model of pillar formation.

Finally, the finding of increased pillar formation under ultra-low shear stress in ECs with reduced VEGFR2 expression is interesting. Sprouting angiogenesis is the most commonly understood and well-studied form of angiogenesis and knowledge of the regulatory mechanisms of this process have been heavily relied upon to inform strategies of therapeutic angiogenesis in patients with PAD (Gupta et al., 2009; Cooke and Losordo, 2015). As such, it is tempting to consider intussusceptive angiogenesis in relation to sprouting, specifically in terms of biochemical regulation. Given the crucial importance of VEGFR2 signalling in sprouting (Ribatti and Crivellato, 2012), one could draw the conclusion that VEGFR2 signalling may also play an important role in intussusception. Studies performed in the vasculature of the mouse skeletal muscle have even suggested this is the case (Gianna-Barrera et al., 2018; Groppa et al., 2018). However, the results in my work suggest instead that the suppression of VEGFR2 signalling is permissive to EC pillar formation. Moreover, previous research performed by our research group in a mouse model of ischemic injury similarly demonstrated that blocking VEGFR2 activation led to an increase in pillar formation in vivo, supporting my findings (Arpino, 2017b). Therefore, I propose that VEGFR2 activity plays a role instead in the decision of endothelial cell to undergo intussusceptive pillar formation. Under high shear stress conditions, VEGFR2 would be activated in a ligand-independent manner, contributing to EC elongation and preventing pillar formation from occurring. However, under ultra-low shear stress conditions, the ligand-independent

activation of VEGFR2 decreases, enabling more individualized cells to undergo pillar formation. This hypothetical scenario is supported by my finding that siRNA-mediated VEGFR2 downregulation enhances the pillar formation of individual ECs under ultra-low shear condition.

In summary, based on the findings in my thesis study, I propose a model of EC transluminal pillar formation wherein ECs adopt a flow-seeking behaviour. Specifically, ultra-low shear stress conditions result in low shear inputs from blood flow and create a need for ECs to become more sensitive to shear. This results in an increase in primary cilia on the plasma membrane of cells within the monolayer, magnifying shear stress signalling. Endothelial cells with a reduced capacity for activation of VEGFR2 are in parallel primed to protrude into the lumen of the vessel where shear stress is elevated and information concerning the magnitude and direction of shear can be more easily sensed by the cell and, possibly, communicated to the EC monolayer.

4.5 Future Directions

The findings of 1) pillar morphogenesis in the progression of intussusceptive angiogenesis and 2) the functional roles of shear stress sensors in transluminal pillar formation require further investigation, as these phenomena are vital to our understanding of intussusceptive angiogenesis and will need to be considered when developing novel therapies for PAD.

To further study pillar morphogenesis, it is important to consider the progression of pillar formation and extension over time. While my findings have suggested that pillar formation occurs in a phased manner whereby a slender pillar will widen and fuse with neighbouring pillars, the exact mechanism of pillar formation remains unknown. Specifically, aside from a protrusive event hypothesis, it is equally possible that formation of a pillar occurs when a cell previously lining the wall of the vessel delaminates from the established basement membrane and moves into the lumen, connecting to a cell on the

adjacent or opposing vessel wall. To interrogate this further, the model I have developed in this study could be used to generate a 3D live cell imaging experiment with fluorescently labelled cells using confocal microscopy. Real time imaging of cells subjected to ultra-low shear would allow the investigation of pillars as they form.

It is also important to further investigate the functional roles of shear stress sensors in pillar formation. My findings have revealed important information concerning primary cilia and VEGFR2, two prominent endothelial shear stress sensors, but there are many others that could contribute to pillar formation, as well as the decision to undergo intussusception instead of sprouting. Immunostaining of select shear stress sensors in my microfluidic design and in microvessels undergoing intussusception, such as GPR68, Notch1, Piezo1, β1 integrin, or Alk1, could quickly and efficiently uncover more precise signalling cascade(s) involved in the regulation of intussusceptive angiogenesis (Ando and Yamamoto, 2013). Moreover, loss-of-function experiments on select shear sensors, such as RNAi- or CRISPR/Cas9-based gene inactivation are warranted to establish their functions in pillariogenesis.

The landscape of shear stress sensors in pillar formation could also be further explored via RNA sequencing. While it may be technically difficult to remove cells from the channel surface without negative consequences, genome-wide sequencing of these cells could reveal important changes in gene regulation in ECs subjected to ultra-low shear stress. Moreover, because of the 3D nature of the microfluidic model developed, these cells would reflect ECs lining microvessels *in vivo* more closely and may present new information regarding cell-cell communication within a 3D environment.

4.6 Conclusions

In conclusion, I have developed the first 3D *ex vivo* microvessel model using microfluidics capable of controlled EC transluminal pillar formation. This

model was then used to interrogate the biomechanical and biochemical regulation of pillar formation. I discovered that, under ultra-low shear stress conditions, ECs had increased primary cilia. I also proved that ECs with a low capacity for VEGFR2 activation are primed to form an EC transluminal pillar under ultra-low shear conditions. These findings uncover vital information on the initiation and progression of intussusceptive angiogenesis in relevance with ischemic skeletal muscle that could inform the development of therapeutic strategies for PAD.

4.7 References

Ahn, S.I., Sei, Y.J., Park, H.J., Kim, J., Ryu, Y., Choi, J.J., Sung, H.J., MacDonald, T.J., Levey, A.I., and Kim, Y. (2020). Microengineered human blood-brain barrier platform for understanding nanoparticle transport mechanisms. Nat Commun *11*, 175.

Aird, W.C. (2005). Spatial and temporal dynamics of the endothelium. J Thromb Haemost *3*, 1392-1406.

Akbari, E., Spychalski, G.B, Rangharajan, K.K., Prakash, S., and Song, J.W. (2018). Flow dynamics control endothelial permeability in a microfluidic vessel bifurcation model. Lab Chip *18*, 1084-1093.

Amann, A., Zwierzina, M., Koeck, S., Gamerith, G., Pechriggl, E., Huber, J.M., Lorenz, E., Kelm, J.M., Hilbe, W., Zwierzina, H., et al. (2017). Development of a 3D angiogenesis model to study tumour – endothelial cell interactions and the effects of anti-angiogeneic drugs. Sci Rep *7,* 2963.

Ando, J., and Yamamoto, K. 2013. Flow detection and calcium signalling in vascular endothelial cells. Cardiovasc Res *99*, 260-268.

Arpino, G.M. (2017b). Angiogenesis And Neo-Microcirculatory Function In Diseased Tissue Revealed By Intravital Microscopy. Electronic Thesis and Dissertation Repository, 4731.

Cooke, J.P., and Losordo, D.W. (2015). Modulating the vascular response to limb

ischemia: angiogenic and cell therapies. Circ Res *116*, 1561-1578.

Djonov, V., Schmid, M., Tschanz, S.A., and Burri, P.H. (2000). Intussusceptive angiogenesis: its role in embryonic vascular network formation. Circ Res *86*, 286-292.

Egginton, S., Zhou, A.L., Brown, M.D., and Hudlická, O. (2001). Unorthodox angiogenesis in skeletal muscle. Cardiovasc Res *49*, 634-646.

Filipovic, N., Tsuda, A., Lee, G.S., Miele, L.F., Lin, M., Konerding, M.A., and Mentzer, S.J. (2009). Computational flow dynamics in a geometric model of intussusceptive angiogenesis. Microvasc Res *78*, 286-293.

Gianna-Barrera, R., Butschkau, A., Uccelli A., Certelli, A., Valente, P., Bartolomeo, M., Groppa, E., Burger, M.G., Hlushchuk, R., Heberer, M. et al. (2018). PDGF-BB regulates splitting angiogenesis in skeletal muscle by limiting VEGF-induced endothelial proliferation. Angiogenesis *21*, 883-900.

Gianna-Barrera, R., Trani, M., Fontanellaz, C., Heberer, M., Djonov, V., Hlushchuk, R., and Banfi, A. (2013). VEGF over-expression in skeletal muscle induces angiogenesis by intussusception rather than sprouting. Angiogenesis *16*, 123-136.

Groppa, E., Brkic, S., Uccelli, A., Wirth, G., Korpisalo-Pirinen, P., Filippova, M., Dasen, B., Sacchi, V., Muraro, M.G., Trani, M. et al. (2018). EphrinB2/EphB4 signaling regulates non-sprouting angiogenesis by VEGF. EMBO Rep *19*, e45054.

Gupta, R., Tongers, J., and Losordo, D.W. (2009). Human studies of angiogenic gene therapy. Circ Res *105*, 724-736.

Kong, J., Luo, Y., Jin, D., An, F., Zhang, W., Liu, L., Li, J., Fang, S., Li, X., Yang, X., et al. (2016). A novel microfluidic model can mimic organ-specific metastasis of circulation tumor cells. Oncotarget *7*, 78421-78432.

Lee, G.S., Filipovic N., Lin, M., Gibney, B.C., Simpson, D.C., Konerding, M.A., Tsuda, A., and Mentzer, S. (2011). Intravascular pillars and pruning in the

extraembryonic vessels of chick embryos. Dev Dyn *240*, 1335-1343.

Lin, J.Y., Lo, K.Y., and Sun, Y.S. (2019). A microfluidics-based wound-healing assay for studying the effects of shear stresses, wound widths, and chemicals on the wound-healing process. Sci Rep *9,* 20016.

Maoz, B.M., Herland, A., FitzGerald, E.A., Grevesse, T., Vidoudez, C., Pacheco, A.R., Sheehy, S.P., Park, T.E., Dauth, S., Mannix, R., et al. (2018). A linked organ-on-a-chip model of the human neurovascular unit reveals the metabolic coupling of endothelial and neuronal cells. Nat Biotechnol *36*, 865-874.

Mentzer, S.J., and Konerding, M.A. (2014). Intussusceptive angiogenesis: expansion and remodeling of microvascular networks. Angiogenesis *17*, 499-509.

Myers, D.R., Sakurai, Y., Tran, R., Ahn, B., Hardy, E.T., Mannino, R., Kita, A., Tsai, M., and Lam, W.A. (2012). Endothelialized microfluidics for studying microvascular interactions in hematologic diseases. J Vis Exp *64*, e3958.

Ogawa, Y. (1977). On the fine structural changes of the microvascular beds in skeletal muscle. J Yokohama City Univ Ser Sport Sci Med *6*, 1-19.

Park, J.Y., White, J.B., Walker, N., Kuo, C.H., Cha, W., Meyerhoff, M.E., and Takayama, S. (2011). Responses of endothelial cells to extremely slow flows. Biomicrofluidics *5*, 22211.

Park, T.E., Mustafaoglu, N., Herland, A., Hasselkus, R., Mannix, R., FitzGerald, E.A., Prantil-Baun, R., Watters, A., Henry, O., Benz, M., et al. (2019). Hypoxia-enhanced Blood-Brain Barrier Chip recapitulates human barrier function and shuttling of drugs and antibodies. Nat Commun *10*, 2621.

Ribatti, D., and Crivellato, E. (2012). "Sprouting angiogenesis", a reappraisal. Dev Biol *372*, 157-165.

Said, S.S., Pickering, J.G., and Mequanint, K. (2013). Advances in growth factor delivery for therapeutic angiogenesis. J Vasc Res *50*, 35-51.

Sfriso, R., Zhang, S., Bichsel, C.A., Steck, O., Despont, A., Guenat, O.T., and

Rieben, R. (2018). 3D artificial round section micro-vessels to investigate endothelial cells under physiological flow conditions. Sci Rep *8*, 5898.

Shih, H.C., Lee. T.A., Wu, H.M., Ko, P.L., Liao, W.H., and Tung, Y.C. (2019). Mircofluidic Collective Cell Migration Assay for Study of Endothelial Cell Proliferation and Migration under Combinations of Oxygen Gradients, Tensions, and Drug Treatments. Sci Rep *9*, 8234.

Tojkander, S., Gateva, G., and Lappalainen, P. (2012). Actin stress fibres—assembly, dynamics and biological roles. J Cell Sci *125*, 1855-1864.

Tovar-Lopez, F., Thurgood, P., Gilliam, C., Nguyen, N., Pirogova, E., Khoshmanesh, K., and Baratchi, S. (2019). A Microfluidic System for Studying the Effects of Disturbed Flow on Endothelial Cells. Front Bioeng Biotechnol *7*, 81.

Tsai, M., Kita, A., Leach, J., Rounsevell, R., Huang J.N., Moake, J., Ware, R.E., Fletcher, D.A., and Lam, W.A. (2012). In vitro modeling of the microvascular occlusion and thrombosis that occur in hematologic diseases using microfluidic technology. J Clin Invest *122*, 408-418.

Tzima, E., Irani-Tehrani, M., Kiosses, W.B., Dejana, E., Schultz, D.A., Engelhardt, B., Cao, G., Delisser, H., and Schwartz, M. A. (2005). A mechanosensory complex that mediates the endothelial cell response to fluid shear stress. Nature *437*, 426-31.

Zhou, A., Egginton, S., Hudlická, O., and Brown, M.D. (1998). Internal division of capillaries in rat skeletal muscle in response to chronic vasodilator treatment with alpha1-antagonist prazosin. Cell Tissue Res *293*, 292-303.

APPENDIX

Appendix A: Legends for Supplemental Video Files

Online Video 4.1: Video rotating along the X-axis of a 3D volume image reconstructed from 150 confocal z-slices (0.25 μm step-size) showing multiple endothelial cell transluminal pillars stained for F-actin and nuclei bridging from the bottom surface to the side wall of a microfluidic channel.

Online Video 4.2: Video rotating along the X-axis of a 3D volume image reconstructed from 150 confocal z-slices (0.25 μm step-size) showing an endothelial cell transluminal pillar immunostained for VE-Cadherin and stained for F-actin bridging from the bottom surface to the side wall of a microfluidic channel lined with a confluent layer of endothelial cells.

CURRICULUM VITAE

Emma Prescott

MSc Candidate

EDUCATION

The University of Western Ontario — London, ON
MSc, Medical Biophysics (Candidate) — 2018-Present
Thesis: *A 3D Microvessel Model for the Study of Endothelial Cell Transluminal Pillar Formation*

The University of Western Ontario — London, ON
Bachelor of Medical Sciences, Honors Specialization in Biochemistry and Cell Biology — 2014-2018

Robert F. Hall Catholic Secondary School — Caledon East, ON
Ontario Secondary School Diploma — 2010-2014

RESEARCH EXPERIENCE

The University of Western Ontario — London, ON
Honors Undergraduate Researcher; — 2017-2018
Supervisor: Dr. J. Geoffrey Pickering

- Worked with Dr. Tamie Poepping and Dr. David Holdsworth at The University of Western Ontario to develop a novel *in-vitro* microvessel model using microfluidics

- Used novel microfluidic model to characterize endothelial cell responses to ultra-low flow rates seen in diseased-states, namely in the skeletal muscle of peripheral vascular disease models

The University of Western Ontario London, ON
Research Assistant; 2016-2017
Supervisor: Dr. Jamie Kramer

- Aided in the upkeep and preparation of behavioral assays using *Drosophila* in order to characterize the role of epigenetic regulation in intellectual disability.

LEADERSHIP EXPERIENCE

EMPLOYMENT

The University of Western Ontario London, ON
Front Desk Clerk, Division of Housing and Ancillary Services 2016-Present

- Work with Residence Life to keep first year students living in residence safe and help with emergencies, such as fires or mental health. Keep track of mail and answer phones.

VOLUNTEER ACTIVITIES

ANOVA London, ON
Child Care Assistant 2018-Present

- Plan activities for and help care for children in a shelter for women and children escaping abusive homes, giving mothers time to have meetings, rest, or shower.

The University of Western Ontario London, ON
Poster Judge, Medical Biophysics Undergraduate Research Day 2019

- Judge medical biophysics undergraduate student posters, asking students questions about their research and rating performance.

The University of Western Ontario London, ON

Charity Ball Committee Member, University Students' Council 2017-2018

- Acting under the Western's University Student Council to organize an event/dance to fundraise for the Make-A-Wish Foundation.

PUBLICATIONS

Chevalier, J., Yin, H., Arpino, J.M., O'Neil, C., Nong, Z., Gilmore, K.J., Lee, J.J., **Prescott, E.**, Hewak, M., Rice, C.L., Dubois, L., Power, A.H., Hamilton, D.W., and Pickering, J.G. (2020). Obstruction of Small Arterioles in Patients with Critical Limb Ischemia due to Partial Endothelial-to-Mesenchymal Transition. iScience *23*, 101251.

PRESENTATIONS

E. Prescott, J. Arpino, H. Yin, J. Chevalier, C. O'Neil, D. Lorusso, T. Poepping, D. Holdsworth, and J. G. Pickering. A Novel 3D Microvessel Model to Study Endothelial Cell Dynamics Under Ultra-Low Flow. Abstract for London Health Research Day, 2019.

E. Prescott, J. Arpino, H. Yin, J. Chevalier, C. O'Neil, D. Lorusso, T. Poepping, D. Holdsworth, and J. G. Pickering. A Novel 3D Microvessel Model to Study Endothelial Cell Dynamics Under Ultra-Low Flow. Abstract for Robarts Research Retreat, 2019.

J. Chevalier, J. Arpino, H. Yin, C. O'Neil, Z. Nong, K. Gilmore, J. Lee, **E. Prescott**, M. Hewak, C. L. Rice, L. Dubois, A. H. Power, D. W. Hamilton, J. G. Pickering. Microvascular Stenosis in End-Stage Peripheral Artery Disease: Role

of Partial Endothelial to Mesenchymal Transition. Abstract for Vascular Discovery: From Genes to Medicine Scientific Sessions, 2019. Abstract 242.

J. Chevalier, J. Arpino, H. Yin, C. O'Neil, Z. Nong, K. Gilmore, J. Lee, **E. Prescott**, M. Hewak, C. L. Rice, L. Dubois, A. H. Power, D. W. Hamilton, J. G. Pickering. Microvascular Stenosis in End-Stage Peripheral Artery Disease: Role of Partial Endothelial to Mesenchymal Transition. Abstract for the Canadian Vascular & Lipid Summit, 2019.

E. Prescott. Engineering a Miniature Blood Vessel. Presented at the Celebrating Science and Discovery Dinner as a part of the 2019 J. Allyn Taylor International Prize in Medicine Symposium, 2019.

AWARDS

The University of Western Ontario
London, ON
Robarts Research Retreat, Poster Award
2019

The University of Western Ontario
London, ON
Dean's Honour Roll
2014-2018

The University of Western Ontario London, ON
Continuing Admissions Scholarship 2014-2018
for 95% admittance average

Robert F. Hall Catholic Secondary School Caledon East, ON
Ontario Scholar's Certificate 2014
Outstanding Achievement in Calculus & Vectors

Academic Excellence in Chemistry

Excellence in Advanced Functions

The Royal Lepage Scholarship

The Canadian Federation of University Women Scholarship